

Control source development for reduction of noise transmitted through a double panel structure



**Control source development for reduction
of noise transmitted through a double
panel structure**

Jen-Hsuan Ho

Graduation committee:

Chair:

Prof.dr. S.J.M.H. Hulscher University of Twente

Promotor:

Prof.dr.ir A. de Boer University of Twente

Co-promotor:

Dr.ir. A.P. Berkhoff TNO/University of Twente

Internal Members:

Prof.dr.ir. T.H. van der Meer University of Twente

Prof.dr.ir. C.H. Slump University of Twente

Dr.ir. J. van Dijk University of Twente

External Members:

Prof.dr.-ing. T. Bein Fraunhofer-Institut LBF/
Technische Universität Darmstadt

Prof. ir. E. Gerretsen TNO/Eindhoven University of Technology

This work was supported by STW (De Stichting voor de Technische Wetenschappen, The Foundation for Technical Sciences), Project no.10602 IMPEDANCE (Integrated Modules for Power Efficient Distributed Active Noise Cancelling Electronics).

Chair of Structural Dynamics and Acoustics, Section of Applied Mechanics
Faculty of Engineering Technology, University of Twente
P.O. Box 217, 7500 AE Enschede, The Netherlands

Cover design: Ren-Wei He

Copyright © Jen-Hsuan Ho, Enschede, 2014

Printed by Ipskamp Drukkers B.V., Enschede, The Netherlands

No part of this publication may be reproduced by print, photocopy or any other means without the permission of the copyright owner.

ISBN 978-90-365-3702-5

DOI 10.3990/1.9789036537025

**CONTROL SOURCE DEVELOPMENT FOR
REDUCTION OF NOISE TRANSMITTED
THROUGH A DOUBLE PANEL STRUCTURE**

DISSERTATION

to obtain
the degree of Doctor at the University of Twente,
on the authority of the Rector Magnificus,
Prof. dr. H. Brinksma,
on account of the decision of the graduation committee,
to be publicly defended
on Friday 11 July, 2014 at 14:45

by

Jen-Hsuan Ho

born on 07 July, 1984
in Taichung, Taiwan

This dissertation has been approved by:

Prof. dr. ir. A. de Boer (promotor)

Dr. ir. A. P. Berkhoff (co-promotor)

To my grandparents
獻給我的爺爺奶奶

Abstract

A double panel structure, which consists of two panels with air in between, is widely adopted in many applications such as aerospace, automotive industries, and buildings due to its low sound transmission at high frequencies, low heat transmission, and low weight. Nevertheless, the resonance of the cavity and the poor sound transmission loss at low frequencies limit the double panel's noise control performance. Applying active structural acoustic control to the panels or active noise control to the cavity has been discussed in many studies. In this thesis, the resonances of the panels and the cavity are considered simultaneously to further reduce the transmitted noise through an existing double panel structure. Various control strategies have been compared and developed to improve the noise control performance. Both numerical and experimental studies are presented.

A validated structural-acoustic coupled model, which can sufficiently accurately predict the interactions between the structure vibration and acoustic wave propagation for our purpose, has been developed. Various combinations of decentralized structural and cavity feedback control strategies are numerically studied and compared. The comparison is based on identical control stability indexes. Moreover, three types of cavity control sources are presented and compared. The results indicate that the largest noise reduction within the frequency range from 10 Hz to 1 kHz is obtained with cavity control by loudspeakers modified to operate as incident pressure sources. This cavity control source has been numerically developed and applied to the double panel structure by using a dynamic loudspeaker, a distributed microphone, and a distributed velocity sensor with feedback control. Furthermore, a one-dimensional incident pressure source has been realized by using a dynamic loudspeaker, a microphone, and a particle velocity sensor with feed-forward control.

An alternative control method is by using flat acoustic sources to reduce the transmitted noise. A flat acoustic source with a small thickness that provides an even sound frequency response has been developed and realized. Multiple

actuators are used to drive the moving panel of the acoustic source. Control of the acoustic resonances and structural resonances is required to obtain an even frequency response. Collocated decentralized feedback control based on velocity sensing was found to be ineffective in controlling these resonances due to the destabilizing asymmetric modes caused by the coupling of the internal acoustic cavity and the rigid body vibration of the moving part. Resonances can be controlled by a set of independent combinations of symmetric driving patterns with corresponding velocity feedback controllers such that the fundamental mass-air resonance is effectively controlled, as is the lowest bending mode of the moving part. Finally, a compensation scheme for low frequencies is used, leading to a flat frequency response in the range of 30 Hz to 1 kHz with deviations smaller than 3 dB.

Samenvatting

Een dubbel paneel bestaande uit twee platen en een luchtsponw wordt veelvuldig toegepast in de luchtvaart, de autoindustrie en gebouwen vanwege de lage geluidtransmissie bij hoge frequenties, de lage warmtegeleiding en het lage gewicht. De resonantie van de spouw en de beperkte geluidsisolerende eigenschappen bij lage frequenties beperken de prestatie bij gebruik als geluidbeheersend element. In dit proefschrift worden de resonanties van de panelen en van de spouw gelijktijdig in beschouwing genomen voor een verdere reductie van het doorgelaten geluid. Verschillende regelstrategieën worden vergeleken en verder uitgewerkt ter verbetering van de akoestische prestatie. Numerieke en experimentele resultaten worden beschreven.

Een gevalideerd vibro-akoestisch model voorspelt voldoende nauwkeurig de interactie tussen de trillingen van de structuur en de akoestische golfvoortplanting. Verschillende combinaties van regelstrategieën bestaande uit een decentrale terugkoppeling van trillingen en akoestische grootheden worden numeriek vergeleken. Daarnaast worden drie typen bronnen voor de besturing van het akoestisch veld in de luchtsponw gepresenteerd en vergeleken. De resultaten laten zien dat in het frequentiegebied van 10 Hz tot 1 kHz de grootste geluidreductie wordt verkregen met een regeling van het akoestisch veld in de spouw door middel van luidsprekers die worden aangepast tot reflectievrije drukbronnen. Deze regeling van het akoestisch veld in de luchtsponw werd numeriek ontwikkeld en toegepast op het dubbele paneel met behulp van een electrodynamische luidspreker, een gedistribueerde microfoon, en een gedistribueerde snelheidssensor met een teruggekoppelde regeling. Ook werd een een-dimensionale reflectievrije drukbron gerealiseerd door middel van een electrodynamische luidspreker, een microfoon, en een deeltjessnelheidssensor met vooruitregeling.

Een alternatieve regelstrategie voor de vermindering van het doorgelaten geluid kan gebruik van een platte akoestische bron. In dit onderzoek werd een platte akoestische bron met kleine dikte en een vlakke frequentieresponsie ontwikkeld en gerealiseerd. Meervoudige actuatoren sturen het be-

wegende paneel van de akoestisch bron. Beheersing van de akoestische resonanties en de structuurresonanties is nodig om een vlakke frequentieresponsie te bewerkstelligen. Een decentrale teruggekoppelde regeling met actuator- en sensorcolocatie gebaseerd op snelheidsmeting bleek geen effectieve methode voor de beheersing van de resonanties vanwege de destabiliserende asymmetrische modi veroorzaakt door de koppeling tussen het akoestische veld in de luchtspouw en de rotatie van de bewegende plaat. Beheersing van de resonanties is wel mogelijk door middel van onafhankelijke combinaties van symmetrische bewegingspatronen met bijbehorende teruggekoppelde snelheidssignalen waarmee de fundamentele resonantie bepaald door de bewegende massa en de stijfheid van de lucht effectief kan worden onderdrukt, evenals de laagste-orde buigmodus van de bewegende plaat. Tot slot werd een compensatieschema toegevoegd, hetgeen resulteert in een vlakke frequentieresponsie in het frequentiegebied van 30 Hz tot 1 kHz met afwijkingen kleiner dan 3 dB.

Contents

1	Introduction	1
1.1	Background	1
1.2	Noise control methods	2
1.2.1	Passive noise control	2
	Helmholtz resonators	3
	Shunt piezoelectric damping	4
	Tuned vibration absorber	5
1.2.2	Active noise control	6
	Active noise control and active structural acoustic control	6
	Feed-forward and feedback control	9
	Adaptive control	10
	Centralized, decentralized and distributed control	11
1.2.3	Combination of passive and active control	12
1.3	Double panel structure	12
1.4	Flat acoustic source	14
1.5	Patent research	15
1.6	Research scope and objectives	16
1.7	Thesis outline	17
2	Control methods	19
2.1	Introduction	19
2.2	Feed-forward control	20
2.2.1	Decentralized harmonic feed-forward control	20
2.2.2	Stability: control effort weighting factor	21
2.2.3	Internal model control	21
2.3	Feedback control	22
2.3.1	Multiple decentralized feedback control	22
2.3.2	Nyquist criterion	23
2.3.3	Generalized Nyquist criterion	24
2.3.4	Collocated sensor-actuator control pairs	25

2.4	Adaptive control	27
2.4.1	Steepest-descent algorithm	27
2.4.2	Regularized modified filtered-error LMS algorithm	28
2.5	Conclusions	30
3	Finite element method model and experimental setup	31
3.1	Introduction	31
3.2	Structural-acoustic coupled model	31
3.3	Near field sound pressure	33
3.4	Kinetic energy estimation	35
3.5	Equivalent piezoelectric load	37
3.6	Experimental setup	37
3.7	Model validation	39
3.8	Conclusions	41
4	Structural, cavity, and combined control	43
4.1	Introduction	43
4.2	Feedback structural control	43
4.2.1	Radiating and incident panel control	44
4.2.2	Resonant modes analysis	47
4.2.3	Real-time control	51
4.3	Feedback cavity control	53
4.4	Feedback combined control and comparisons	55
4.5	Conclusions	59
5	Comparison of cavity control strategies	61
5.1	Introduction	61
5.1.1	Acceleration source loudspeaker	62
5.1.2	Incident pressure source loudspeaker	63
5.1.3	Pressure-controlled source loudspeaker	64
5.2	Cavity control performance comparisons	65
5.3	Feed-forward control	68
5.4	Conclusions	72
6	Development of incident pressure sources	73
6.1	Introduction	73
6.2	Development of an incident pressure source	74
6.2.1	System configuration	74
6.2.2	Wave separation technique	75

6.3	One-dimensional realization with feed-forward control	76
6.3.1	Experimental setup	76
6.3.2	Real-time control results	77
6.4	Numerical development with feedback control	81
6.4.1	Performance in a duct	81
6.4.2	Performance in a double panel structure	85
	Reflecting pressure direction selection	86
	MIMO control results	90
6.5	Conclusions	92
7	Flat acoustic sources	93
7.1	Introduction	93
7.2	Method	94
7.2.1	Perforated honeycomb panel	94
7.2.2	Multiple decentralized feedback control	96
7.2.3	Feed-forward response correction filter	98
7.3	Implementation and numerical model	100
7.3.1	Implementation	100
7.3.2	Numerical model	102
	FEM model	102
	Model validation	104
7.4	Control stability	106
7.4.1	Excitation positions	107
7.4.2	Nyquist stability analysis	109
7.5	Control results	111
7.5.1	Feedback control configurations	111
	SISO control system	111
	MIMO control system	113
	Example	115
7.5.2	Response equalization at low frequencies	117
7.6	Conclusions	119
8	Conclusions	121
8.1	Conclusions	121
8.2	Answers to the research questions	124
8.3	Potential directions for future work	125
	Bibliography	127

Nomenclature	137
Appendices	141
A Datasheet of the voice coil actuator	143
B Datasheet of the accelerometer	145
C Amplifier	149
Appendices	141
About the author	151
Acknowledgments	153

Introduction

1.1 Background

Traditionally, noise control methods are based on passive noise control, which means applying damping materials, adding mass, adding resilient elements or installing absorbing resonators in the system. Passive noise control can effectively reduce noise at high frequencies [1]. However, there is typically much less noise reduction at low frequencies, and reduction requires a substantial implementation cost because the acoustic wavelengths are much longer than the damping device [2,3]. Conversely, active noise control offers the potential advantages of decreased weight and better performance at low frequencies. With the development of smart materials and computational power, active noise control has received increasing attention in the past few decades. Traditional active noise control (ANC) for reducing broadband noise has been successfully applied in relatively small spaces [4,5]. However, for a larger control volume, the 3D wave propagation problem causes the control implementation to become complicated and inefficient. Therefore, active structural acoustic control (ASAC) has been proposed to simplify the control computation. ASAC can simplify a 3D problem to a 2D problem by directly controlling the vibrating structure to reduce the structure's radiating sound field instead of addressing 3D acoustic wave propagation [4,6]. Furthermore, for a large configuration, decentralized control or distributed control can make the controller suitable for practical implementations [7–11]. For specific configurations a decentralized feedback control strategy can be effective [12,13].

A double panel structure, which consists of two panels with air in the gap, is another common implementation for noise reduction. The double panel structure offers the advantages of low sound transmission at high frequencies, low heat transmission, and low weight [1, 14–16]. The double panel structure is

widely used, such as in the aerospace and automotive industries. Nevertheless, the resonance of the cavity and the poor sound transmission loss at low frequencies limit the double panel's noise control performance. Applying active structural acoustic control to the panels or active noise control to the cavity has been discussed in many papers. However, the improvement of the transmitted noise reduction is limited. The current work compares various control strategies and provides an effective control strategy for the transmitted noise reduction through the double panel structure.

This chapter is structured as follows. (1) Firstly, various noise control methods are introduced. (2) Subsequently, the state-of-the-art of noise control strategies for the double panel structure is described. (3) The need for a flat acoustic source is addressed. (4) A patent research is presented since industrial research is relevant in this field. (5) Research questions and objectives are given. (6) The outline of this thesis is provided.

1.2 Noise control methods

Noise control methods can be passive, active, or both passive and active. The passive approach has been investigated and developed for several decades. The limitation of the degree of noise reduction and the addition of weight are the main bottlenecks. However, recently, some research groups have proposed new passive noise reduction methods such as multiple optimal Helmholtz resonators, distributed vibration absorbers and shunt damping, which improve the performance of passive noise reduction. These research results are introduced in the following section. On the other hand, active noise control has the potential of lighter implementations if the noise and vibration levels are not too high. Furthermore, active control may result in higher reductions of noise and vibration. However, if the control computation is complicated then the need for expensive hardware restricts its practical implementation. Recent research results are described in the second part of this section. Moreover, some researches combining passive and active controls are also presented in this section.

1.2.1 Passive noise control

Passive control is the traditional solution for noise and vibration reduction [2, 17]. The main concept of passive noise reduction is to increase the damping of the vibrating plate and the cavity, or to add the resonator in the

cavity. For instance, adding visco-elastic layers on fuselage skin panels or trim panels is a common solution to reduce noise in aircraft [18–21]. Tube resonators have been proposed for noise reduction in aircraft cabins and have shown good performance in the frequency range of 500 Hz to 2 kHz [22]. Passive control can avoid sensors, actuators, and control electronics. It works well in the high frequency range where the acoustic wavelengths are much shorter than the passive control device [3]. However, passive control at low frequencies usually leads to much less noise reduction and comes with a heavy implementation. The main passive control methods and their recent developments are addressed in this section.

Helmholtz resonators

A Helmholtz resonator consists of a cavity connected to the system of interest through a narrow tube as shown in Fig. 1.1. In such a way, the Helmholtz resonator acts like a mass on a spring, the air inside the cavity acts like the spring and the air in the narrow tubes acts like the oscillating acoustic mass. Damping appears because of the radiation losses at the tube ends and the friction of the oscillating air in the narrow tubes.

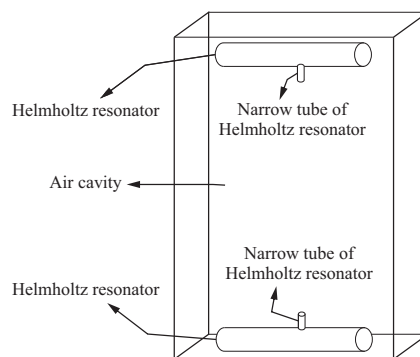


Figure 1.1: Helmholtz resonators for noise reduction in an air cavity.

Helmholtz resonators have been used to control sound transmission between infinite double plates [23, 24]. Those resonators are tuned to the main noise frequency. However, the finite double plate is more complex than the infinite case. Therefore, the modeling and investigating on finite double plate has been studied. A structural-acoustic coupling model of finite double

plate sound transmission with Helmholtz resonators has been presented in Ref. [25], which shows how the Helmholtz resonators need to be optimized. Only tuning the resonator to the mass-air-mass resonance frequency cannot obtain the biggest reduction of noise transmission. It is more effective to tune the frequency of the resonator by using average noise transmission loss as an index. Some traffic noises like jet-aircraft, train, helicopter highway noises are used as excitation sources in experiments and the results show the effect of Helmholtz resonators in a practical implementation [25]. Even this method can improve the isolation of sound transmission; the reduction of sound pressure is limited to about 10 dB with 6 Helmholtz resonators [26]. Furthermore, the control performance is affected by the angle of incident sound wave [26].

Shunt piezoelectric damping

Shunt piezoelectric damping uses piezoelectric materials to convert mechanical vibration energy into electrical energy, and then use the resistive component of the shunt circuit to eliminate the energy [27]. Tuning the resonance frequency of the circuit to the resonance frequency of the structure can effectively reduce the vibration. However, if the resonance frequency of the structure changes due to environmental changes, the resonant circuit becomes 'detuned' and leads to drastically reduced effectiveness of this method. Therefore, another shunt circuit called state-switched shunt piezoelectric damping has been proposed, which changes the stiffness by switching between open-circuit (high stiffness) and short circuit (low stiffness) [28]. Consequently, the system can effectively store the energy with high stiffness and dissipate the energy by changing to low stiffness. This method is less sensitive to environmental changes than the traditional shunt piezoelectric damping method [28, 29].

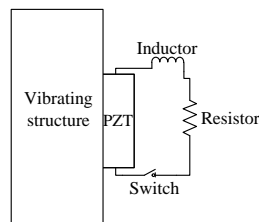


Figure 1.2: Pulse-switched shunt piezoelectric damping.

Furthermore, a pulse-switched shunt piezoelectric damping method has been proposed as shown in Fig. 1.2. The piezoelectric element is briefly switched to a resistor/inductor shunt circuit in such a way that the piezoelectric element can generate force opposite to the velocity of the structure [29–31]. This method is similar to the direct velocity feedback control and is considered as a good noise control method [14].

Tuned vibration absorber

A tuned vibration absorber (TVA) can absorb a certain frequency of structural vibration by transferring the vibrating energy from the structure to the vibration of the secondary mass, being the absorber [32, 33]. As shown in Fig. 1.3, the vibrating structure consists of the mass M_s , the spring K_s and the damper C_s ; the absorber consisting of the mass M_a , the spring K_a and the damper C_a is attached to the vibrating structure.

The TVA has been used for a long time in civil engineering to protect tall buildings from wind or earthquake loading. Furthermore, the TVA has also been designed to reduce the vibration of the aircraft fuselage and the aircraft interior noise [34]. However, for a broadband disturbance this tonal vibration absorber is not enough. The absorber frequency should be tunable to achieve better control performance. Therefore, adaptive tuned vibration absorbers (ATVAs) have been proposed, where the absorber frequency can be tuned by varying its stiffness element. The varying stiffness technique can be realized by a motor-driven mechanism, by piezoelectric stack actuators, by shape-memory alloys, and by magneto-rheological(MR) fluid [35–37]. For example, in MR fluid design, the natural frequency can be changed from 106 Hz to 149 Hz, which is almost a 40 % change [37].

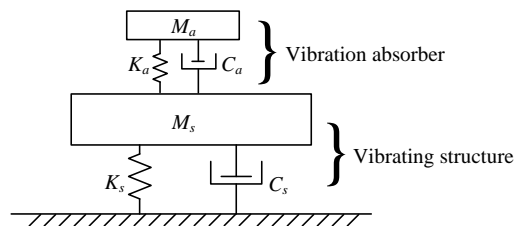


Figure 1.3: Tuned vibration absorber.

1.2.2 Active noise control

Because of the heavy implementation, passive noise control leads to increased fuel cost in practical applications. Furthermore, passive noise control has poor performance in the low frequency range where the acoustic wavelengths are much longer than the passive control device or the noise reduction can only be obtained in a narrow frequency range [3]. To decrease the weight of the implementation and to increase the reduction of noise, more and more researches focus on active noise control (ANC) [7]. In early studies, active noise control could obtain reductions of 14 dB (sum of measured squared pressure with 32 sensors) at certain frequencies [38]. With the development of more advanced control hardware, algorithms, and control theory, the reduction of active noise control can achieve 10 to 18 dB (radiated sound power at low-frequency resonances of the system) for broadband disturbances [16]. Furthermore, the combination of passive and active noise control can be particularly effective and has become the trend for broadband noise control, since passive control is more effective at high frequencies and active control is more effective at low frequencies [39]. This section introduces the principles of active noise control, active structural acoustic control, and active control schemes.

Active noise control and active structural acoustic control

Generally, an active noise control system consists of sensors (microphones), secondary sound sources (loudspeakers), and a controller. The control principle uses a loudspeaker to produce a secondary source, which has the same amplitude but with anti-phase to the original noise source. In such a way, the control source can cancel the noise source as shown in Fig. 1.4. However, in

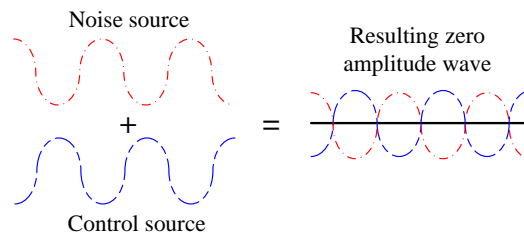
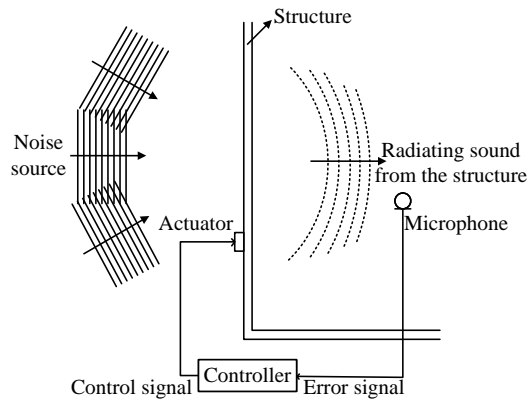
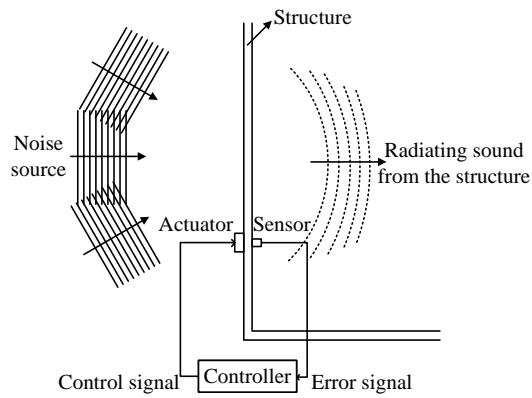


Figure 1.4: Active noise control principle.

order to cancel an acoustic wave in 3D space, 3D modeling, calculations, and measurements are necessary. This makes active noise control become ineffective and expensive in relatively large spaces [4, 5]. To solve this problem, active structural acoustic control (ASAC) has been proposed [40]. ASAC focuses on the control of a vibrating plate in order to reduce the sound transmission through a plate. This means the control objective is simplified to two dimensions. Relationships between the structural vibrations and the sound radiations have been studied at the primary stage [41–43]. Strategies minimizing the far-field radiated sound power by the near-field sensors have been investigated [44]. Furthermore, the vibration patterns of the structure that produce effective radiated sound power are called radiation modes. Sensor configurations and radiation mode estimation have been described in Refs. [8, 45]. Moreover, various structural actuators and sensors have been modeled and compared [46, 47]. Figure 1.5(a) presents an implementation scheme of ASAC with a microphone as the error sensor and Fig. 1.5(b) uses an accelerometer as the error sensor. It has been reported that the control performance of ASAC and ANC shows no clear difference [14]. In the ASAC system, the position and number of sensors and actuators can be optimized to improve the control performance [40, 48, 49]. Piezoelectric actuators, voice coil actuators and electrodynamic proof-mass actuators have been used as the control actuators [16, 50, 51]. Control stabilities have been addressed in Refs. [51, 52].



(a)



(b)

Figure 1.5: Active structural acoustic control: (a) using a microphone as the error sensor; (b) using an accelerometer on the structure as the error sensor.

Feed-forward and feedback control

In an active control system, there are two main control strategies: feed-forward control and feedback control. When a signal correlated to the primary noise is available, feed-forward control is attractive because it can reduce the noise for any frequency and attempt to cancel the noise by generating a secondary signal with opposite phase to the primary noise. Therefore, it is widely used as an active control methodology. The more accurate the reference signal, the better the control performance. Figure 1.6(a) presents an ANC controller with feed-forward control scheme, where the control signal relies on the reference signal. Filtered-reference least mean square (Filtered-x LMS/FXLMS) feed-forward control is the most often used for harmonic disturbances [53]. However, the reference signal is not always available. For instance, the noise in aircraft mainly comes from the air turbulence and the engine which means the vibration comes from everywhere and has a broadband nature as well. There are too many primary sources to observe and the reference signal cannot be detected accurately [54]. Therefore it is difficult to obtain good noise reduction performance in such a situation with feed-forward control. In contrast to feed-forward control, feedback control does not rely on the availability of a reference signal. Consequently, many studies choose feedback control to reduce the noise when the reference signal is unavailable [9–13, 55]. Figure 1.6(b) presents an ANC controller with a feedback control scheme, where the control signal relies on the error signal. Moreover, direct velocity feedback (DVFB) control offers an unconditionally stable control system if appropriate sensors and actuators are used. Modeling and designing of DVFB control in noise control have been presented in Refs. [52, 56]. Although the reference signal correlating to the primary disturbance for the feed-forward controller is not always available, a reformulation method can transform a feedback controller into an equivalent feed-forward controller [57]. This method is known as internal model control (IMC). IMC methods applied to a double panel structure have been shown [58]. Further theories of the feed-forward, feedback and internal model control are discussed in Chapter 2.

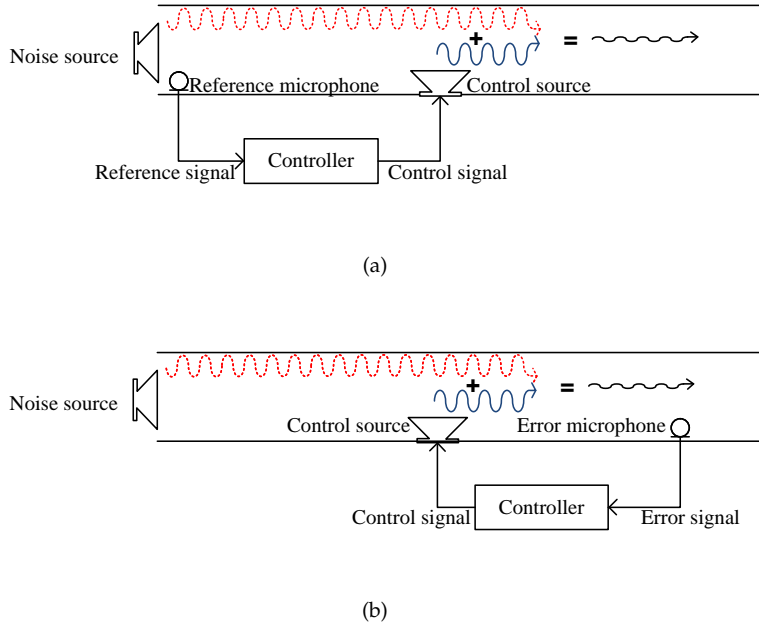


Figure 1.6: Control scheme (a) feed-forward ANC; (b) feedback ANC. The transfer of the control source to the reference sensor is not included, it will be taken into account later in Chapter 2.

Adaptive control

The characteristics of the environments can vary with time. When the variation of the environment is too large, a control system based on a fixed control law may become unstable. Therefore, an adjustable control law is necessary in a control environment with large parameter variations. Adaptive control provides a control system with time-varying parameters [59]. The adaptive control adjusts its coefficients in response to new data. It can potentially control a system with non-stationarity caused by changes in the primary noise. Some implementations of adaptive controllers can also be made adaptive with respect to changes of the secondary path [60]. Adaptive control has been investigated intensively because of the development in aircraft industry. Aircraft are oper-

ated in a wide range of speeds and altitudes; control design based on one operation condition cannot make the control system stable [61]. Still more theories and practical applications of adaptive control are becoming available [61–64]. Moreover, by iteratively adjusting the coefficients of the controller, adaptive control uses fewer calculations per sample than directly computing the optimal coefficients in one step.

Centralized, decentralized and distributed control

Active control implementations have adopted centralized control for a long time [65,66]. A centralized control system uses only one controller for all the sensors and all the actuators. The controller relies on the prediction of the transfer functions and uses actuators to control different modes. The predictions are accurate only at the lower-order modes, which are less sensitive to the environment [67]. The control performance is easily affected when the environment conditions change. Moreover, failure of one control channel could damage the whole control system. Most importantly, the computation of centralized control is often too complicated and expensive especially for broadband disturbances. It is hard to use centralized control in practical systems because of the expensive hardware. This problem becomes particularly serious in aircraft for its extremely large vibrating area. A simplified method, which is called decentralized control, is separating the control units to decrease the complexity in conventional centralized control. A decentralized control system uses pairs of sensors and actuators as independent control units. The error signal from the sensor(s) in such a system controls only the corresponding actuator(s). When the sensors and actuators are collocated and dual, the system can be unconditionally stable [67–69]. Therefore, the control loops become simpler, and the stability of control system also becomes more robust [70,71]. Research shows that the control system can maintain the same performance when there are 3 of 16 channels that have a failure [72].

In spite of the reduction of computational complexity and the increasing stability of decentralized control, the noise reduction performance also becomes worse. Therefore, control concepts based on distributed control have been proposed. The control units of the distributed control system are basically independent, but there are reference signals which could be passed through each control unit. Instead of the weak connection between each control unit in decentralized control, distributed control has a stronger connection between control units [73]. The control units could share the sensor information to improve the control results. In this way, the global control performance can be

improved [74,75]. The comparison between centralized, decentralized and distributed control has been investigated, the performance of distributed control is better than decentralized control in the fundamental mode and is close to the traditional centralized control [76]. The distributed control system not only reduces the computational complexity but also achieves performance close to that of a centralized control system. Active control applied to large-scale objectives by adopting a distributed control system seems promising [77].

1.2.3 Combination of passive and active control

Since passive control can effectively reduce noise transmission at high frequencies, and active control performs better at low frequencies, the combination of these two noise control methods becomes an important concept of noise reducing design. Here are some examples of this passive and active combined control. An implementation consisting of active noise control, distributed vibration absorber and viscoelastic constrained layer damping has been presented in Refs. [39]. This combination can increase transmission losses by 9.4 dB and only add 285 g to the panel (approximately 5 % of the total weight) between 15 Hz - 1 kHz. Combination of loudspeakers and a micro-perforated absorber can provide effective noise reduction from 100 Hz to 1600 Hz [78]. Therefore, further development of active noise control strategies applied to structures with passive noise control leads to high potential in noise control design.

1.3 Double panel structure

A double panel structure, which consists of two panels with air in a gap as shown in Fig. 1.7, is another common implementation for noise reduction. The double panel structure offers the advantages of low sound transmission at high frequencies, low heat transmission, and low weight [1, 14–16]. However, the reduction is not enough, especially in the low frequency range. Moreover, there are cavity resonance problems and good acoustical coupling between incident panels and radiating panels. Accordingly, active noise control has been applied to the double panel structure to improve the noise reduction [6, 53, 79–82]. Acoustic and vibration coupled models have been investigated in analytical and numerical forms [4, 79, 83]. The research of active double panel noise control focuses on the optimized position of sensors and actuators (putting them on the incident/radiating panel or using loudspeakers in the cavity), the acoustical coupling between incident panel and radiating panel,

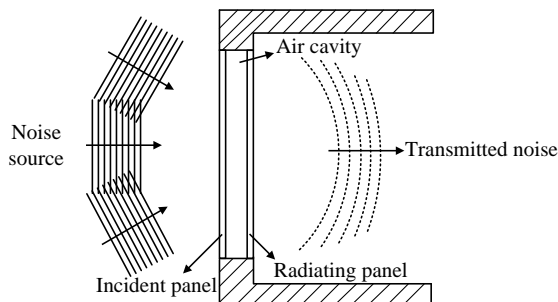


Figure 1.7: Double panel structure.

and the cavity resonant behaviors. Comparisons of incident panel control and radiating panel control have been given in Refs. [81, 84]. Results have shown that if the properties of the incident panel and the radiating panel are very dissimilar, then control of the incident panel control will be useless; the control should be on the radiating panel. Moreover, less coupling between the incident panel and the radiating panel, which is offered by less similarity between the properties of incident panel and radiating panel, increases the transmission loss and the control efficiency [6]. If the incident panel and the radiating panel have identical thickness and material property, the panels would have in-phase resonant modes, which are the uncontrollable cavity modes [14, 85]. Furthermore, theoretical analysis of applying ideal skyhook actuators and reactive actuators to both panels for active damping control has been discussed in Refs. [15, 52]. The latter reference also discusses the critical aspect of control stability for these control configurations. A blended velocity feedback control, where the blended velocity consists of weighted velocity of the incident panel and the radiating panel, has been proposed [16]. Applying passive methods to improve the noise reduction has also been studied. Adding acoustic foam materials or metamaterials between these two panels to absorb the transmitted noise is reported [86–89]. Viscothermal effects in the air layer, which can convert vibration energy into heat, for reduction of noise transmitted through the double panel structure have been studied [90]. However, the study shows the dissipative properties of the air layer can only effectively reduce structure-borne noise. The transmitted noise caused by airborne noise is hardly reduced by the viscothermal effects.

1.4 Flat acoustic source

Acoustic sources having small thickness offer practical advantages for active noise control [91, 92] and for audio reproduction [93] because the available space is often limited. Electroacoustic efficiency of moving coil loudspeaker at low frequencies is proportional to internal enclosure volume [94, 95]. Therefore the available internal volume of the loudspeaker should be used as efficiently as possible. Furthermore, conventional moving-coil loudspeakers attempt to move the membrane or panel as a rigid piston [94]. However, in reality, the membrane exhibits bending waves. These unwanted bending modes of the membrane cause the frequency response of the loudspeaker to be colored and uneven. To achieve an even frequency response, many researchers have designed the materials, structure, and suspension of the membrane to eliminate these unwanted resonances. Instead of eliminating these unwanted bending modes, distributed mode loudspeakers (DMLs) technique uses these bending modes to cause an acoustic output [96–98]. The excitation position is designed to obtain an evenly distributed modal density, which produces a similar effect as a continuous spectrum. Various filter topologies have been studied to further equalize the uneven frequency response. This technique offers the advantages of compactness and omnidirectionality. However, the panel resonances are complex and difficult to control, which often leads to complicated computations and an insufficient low-frequency response. In further development of DMLs, multiple exciters are applied to the panel, which is known as a multi-actuator panel (MAP) [99, 100]. However, the panel response is dependent on the excitation positions. Therefore, dedicated filters based on the excitation positions for each individual exciter are essential [101], although commercial DML products have been seen on the market and further applications of MAPs have been proposed. For instance, MAPs can function as array loudspeakers for wave field synthesis (WFS) applications [99]. The DMLs and MAPs still suffer from poor acoustic response at low frequencies. In a recent study, the bandwidth of a MAP loudspeaker was extended down to 100 Hz by a physical-psychoacoustic combined method [102]. Furthermore, air cavities between two panels are often used to improve noise insulation by passive means [14, 82, 103]. A larger air gap provides larger acoustic compliance, and therefore, less coupling is obtained. Compact partitions with narrow air gaps lead to less acoustic insulation, especially at low frequencies. Nevertheless, if a flat acoustic source with small thickness and sufficient acoustic output at low frequencies is provided, the acoustic insulation at low frequencies can be improved by applying an acoustic source for active noise control, while sufficient insulation at high

frequencies is provided by a narrow air gap.

1.5 Patent research

This section presents results of a patent search to give an overview of practical noise control implementations. The noise problem is more significant in vehicle design, because the noise coming from the engines and the air turbulence is directly experienced by the passengers in the vehicles. Passive noise control is the conventional noise reduction method; however, its heavy implementation increases the fuel cost, especially in aircraft. Active control such as Active Noise Control (ANC), Active Vibration Absorbers (AVAs), and Active Structural Control (ASC) not only avoids this problem but can also improve the performance of noise reduction in the low frequency range [104–107]. In general, vehicle structure is an enclosure space. The design of active noise control for the enclosure space has been shown in Refs. [108,109]. Furthermore, for a large-scale control system, multiple control units (multiple sensors and multiple actuators) are necessary. The design of multiple adaptive noise control systems is reported in Refs. [110,111]. Nevertheless, the complex computation limits the practical implementation of active noise control. Therefore, a decentralized control system was designed, in which each of the control units is independent and the calculation is simplified [112]. However, the noise reduction performance of a decentralized control system is worse than the noise reduction performance of a centralized control system. Later, another control system, which uses the signals from neighboring sensors to produce the actuating signals, was introduced [113]. Moreover, methods to improve control stability have been proposed. For instance, to establish a stability detecting system to evaluate the stability of the adaptive control system and to improve the speed and performance as well [114]. The double panel structure, defined by the exterior fuselage wall and the interior trim panel, is a common design in aircraft. The resonance of the cavity also has a considerable effect on the noise transmission. However, only a small region of the cavity is controlled [115]. The control performance is also affected by the properties of the actuators. Consequently, the design of the actuators is another important issue. The control force, which is the product of the mass and the acceleration of the inertial mass shaker for well above the resonance frequency, is applied to the vibrating structure in the conventional shaker control design. To reduce the displacement of the mass, the reduction of the mass cannot be too large. Instead of the conventional oscillatory force, an oscillatory torque is used on the vibration control to remove

the constraints on mass reduction in a vibration generator design [116].

1.6 Research scope and objectives

The core objective of this research is to develop a further understanding of resonance in a double panel structure and to provide a more effective control strategy for reduction of noise transmitted through a double panel structure. Therefore, the research questions are:

- What kind of resonance dominates transmitted noise through a double panel structure?
- With decentralized feedback control, controlling which part of the double panel structure offers more transmitted noise reduction: the cavity, the incident panel, or the radiating panel?
- Can the decentralized feedback control performance be further improved by combining other control strategies?
- Do we already have good control sources for the transmitted noise control? If not, what kind of control source is needed?

To answer the research questions and to accomplish our core research objectives, we have set the following goals for the current work:

- To develop a structural-acoustic coupled Finite Element Method (FEM) model, which can accurately predict the interactions between the structural vibration and acoustic wave propagation.
- To analyze the dominant structural/acoustic modes of the double panel structure at resonance frequencies.
- To compare various decentralized control strategies, including structural and acoustic sensor-actuator configuration designs, to reduce noise transmission through a double panel structure.
- To develop an effective control strategy for the transmitted noise reduction through a double panel structure.

1.7 Thesis outline

This thesis is organized as follows. Chapter 2 introduces our control methods, which include feedback control, feed-forward control, and adaptive methods taking into account control stability. Chapter 3 describes the details of our numerical model and the experimental setup. Chapter 4 presents the resonant behavior analysis of the double panel structure. Decentralized structural and cavity feedback control results are numerically compared. Chapter 5 introduces and compares three acoustic sources used as decentralized cavity feedback control sources in the double panel structure: an acceleration source loudspeaker, an incident pressure source loudspeaker, and a pressure-controlled source loudspeaker. Moreover, to further improve the transmitted noise reduction, a combination of feedback and feed-forward decentralized control is presented. Chapter 6 presents the development of the so-called incident pressure source by modifying a dynamic loudspeaker with feed-forward or feedback control. Chapter 7 introduces the development of flat acoustic sources, which can be used as cavity control sources for noise reduction. Finally, Chapter 8 summarizes our research results, answers the research questions and suggests potential directions for future work.

Control methods

2.1 Introduction

As introduced in Chapter 1, there are several possible active control strategies to reduce acoustic noise. This chapter describes a few of these strategies as they apply to our system, and their operating principles. When a signal correlated to the primary noise is available, feed-forward control is attractive because it can reduce the noise for any frequency and attempt to cancel the noise by generating a secondary signal with opposite phase to the primary noise. In contrast to feed-forward control, feedback control does not rely on the availability of a reference signal. Direct velocity feedback (DVFB) control provides active damping, offering an unconditionally stable control system if appropriate sensors and actuators are used. These control systems can also be realized in larger configurations through decentralized or distributed control, making the controller more practical to implement [7,9–11,117]. Decentralized feedback control for a broadband objective has been shown to be remarkably effective [13]. As stability is an essential requirement for the control system, this chapter also describes methods used to determine and improve the stability. Furthermore, the primary noise can vary with time, if the variation is too large, a controller with fixed control parameters may become unstable. A control system with time-varying parameters, which is called adaptive control, can be applied.

2.2 Feed-forward control

2.2.1 Decentralized harmonic feed-forward control

Figure 2.1 shows the signal block diagram of a MIMO feed-forward control system with L error sensors and M actuators, where the noise sources are used as the reference signals. $\mathbf{e}(j\omega)$ is the $M \times 1$ -dimensional vector of error signals, where ω is the angular frequency [rad s⁻¹] and $j = \sqrt{-1}$. $\mathbf{G}(j\omega)$ is the $L \times M$ -dimensional plant transfer function; $\mathbf{u}(j\omega)$ is the $M \times 1$ -dimensional vector of control signals; $\mathbf{d}(j\omega)$ is the $L \times 1$ -dimensional noise source vector, which is the vector of error signals without the input control signal.

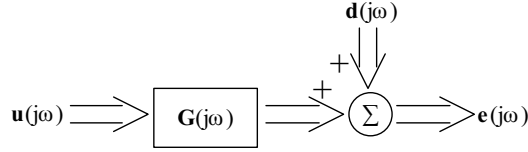


Figure 2.1: Feed-forward control systems.

From the block diagram in Fig. 2.1, the error signals $\mathbf{e}(j\omega)$ can be derived as

$$\mathbf{e}(j\omega) = \mathbf{d}(j\omega) + \mathbf{G}(j\omega)\mathbf{u}(j\omega). \quad (2.1)$$

For simplicity, the explicit dependence on $j\omega$ is dropped in the following notation. The cost function is defined as the sum of the square error signals

$$J = \mathbf{e}^H \mathbf{e} = \mathbf{u}^H \mathbf{G}^H \mathbf{G} \mathbf{u} + \mathbf{u}^H \mathbf{G}^H \mathbf{d} + \mathbf{d}^H \mathbf{G} \mathbf{u} + \mathbf{d}^H \mathbf{d}, \quad (2.2)$$

where H denotes the Hermitian transpose. Alternatively, the trace of an outer product of the cost function can be used,

$$J = \mathbf{e}^H \mathbf{e} = \text{trace}(\mathbf{e}\mathbf{e}^H). \quad (2.3)$$

The derivative of the cost function with respect to the control signal is written as

$$\frac{\partial J}{\partial \mathbf{u}_R} + j \frac{\partial J}{\partial \mathbf{u}_I} = 2\mathbf{G}^H \mathbf{G} \mathbf{u} + 2\mathbf{G}^H \mathbf{d}, \quad (2.4)$$

where \mathbf{u}_R and \mathbf{u}_I are the real part and the imaginary parts of \mathbf{u} . By setting the above equation to zero, the optimal control signals \mathbf{u}_{opt} can be derived as

$$\mathbf{u}_{opt} = - [\mathbf{G}^H \mathbf{G}]^{-1} \mathbf{G}^H \mathbf{d}. \quad (2.5)$$

2.2.2 Stability: control effort weighting factor

As some decentralized control systems are inherently unstable, adding an effort weighting term to the system can improve the stability. Instead of only using the squared error signals in the cost function (as described by Eq. (2.2)), the squared control signal with an effort weighting factor β is added. The cost function J is now defined as

$$J = \mathbf{e}^H \mathbf{e} + \beta \mathbf{u}^H \mathbf{u}. \quad (2.6)$$

The control signal is then derived as

$$\mathbf{u} = - [\hat{\mathbf{G}}^H \mathbf{G} + \beta \mathbf{I}]^{-1} \hat{\mathbf{G}}^H \mathbf{d}, \quad (2.7)$$

where $\hat{\mathbf{G}}$ is an estimated plant transfer function. In a practical implementation, the plant transfer function \mathbf{G} might not be perfectly known, $\hat{\mathbf{G}}$ is used in an adaptation algorithm to update the control signals. If the plant transfer function is perfectly known and can be reliably measured, we can then assume $\hat{\mathbf{G}} = \mathbf{G}$. The stability of the decentralized MIMO feed-forward control system is guaranteed when the real parts of the eigenvalues λ of the matrix $\hat{\mathbf{G}} \mathbf{G}^H + \beta \mathbf{I}$ are positive. If the system is unstable, β can be set to $-\min \text{Re}(\lambda)$ to make the system just stable [118]. However, feed-forward control needs perfect knowledge of the reference signal to provide good control performance.

2.2.3 Internal model control

Although a reference signal correlating to the primary disturbance for the feed-forward controller is not always available, a reformulation method can transform a feedback controller into an equivalent feed-forward controller [57]. This method is known as internal model control (IMC) as shown in Fig. 2.2. The dashed line indicates the complete negative feedback controller \mathbf{H} , which contains a control filter \mathbf{W} and an internal model $\hat{\mathbf{G}}$. This internal model is an estimated model of \mathbf{G} , which is the plant response from the secondary sources

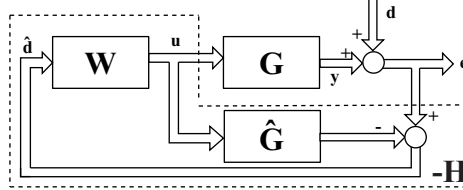


Figure 2.2: Internal model control

to the error sensors. By using this estimated plant model \hat{G} , the influence from the secondary sources to the error signals can be estimated. Subtracting this estimated influence from the error signals e can obtain the estimated noise signals \hat{d} of the true noise signals d , which are used as the reference signals. \hat{d} are fed to the control filter W as the estimated reference signals, and the output control signals u drive the plant G to produce the secondary signals y .

2.3 Feedback control

2.3.1 Multiple decentralized feedback control

Figure 2.3 illustrates the signal block diagram of a multiple-input and multiple-output (MIMO) feedback control system, assuming there are L error sensors and M actuators. $e(j\omega)$ is the $M \times 1$ -dimensional vector of error signals, where ω is the angular frequency [rad s^{-1}] and $j = \sqrt{-1}$. $G(j\omega)$ is the $L \times M$ -dimensional plant transfer function; $u(j\omega)$ is the $M \times 1$ -dimensional vector of control signals; $d(j\omega)$ is the $L \times 1$ -dimensional noise source vector, which is the vector of error signals without the input control signals; and $H(j\omega)$ is the $M \times L$ -dimensional control matrix, which is a constant for this system. The time-dependent signals are the real part of the complex vectors (i.e., the time-dependent error signals $e(t) = \text{Re}\{e(j\omega)e^{j\omega t}\}$).

From the block diagram in Fig. 2.3, $e(j\omega)$ can be derived as

$$e(j\omega) = [\mathbf{I} + \mathbf{G}(j\omega)\mathbf{H}(j\omega)]^{-1}d(j\omega), \quad (2.8)$$

where \mathbf{I} is an identity matrix of dimensions L . To present the physical interactions between each control unit in a MIMO control system, a fully coupled

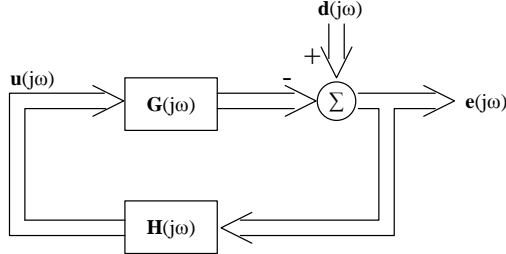


Figure 2.3: Direct feedback control system.

multiple channel plant transfer function $\mathbf{G}(j\omega)$ is applied:

$$\mathbf{G}(j\omega) = \begin{bmatrix} \mathbf{G}_{11}(j\omega) & \cdots & \mathbf{G}_{1m}(j\omega) \\ \vdots & \ddots & \vdots \\ \mathbf{G}_{l1}(j\omega) & \cdots & \mathbf{G}_{lm}(j\omega) \end{bmatrix}, \quad (2.9)$$

where $\mathbf{G}_{lm}(j\omega)$ is the transfer function from the m -th actuator to the l -th sensor.

2.3.2 Nyquist criterion

In theory, the stability of a feedback control system can be unconditionally guaranteed when the sensors and actuators are dual and collocated [68]. Therefore, the control gain can be increased infinitely to decrease the error signals of Eq. (2.8) to zero. In practice, determining the system stability is essential for operating the control system. The Nyquist plot of the open-loop system provides the stability information of the close-loop system, and provides insight on how to improve the stability. The system is stable if and only if the Nyquist plot of $\mathbf{G}(j\omega)\mathbf{H}(j\omega)$ does not cross or encircle $(-1, 0)$. However, a stable system can become unstable in the presence of perturbations. The ability of the system to withstand perturbations is defined by stability margins (e.g. gain margin, phase margin, and modulus margin) in a single-input and single-output (SISO) control system as shown in Fig. 2.4. The gain margin g_m is the minimum increased gain to make the Nyquist plot of $\mathbf{G}(j\omega)\mathbf{H}(j\omega)$ cross or encircle $(-1, 0)$. The phase margin p_m is the minimum extra phase to make the Nyquist plot cross or encircle $(-1, 0)$. The modulus margin s_m is the minimum distance between $(-1, 0)$ to the Nyquist plot. Practical requirements are $g_m > 2$ and $30^\circ < p_m < 60^\circ$.

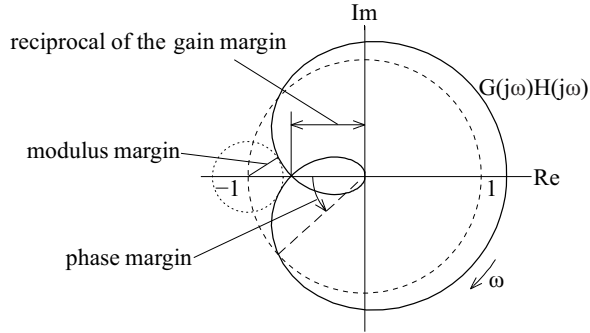


Figure 2.4: Stability margins for a SISO control system.

2.3.3 Generalized Nyquist criterion

The generalized Nyquist criterion can be applied to determine the stability of practical MIMO decentralized control systems [13]. The system is stable if and only if the locus of $\det [\mathbf{I} + \mathbf{G}(j\omega)\mathbf{H}(j\omega)]$ does not cross or encircle the origin $(0, 0)$. On the other hand, in a MIMO system, even a simultaneous change in the gain or phase in all of the loops may change the shape of the locus of $\det [\mathbf{I} + \mathbf{G}(j\omega)\mathbf{H}(j\omega)]$. Therefore, the margins of a MIMO control system give different meanings to the classical definitions. One method to access the classical stability margins in a MIMO system is to use the eigenvalue loci. The eigenvalue loci are the eigenvalues of the frequency response of $\mathbf{G}(j\omega)\mathbf{H}(j\omega)$, which can provide Nyquist plots with the classically defined margins. Nevertheless, these margins are not practically useful since the system is assumed as having a simultaneous and identical change in the gain or phase in all of the loops [119]. Another method is to firstly analyze each individual control loop to govern the stability margins of each single channel. The stability margins of the single channel present the physics and intrinsic limitations of the sensor-actuator feedback loop. And the maximum control gain of each individual control unit can be found. However, the margins from this analysis cannot guarantee the mutual stability of the multiple control units. Therefore, the next step is to apply the generalized Nyquist stability criterion to prove the stability of the multiple feedback control system with the maximum mutual control gain, which is smaller than the maximum single channel control gain

from each individual control unit [16, 120].

Since the main purpose of determining the stabilities in our work is to compare the noise reduction of various control strategies, this thesis applies simple but relatively fair stability criteria. The gain stability index, phase stability index, and modulus stability index in a MIMO system are defined as the stability margins of the locus of $\det[\mathbf{I} + \mathbf{G}(j\omega)\mathbf{H}(j\omega)]$. The gain stability index is the minimum increased gain to make the locus of $\det[\mathbf{I} + \mathbf{G}(j\omega)\mathbf{H}(j\omega)]$ cross or encircle $(0, 0)$. The phase stability index is the minimum extra phase to make the mentioned locus cross or encircle $(0, 0)$. The modulus stability index is the minimum distance between $(0, 0)$ to the mentioned locus. These three stability indexes are shown in Fig. 2.5. Although these indexes are different to the classical margins in a SISO system, they can provide us with approximations of control stability margins.

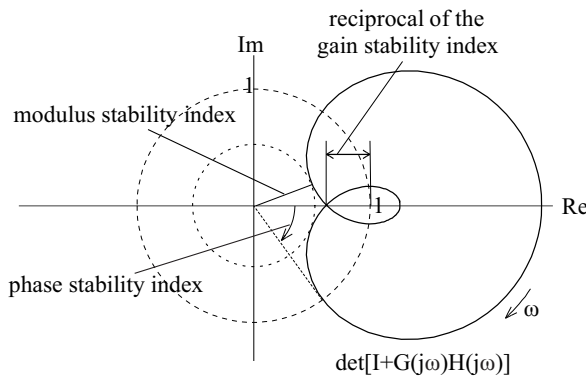


Figure 2.5: Stability indexes for a MIMO control system.

2.3.4 Collocated sensor-actuator control pairs

Direct velocity feedback (DVFB) control may be considered as the simplest method of active damping control [68], which aims to reduce the vibration of the structure by directly feeding the measured signal from a velocity sensor with a fixed gain to a force actuator. DVFB control can provide active damping to the structure without a model of the structure. Moreover, while DVFB control is very simple, it can be unconditionally stable if collocated sensor-actuator pairing is used. A collocated sensor-actuator pair indicates that the sensor and

actuator are physically located at the same position and energetically conjugated, such as a force actuator with a displacement/velocity/acceleration sensor. This stability is unconditionally guaranteed for any position of a sensor-actuator pair in the structure and for any disturbance to the system [71]. An example of a DVFB control system with a collocated sensor-actuator control pair is shown in Fig. 2.6.

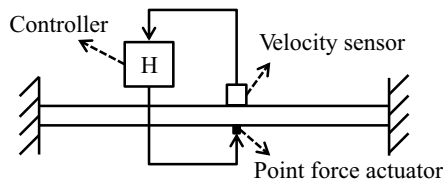


Figure 2.6: A DVFB control system with a collocated sensor-actuator control pair.

In theory, the unconditional stability means the control gain can be increased infinitely to decrease the error signals to zero providing zero residual vibration. While a pair of collocated sensor-actuators guarantees the alternative pole/zero pattern in both SISO and MIMO systems, a flipped pole/zero pattern may exist when non-collocated sensor-actuator pairs are used [68, 121]. In frequency responses, the poles correspond to the resonance frequencies and the zeros correspond to the anti-resonance frequencies. Figure 2.7 presents a bode plot of a collocated velocity sensor response to a point force actuator. A resonance frequency leads to a 180° phase lag and an anti-resonance frequency leads to a 180° phase lead. The unconditional stability of a collocated DVFB control is the consequence of the alternative pole/zero pattern, which ensures the phase response is always between -90° and 90° as shown in Fig. 2.7. Furthermore, this collocated stability concept in structure control has been extended to active noise control systems [122]. As collocated sensor-actuator pairs are not always available in practical applications, the limitations of using non-collocated sensors and actuators has been studied [67, 123]. Regardless, collocated sensors and actuators should be used in DVFB control whenever possible.

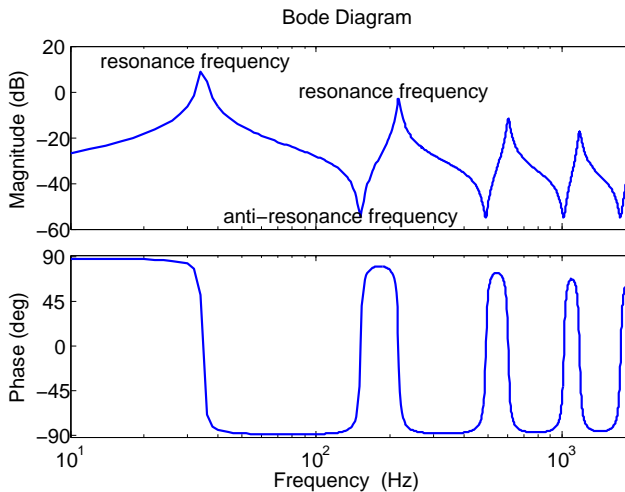


Figure 2.7: Bode plot of a collocated sensor-actuator control pair.

2.4 Adaptive control

Adaptive control provides a control system with time-varying parameters, which are altered to minimize the mean-square error. Therefore, by iteratively adjusting the coefficients of the controller, adaptive control uses fewer calculations per sample than directly computing the optimal coefficients in one step. Moreover, since the adaptive control adjusts its coefficients in response to each new data, it can potentially control a non-stationary system, which may be caused by changes in the primary noise. This section introduces two adaptive control algorithms applied to our system.

2.4.1 Steepest-descent algorithm

Assuming there are L error sensors and M actuators, \mathbf{e} is defined as the $M \times 1$ -dimensional vector of error signals, \mathbf{G} is the $L \times M$ -dimensional plant transfer function, and \mathbf{u} is the $M \times 1$ -dimensional vector of control signals. The steepest-descent algorithm adjusts the control signals iteratively to minimize the sum of squared errors $J = \mathbf{e}^H \mathbf{e}$.

The steepest-descent adaptation rule for the controller is

$$\mathbf{u}(n+1) = \mathbf{u}(n) - \mu \left(\frac{\partial J}{\partial \mathbf{u}_R(n)} + j \frac{\partial J}{\partial \mathbf{u}_I(n)} \right), \quad (2.10)$$

where μ is the convergence factor and $\mathbf{u}_R(n)$ and $\mathbf{u}_I(n)$ are the real and imaginary parts of the control signals at the n -th iteration. The steepest-descent algorithm subtracts the vector proportional to the derivative of the cost function with respect to the control signals from the control signals to derive the adapted control signals at the next iteration. If the error signals reach the steady-state value at each iteration, the error signals at the n -th iteration can be written as

$$\mathbf{e}(n) = \mathbf{d} + \mathbf{G}\mathbf{u}(n). \quad (2.11)$$

Using Eqs. (2.4) and (2.11), the steepest-descent adaptive method given in Eq. (2.10) can be written as

$$\mathbf{u}(n+1) = \mathbf{u}(n) - \alpha \mathbf{G}^H \mathbf{e}(n), \quad (2.12)$$

where $\alpha = 2\mu$ is the final convergence coefficient. To guarantee a stable control system, the control effort weighting factor can be included by replacing the cost function with $J = \mathbf{e}^H \mathbf{e} + \beta \mathbf{u}^H \mathbf{u}$. Equation (2.12) with the control effort weighting factor is written as

$$\mathbf{u}(n+1) = (1 - \alpha\beta)\mathbf{u}(n) - \alpha \mathbf{G}^H \mathbf{e}(n). \quad (2.13)$$

If there are modelling errors or plant uncertainties, the estimated plant model $\hat{\mathbf{G}}$ can be used to adjust the control signals, then the control signals become

$$\mathbf{u}(n+1) = (1 - \alpha\beta)\mathbf{u}(n) - \alpha \hat{\mathbf{G}}^H \mathbf{e}(n). \quad (2.14)$$

2.4.2 Regularized modified filtered-error LMS algorithm

Our work uses another adaptive algorithm, which is called regularized modified filtered-error least mean square (RMFeLMS) algorithm. The least mean square (LMS) algorithm provides the advantages of low complexity and relatively good robustness. However, the LMS does not guarantee a rapid convergence. To improve the convergence properties of the adaptive controller, the RMFeLMS eliminates the inherent delay in the adaptive path by using an inner-outer factorization of the transfer path between the actuators and the error sensors. Double control filters combined with a regularization technique

(which can preserve the factorization properties) are used for compensating the delay. Compared to the standard filtered-reference and filtered-error algorithm, RMFeLMS has good convergence properties. A detailed RMFeLMS algorithm description can be found in [124, 125]. A block diagram of the adaptive MIMO RMFeLMS scheme, where the dashed line indicates the controller, is shown in Fig. 2.8. Assuming there are K reference signals, L error sensors and M actuators. \mathbf{P} , the primary model, is the $L \times K$ -dimensional transfer function between the reference signals and the error signals; \mathbf{d} is the $L \times 1$ -dimensional vector of the primary noise source. \mathbf{G} , the plant model, is the $L \times M$ -dimensional transfer function between the actuators and the error sensors. \mathbf{W} is the $M \times K$ -dimensional control filter and \mathbf{D} represents a delay operator. The $(L + M) \times M$ -dimensional augmented plant $\bar{\mathbf{G}}$ consists of \mathbf{G} and a $M \times M$ -dimensional regularization function \mathbf{G}_{reg} to avoid saturated control signals. To improve the convergence and to ensure stability, an $L \times M$ -dimensional all-pass function $\bar{\mathbf{G}}_i$ and $M \times M$ -dimensional minimum phase function $\bar{\mathbf{G}}_o$ are used to perform the inner-outer factorization, where $\bar{\mathbf{G}} = \bar{\mathbf{G}}_i \bar{\mathbf{G}}_o$, $\bar{\mathbf{G}}_o^{-1}(q) \bar{\mathbf{G}}_o = \mathbf{I}_L$, in which q is the unit delay operator and \mathbf{I}_L is the identity matrix of dimensions L , and $\bar{\mathbf{G}}_i^*(q) = \bar{\mathbf{G}}_i^T(q^{-1})$, where T denotes the transpose. Internal model control (IMC) can be realized by subtracting the contribution of the secondary sources on the reference signals, where the $K \times M$ -dimensional transfer function is \mathbf{G}_{rp} and the $K \times 1$ -dimensional vector

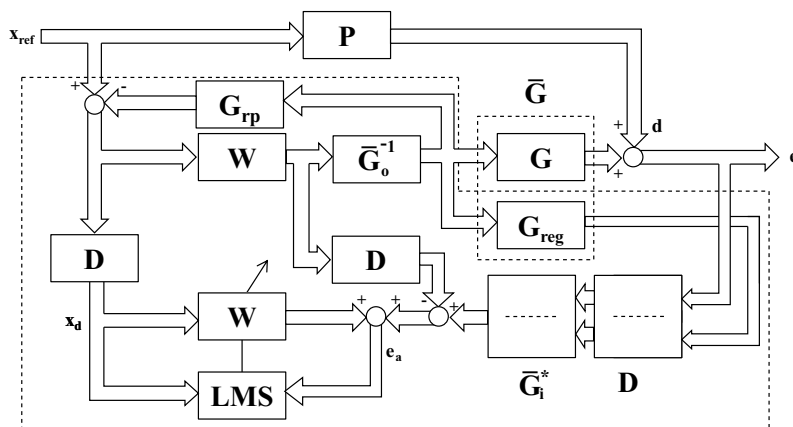


Figure 2.8: Regularized modified filtered-error adaptive least mean square (RMFeLMS) control scheme with IMC.

of reference signals is \mathbf{x}_{ref} [54,57]. The adaptation rule for the controller based on the LMS algorithm is obtained as

$$\mathbf{W}_i(n+1) = \mathbf{W}_i(n) - \alpha \mathbf{e}_a(n) \mathbf{x}_d(n-i), \quad (2.15)$$

where $\mathbf{W}_i(n)$ is the i -th filter at the n -th iteration, \mathbf{e}_a is the $M \times 1$ -dimensional vector of auxiliary error signals, α is the convergence coefficient and \mathbf{x}_d is the $K \times 1$ -dimensional vector of delayed reference signals.

2.5 Conclusions

In this chapter, a description is given of control strategies and their operating principles as they apply to our system. Stability is an essential requirement for the control system. Methods to determine and improve the stability are given as follows. (1) The control effort weighting factor can improve the stability of a feed-forward control system. (2) The Nyquist criterion can determine the stability of a SISO feedback control system. (3) The generalized Nyquist criterion can be used to determine the stability of a MIMO feedback control system. Moreover, DVFB control can be unconditionally stable if collocated sensor-actuator pairing is used. If the reference signal for a feed-forward controller is not available, applying IMC can reformulate a feedback controller into a equivalent feed-forward controller. Furthermore, two adaptive algorithms are given. (1) The steepest-descent algorithm adjusts the control parameters to minimize the sum of squared errors. (2) The RMFeLMS algorithm uses regularization and an inner-outer factorization technique to provide an adaptive algorithm with low complexity, good robustness and good convergence.

Finite element method model and experimental setup

This chapter is based on:

J. H. Ho and A. Berkhoff, "Comparison of various decentralised structural and cavity feedback control strategies for transmitted noise reduction through a double panel structure," Journal of Sound and Vibration, vol. 333, no. 7, pp. 1857–1873, 2014.

3.1 Introduction

This chapter describes our numerical model, assumptions, experimental setup and model validation. First, a finite element method model including both acoustic and structural properties is introduced. The near field sound pressure is related to the kinetic energy of the radiating panel at lower modes [122]. A minimum amount of sensors was found to provide precise estimation of the panel's kinetic energy. Moreover, an equivalent piezoelectric load equation, which is used to simplify the model, is given. Then a detailed experimental setup is described. Finally, the model validation, where we excited the system with a piezoelectric patch and validated the kinetic energy response of the radiating panel, is presented.

3.2 Structural-acoustic coupled model

We use the finite element method (FEM) with the COMSOL Multiphysics 4.3b (COMSOL, Inc., Burlington, MA 01803, USA) to model and analyze the characteristics of our system. To accurately model the system, the acoustic and structural properties must be considered simultaneously. Moreover, the interactions between the properties should be applied to both sides to achieve a

more accurate result. Therefore, there are two domains in our model: the fluid domain and the solid domain. The relationship of the acoustic pressure in the fluid domain to the structural deformation in the solid domain is linked as described below. In the solid domain, the pressure load (normal force per unit area) on the structure \mathbf{F}_p [N m^{-2}] produced by the fluid pressure p_a [Pa] on the fluid-solid interacting boundaries is given by

$$\mathbf{F}_p = -\mathbf{n} \cdot p_a, \quad (3.1)$$

where \mathbf{n} is the normal vector of the solid boundaries. In the acoustic fluid domain, the normal acceleration to the acoustic pressure a_n [m s^{-2}] on the fluid-solid interacting boundaries can be derived from the second derivatives of the structural displacements with respect to time \mathbf{u}_{tt} [m s^{-2}]:

$$a_n = \mathbf{n} \cdot \mathbf{u}_{tt}. \quad (3.2)$$

By applying Eqs. (3.1) and (3.2), the interaction between the acoustic field and solid structure can be investigated. The resonant behavior and sound transmission of a double panel structure are investigated based on the model shown in Fig. 3.1. A spherical incident pressure wave acts as the primary noise source. To produce an asymmetric incident noise wave, this wave is generated from the bottom corner of the source cavity. This primary noise source from the source cavity first enters an aluminum panel (the incident panel), then a 35-mm-thick

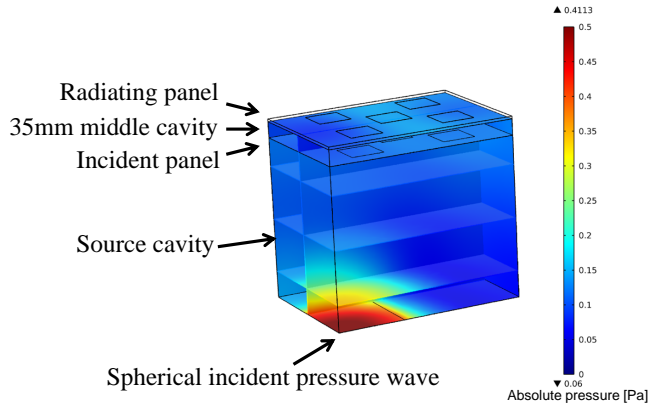


Figure 3.1: Structural-acoustic interaction model.

layer of air (the middle cavity), followed by a honeycomb panel (the radiating panel). These two panels are simply supported. Furthermore, high absorbing materials are applied to the surface of the source cavity to reduce the resonant energy from the source cavity. The detailed model parameters are provided in Table 3.1.

3.3 Near field sound pressure

The energy of the near field sound pressure wave is related to the kinetic energy of the radiating panel at lower modes [122]. Figure 3.2 shows the near field sound pressure wave from the radiating panel of the double panel structure. Directly calculating the near field sound pressure requires more computation than calculating the kinetic energy of the radiating panel. Therefore, to analyze the control performance of various control strategies, we use the kinetic energy of the radiating panel to represent the near field sound. Although the surface mass density affects the ratio of the kinetic energy of the radiating panel to the radiated sound pressure above the radiating panel, all the kinetic energy frequency response in the current work is obtained from the same honeycomb material, which means the ratio is fixed. Moreover, the current work presents

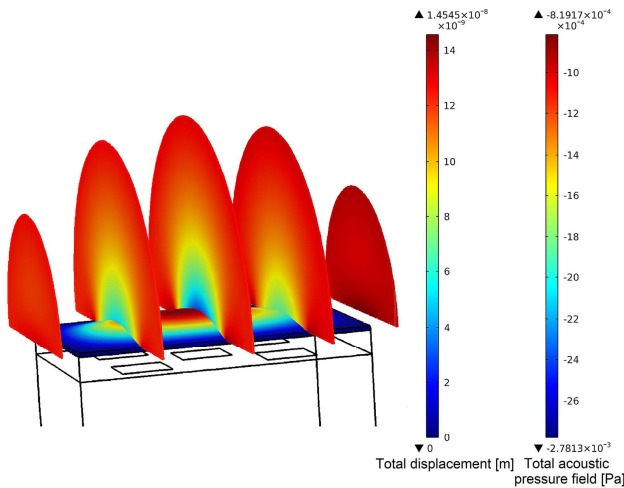


Figure 3.2: Near field sound pressure wave from the radiating panel.

Table 3.1: Model parameters.

Parameters	Values	Unit
Dimensions		
1. Validation model		
Aluminum panel (incident panel)	420 * 297 * 1	[mm ³]
	420 * 297 * 2	[mm ³]
2. Controlled analysis model		
Density	2700	[kg m ⁻³]
Young's modulus	70	[GPa]
Poisson's ratio	0.33	
Loss factor	0.03	
Honeycomb panel (radiating panel)		
Dimensions		
Density	420 * 297 * 5.8	[mm ³]
Young's modulus	409	[kg m ⁻³]
Poisson's ratio	3.7	[GPa]
Loss factor	0.33	
	0.03	
Piezoelectric patches		
Dimensions		
Density	72.4 * 72.4 * 0.264	[mm ³]
Young's modulus	7800	[kg m ⁻³]
Poisson's ratio	52	[GPa]
Strain coefficient d ₃₁	0.33	
	-190	[m V ⁻¹]
Source cavity		
Inner dimensions		
High absorbing surface, acoustic impedance	420 * 297 * 350	[mm ³]
	1000	[Pa s m ⁻¹]
Middle cavity		
Inner dimensions		
Rigid boundary	420 * 297 * 35	[mm ³]

the transmitted noise reduction comparison of various control strategies applied to the same double panel structure. We compared the structure's near field sound pressure, which can be represented by the kinetic energy of the radiating panel. Therefore, the far field radiation efficiency of the radiating panel does not affect the presented comparison results. However, to fully present the controlled results of various control methods, the sound pressure level at 10 cm above the radiating panel surface and the radiated sound power level of the radiating panel are given in Sections 4.4 and 5.2.

3.4 Kinetic energy estimation

As mentioned above, we used the kinetic energy of the radiating panel to represent the near field sound pressure from the panel. The measured kinetic energy of the panel was derived from the sensors on the panel. These sensors were equally distributed on the panel. We used the average velocity of these sensor points to calculate the kinetic energy of the panel. Therefore, more sensor points can improve the accuracy of the kinetic energy estimate, particularly for the higher vibration modes. However, in practice, the number of detecting sensors is limited. The required number of sensors depends on the mode shape complexity of the panel. To guarantee the accuracy of our kinetic energy estimate and to avoid estimation errors because of an insufficient number of sensors, we first compared the accuracy of various sensor numbers using the FEM model. A panel was excited by an incident acoustic wave, and the kinetic energy estimates for this panel from 1, 2, 4, 5, 9, 16, and 25 velocity sensor points were compared with the integral kinetic energy of the entire panel. To provide an accurate approximation of the panel response, the distance between two adjacent monitoring positions should be smaller than half a bending wavelength of the panel. The bending wave speed of the radiating panel was 259 m s⁻¹ and the half bending wavelength of the panel was 6.5 cm at the maximum frequency 2 kHz. The panel model was divided up into 1718 elements and the distance between two adjacent positions was less than 15 mm, which is smaller than the half bending wavelength of the panel. Figure 3.3 shows the kinetic energy frequency response of the panel from 10 Hz to 2 kHz. At each frequency, the error is the absolute difference in dB between the estimated kinetic energy and real kinetic energy. We average all of these errors to obtain the estimation error, which is shown in Table 3.2 for the various sensor results. These results show that using only one sensor on the panel is insufficient for obtaining a correct estimate because a single sensor cannot present the characteristics of any

mode shape that is higher than the first mode, such as (2, 1), (1, 2), and (2, 2). However, below 1 kHz, the estimated kinetic energy from 5 and 9 velocity sensor points can precisely match the integral kinetic energy. Therefore, we can use the average velocity from 5 or 9 sensors to estimate the kinetic energy of the entire panel. In our model validation, the measured kinetic energy was derived from 9 sensors on the panel. In our real-time control, we used 5 sensors, which were the error sensors in the feedback control loop, to derive the kinetic energy of the panel.

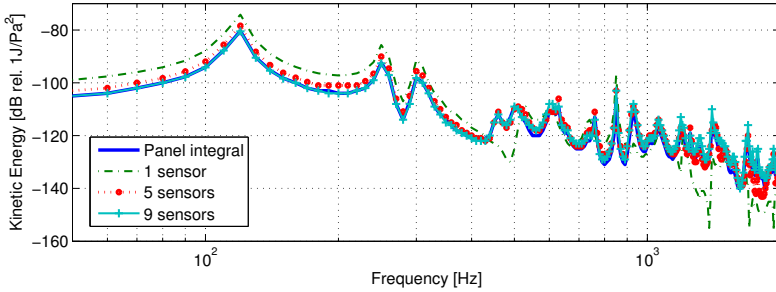


Figure 3.3: Kinetic energy numerical analysis of the radiating panel derived from different numbers of sensor points.

Table 3.2: Kinetic energy difference.

Sensor number(s)	Average difference of kinetic energy[dB] (Average(abs(10 log ₁₀ (ΣKE _{sensors} /ΣKE _{panel integral}))))						
	1	2	4	5	9	16	25
10 Hz–500 Hz	6.622	3.982	0.989	1.739	0.145	0.017	0.030
10 Hz–1 kHz	6.064	4.810	1.500	2.037	1.073	0.200	0.059
10 Hz–2 kHz	7.121	5.512	2.157	2.277	1.879	0.884	0.513

3.5 Equivalent piezoelectric load

In the current work, piezoelectric patches are applied for the structural control. Piezoelectric materials offer the advantages of rapid response and compact dimensions. The equivalent piezoelectric load equation for laminar piezoelectric actuators is adopted to simplify the model, where the piezoelectric force can be represented as line moments on the edges of the piezoelectric patch shown in Fig. 3.4 [71]. The line moment is given by

$$M_p = -E_p d_{31} h V, \quad (3.3)$$

where M_p [N] is the moment per unit length, E_p [GPa] is the Young's modulus of the piezoelectric patch, d_{31} [m Volt⁻¹] is the piezoelectric strain coefficient, h [m] is the distance between the mid-plane of the piezoelectric patch and the mid-plane of the panel, and V [Volt] is the control voltage applied to the patch. In our numerical analysis, the control load from each piezoelectric patch is applied as four line moments on the panel.

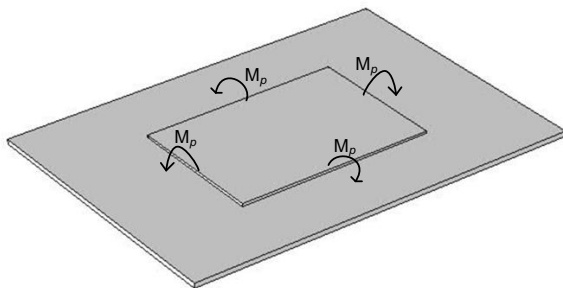


Figure 3.4: Four line moments represent the equivalent piezoelectric load for a laminar piezoelectric actuator.

3.6 Experimental setup

Figure 3.5 shows our experimental setup. The double panel is mounted on a rectangular box, which is referred to as the source cavity. A loudspeaker in the bottom of the rectangular box generated the primary noise. The kinetic energy of the radiating panel can be derived by measuring the velocity of this panel.

The structural control sets on the radiating panel (five piezoelectric actuators and five acceleration sensors) are shown in Fig. 3.6. Furthermore, this box was constructed with 40-mm-thick walls of acrylic plates to prevent the sound from leaking through the side walls. Although we provide only the kinetic energy results, the transmitted sound was also measured by locating a microphone above the top panel.

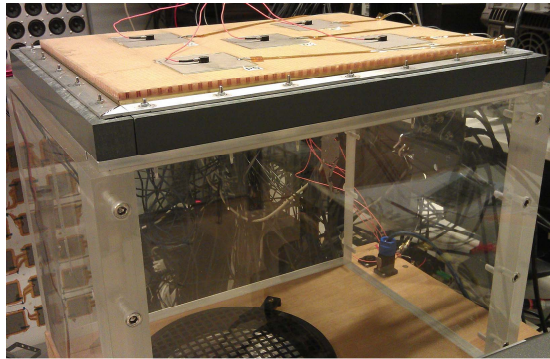


Figure 3.5: Experimental setup for real-time control.

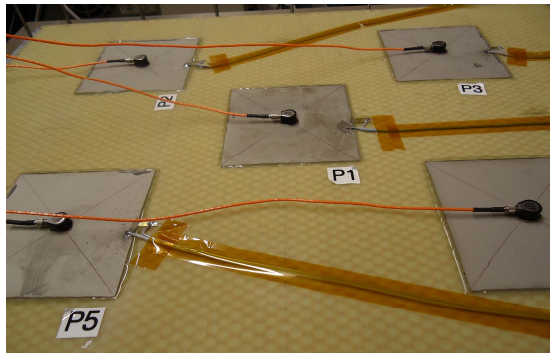


Figure 3.6: Five sensor-actuator pairs on the radiating panel.

3.7 Model validation

To validate our numerical model, a kinetic energy response comparison between the simulation and experiment was performed. We used the kinetic energy response of the radiating panel, whereas there was an excitation force on the radiating panel (the honeycomb panel). Figure 3.7 shows the experimental setup for our model validation. One piezoelectric patch was attached to the honeycomb panel to apply the excitation force. Then, we measured the acceleration of the panel from nine positions to derive the panel's kinetic energy, which is based on the panel integration of the acceleration, and compared the result with that from the numerical simulation, as shown in Fig. 3.8. The figure shows that the numerical model can sufficiently accurately predict the practical sensor-actuator response in a single panel structure for our purpose. To further validate the double panel interaction result, we added another panel below the radiating panel with a 35-mm-thick air gap to change the structure into a double panel structure. This second panel was a 1-mm-thick aluminum panel, which has a high resonance density. The excitation force was only applied on the radiating panel. Figure 3.9 shows that the number of resonance peaks of the double panel structure increases because of the resonance contributions from the incident panel and cavity. However, the numerical model can estimate the practical sensor-actuator response in a double panel structure with reasonable error. The 1-mm-thick aluminum panel with a high resonance density was chosen to obtain a more complex response object to compare with our numerical model. However, because of the concern for control stability, instead of the 1-

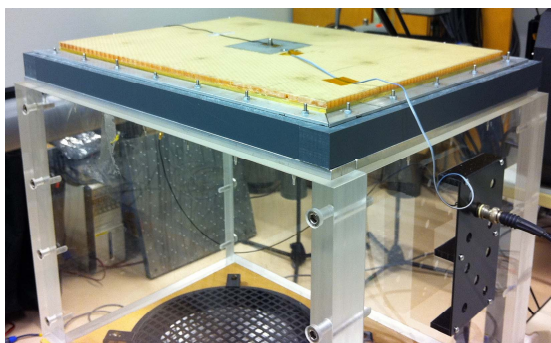


Figure 3.7: Experimental setup for model validation.

mm-thick aluminum panel, a 2 mm-thick aluminum panel was attached to the double panel structure for subsequent analysis and experiments.

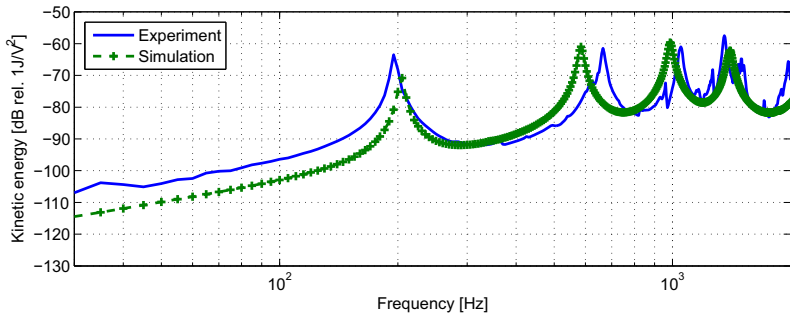


Figure 3.8: Experimental and simulated kinetic energy response of the radiating panel: the single panel structure.

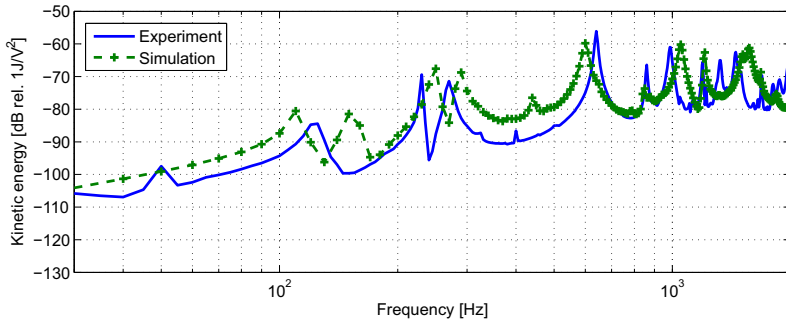


Figure 3.9: Experimental and simulated kinetic energy response of the radiating panel: the double panel structure.

3.8 Conclusions

In this chapter, the details of our numerical model and experimental setup are described. A structural-acoustic coupled FEM model, which can sufficiently accurately predict the interactions between the structure vibration and acoustic wave propagation for our purpose, has been developed and validated. The kinetic energy of the radiating panel is used to represent the structure's near field sound pressure in our study. A minimum amount of 5 sensors has been found to accurately estimate the kinetic energy of our entire radiating panel from 10 Hz to 2 kHz.

Structural, cavity, and combined control

This chapter is based on:

J. H. Ho and A. Berkhoff, "Comparison of various decentralised structural and cavity feedback control strategies for transmitted noise reduction through a double panel structure," Journal of Sound and Vibration, vol. 333, no. 7, pp. 1857–1873, 2014.

4.1 Introduction

In this chapter, we present the results of applying structural control, cavity control, and structural-cavity combination control to the double panel structure. First, we applied piezoelectric patches on the incident panel and radiating panel to control the structure. The limitation of the structural control was analyzed, and the real-time structural control was measured to prove our conclusions obtained from the numerical analysis. Next, we analyzed the cavity control using acceleration source loudspeakers as the cavity sources. Finally, we combined these two methods, which is referred to as the structural-cavity combination control, and compared the various control methods to find the most effective strategy for the transmitted noise reduction.

4.2 Feedback structural control

Two simply supported panels with a 35-mm-thick air gap comprised the double panel structure. The incident panel was a 2-mm-thick aluminum panel, and the radiating panel was a 5.8-mm-thick honeycomb panel. The parameter details are listed in Table 3.1. In the structural control case, an analysis is given of five piezoelectric patches attached to each panel as shown in Fig. 4.1.

On each piezoelectric patch, there is one collocated acceleration sensor that functions as the error sensor for the velocity feedback control system.

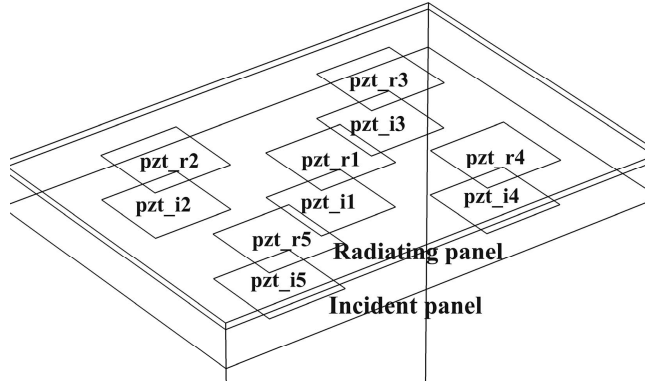


Figure 4.1: Control sets on the panels.

4.2.1 Radiating and incident panel control

Table 4.1 lists the Nyquist plots for the following structure-controlled cases. As described in Section 2.3.3, a MIMO control system is stable if and only if the locus of $\det [\mathbf{I} + \mathbf{G}(j\omega)\mathbf{H}(j\omega)]$ does not cross or encircle the origin $(0, 0)$. Since the accelerometer and the piezoelectric patch were neither dual nor collocated, the feedback loop was not unconditionally stable. The system therefore included a low-pass filter with a cut-off frequency of 1 kHz to prevent instability at higher frequencies. Zoomed figures around the origin are listed in the table to confirm the system stability. In the first and second plots, only the incident panel was controlled with control gain 800. In the third and fourth plots, only the radiating panel was controlled with control gain 330. The plots show that with the low-pass filter, the stability was improved at higher frequencies. Moreover, because these plots do not encircle or cross the origins, the stability of the system is guaranteed.

The control performance of these two cases without and with the low-pass filter is shown in Figs. 4.2 and 4.3. Figure 4.3 shows that the low-pass filter does not weaken the control performance. Moreover, although controlling the radiating panel can effectively reduce the near field sound in a single panel

Table 4.1: Numerical analysis of panel control positions, locus of $\det[\mathbf{I} + \mathbf{G}(j\omega)\mathbf{H}(j\omega)]$ from 10 Hz to 20 kHz: from 10 Hz to 1 kHz (blue solid lines) and from 1 kHz to 20 kHz (green dotted lines).

Control position	Locus of $\det[\mathbf{I} + \mathbf{G}(j\omega)\mathbf{H}(j\omega)]$	Zoomed around (0, 0)
Incident panel		
Incident panel with the low-pass filter		
Radiating panel		
Radiating panel with the low-pass filter		

structure, it cannot reduce all of the resonance peaks in a double panel structure. For instance, for the first few resonance peaks, only the second and fourth peaks can be reduced by controlling the radiating panel. However, the first and third peaks were barely reduced. In contrast, the first and third peaks can be significantly reduced by controlling the incident panel, but the second and fourth peaks were barely reduced.

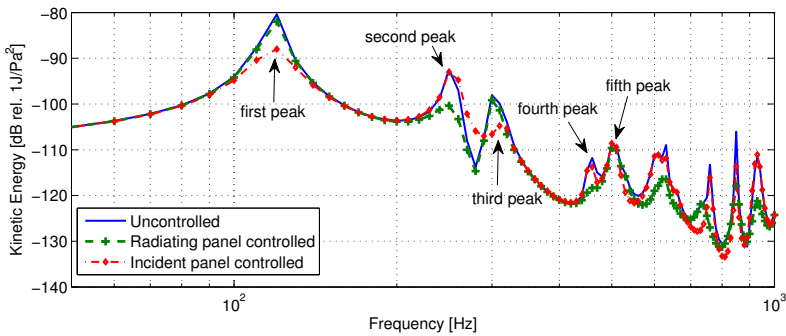


Figure 4.2: Simulated kinetic energy response of the radiating panel with panel control.

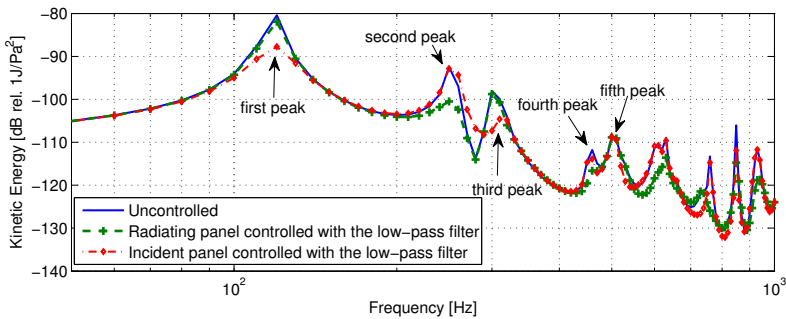


Figure 4.3: Simulated kinetic energy response of the radiating panel with low-pass filtered panel control.

4.2.2 Resonant modes analysis

In the double panel structure, there is a major drop of the sound transmission loss, where the sound transmission loss can even be less than that of a single panel structure. This particular frequency is referred to as the mass-air-mass frequency, where the two panels have anti-phase motion and the air acts as a spring [3]. The calculated mass-air-mass resonance frequency for unbounded panels is 256 Hz in this case, while the resonance frequency at 250 Hz is shown in our FEM simulation result. To further describe the difference, the uncontrolled resonant mode shapes of the panels and the uncontrolled acoustic pressure distribution in the cavity are shown in Table 4.2. The mode shapes show that the first and third resonance frequencies are dominated by the resonant modes of the incident panel. Conversely, the second and fourth resonance frequencies mainly result from the radiating panel. Furthermore, the fifth resonance peak at 500 Hz is dominated by the acoustic resonance of the cavity. Table 4.3 shows the mode shapes of the radiating panel with various structural control methods. From these results, we can observe that the peaks that are dominated by the incident panel resonant modes (120 Hz and 300 Hz) can be effectively reduced by applying the incident-panel piezoelectric actuators. In contrast, the peaks that are dominated by the radiating panel resonant modes (250 Hz and 460 Hz) can be effectively reduced by applying the radiating-panel piezoelectric actuators. Thus, all of the structure-dominated resonance peaks can be reduced when the radiating panel and incident panel are controlled, as shown in the last row of Table 4.3. The control gain for both controlled-panel cases should be readjusted to ensure the stability of the system. The Nyquist plot is shown in Table 4.4, where the control gains for the incident panel and radiating were 500 and 300, respectively. In the second plot, the low-pass filter was applied. Figure 4.4 shows the control performance when both panels were controlled and shows the low-pass filter does not weaken the control performance. Although all of the structure-dominated resonance peaks can be reduced, the size of this reduction decreased. Because of the interference between these two panels, the control gain of both panels was limited. Therefore, the reduction of these resonance peaks was limited. Furthermore, the result shows that although controlling the two panels can reduce most of the resonance peaks, which also include the mass-air-mass resonance frequency, it can barely reduce the resonance peak at the cavity-dominated resonance frequency (500 Hz).

Table 4.2: Simulated mode shapes of the uncontrolled system.

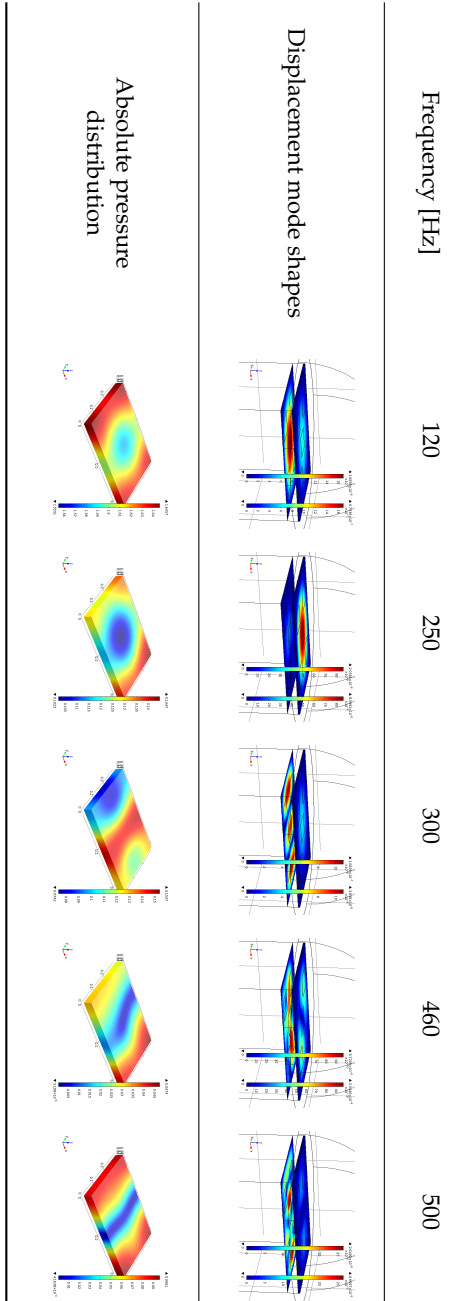


Table 4.3: Simulated mode shapes of the radiating panel with various structural control methods.

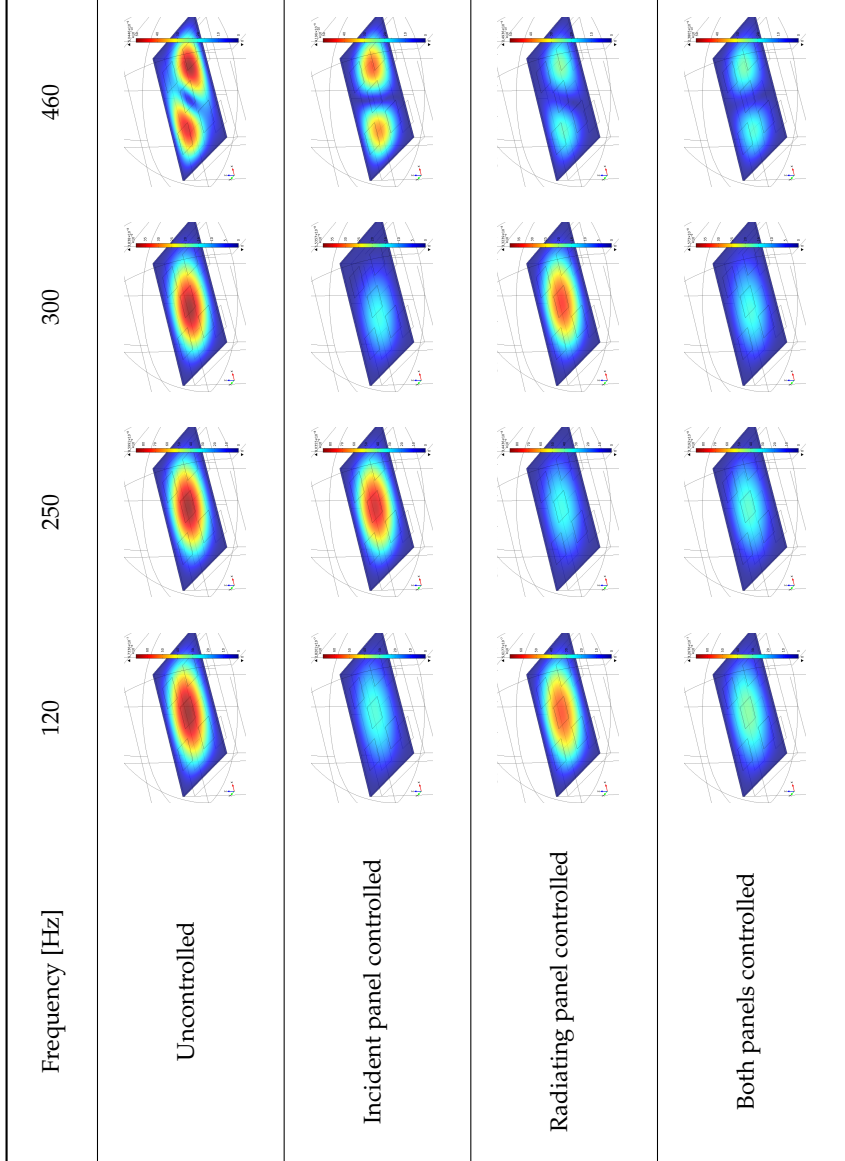


Table 4.4: Numerical analysis of both panels controlled, locus of $\det[\mathbf{I} + \mathbf{G}(j\omega)\mathbf{H}(j\omega)]$ from 10 Hz to 20 kHz: from 10 Hz to 1 kHz (blue solid lines) and from 1 kHz to 20 kHz (green dotted lines).

Control position	Locus of $\det[\mathbf{I} + \mathbf{G}(j\omega)\mathbf{H}(j\omega)]$	Zoomed around (0, 0)
Both panels controlled		
Both panels controlled with the low-pass filter		

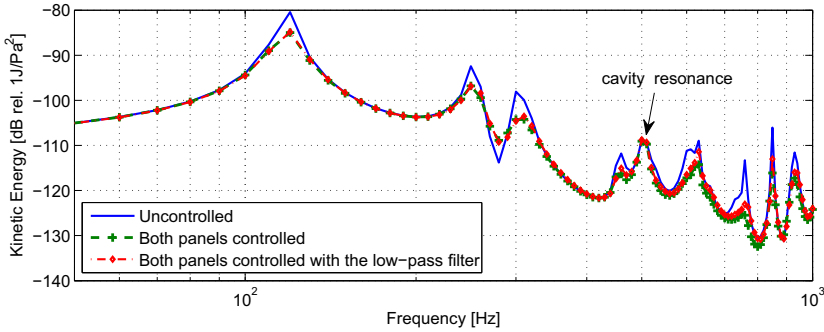


Figure 4.4: Simulated kinetic energy response of the radiating panel with both panels controlled.

4.2.3 Real-time control

To further support the conclusions of the numerical analysis, a real-time structural control measurement was performed. First, we applied the structural control to a single panel structure, whereby five piezoelectric actuators were attached to the panel. The excitation noise source was the acoustic pressure produced by a loudspeaker. The control result indicated that the structural control could effectively reduce the resonant energy in the single panel structure (Fig. 4.5). Next, we added a second panel (the incident panel) under the first panel (the radiating panel) with an air layer between the panels to change the system into a double panel structure. The structural control was only applied to the radiating panel, and the control result is shown in Fig. 4.6. The figure shows that controlling only the radiating panel in a double panel structure can only reduce certain peaks instead of all of the resonance peaks because these resonance peaks were not only determined by the resonant modes of the radiating panel. This result agreed with our numerical analysis. The resonance frequencies of a double panel structure result from not only the radiating panel but also the incident panel. Therefore, both panels should be controlled simultaneously in a double panel structure. Nevertheless, resonant energy also emerges from the cavity, such as the frequency at 500 Hz. This resonant energy can be barely reduced by adding active damping to the structure. This limitation of the structural control should be considered in the system design.

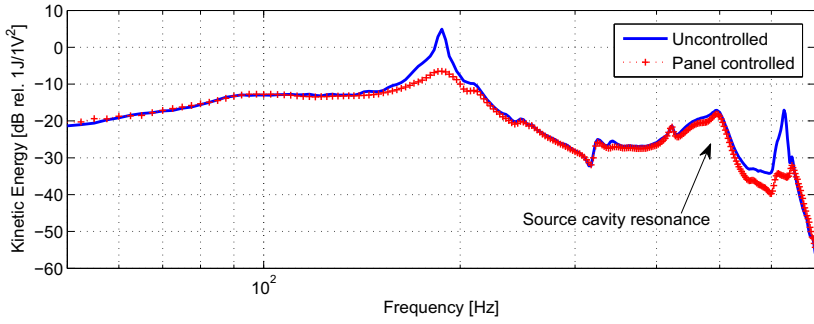


Figure 4.5: Experimental kinetic energy response of the radiating panel: single panel control result.

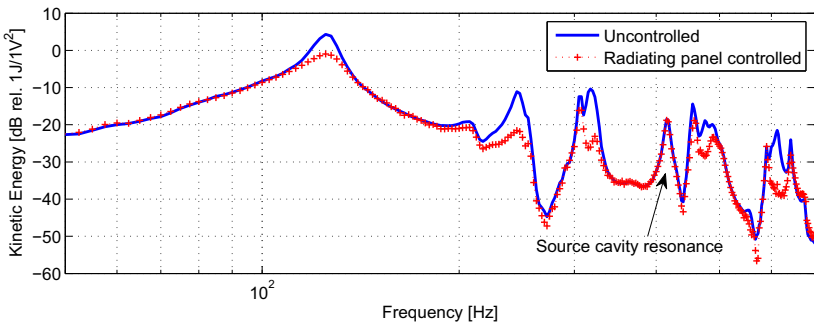


Figure 4.6: Experimental kinetic energy response of the radiating panel: double panel control result.

4.3 Feedback cavity control

The previous section has shown that applying direct velocity feedback control to the structure cannot effectively control the cavity-dominated resonance in a double panel structure. To solve this problem, six decentralized cavity controllers were modeled in the middle cavity between the double panels. An analysis is given of six loudspeakers installed in the cavity between these double panels (Fig. 4.7). In front of each loudspeaker, there is one microphone that functions as the error sensor for the feedback control system. The microphone positions are the circles marked with red in Fig. 4.7. The loudspeaker was a dynamic loudspeaker and thus assumed to operate as an acceleration source above the resonance frequency. The Nyquist plot of this MIMO decentralized control system with a control gain of 0.0003 is shown in Table 4.5. In the second plot, a low-pass filter with a cut-off frequency of 1 kHz to prevent instability at higher frequencies was applied to the control system. The locus of $\det[\mathbf{I} + \mathbf{G}(j\omega)\mathbf{H}(j\omega)]$ does not encircle or cross the origin, which guarantees the stability of the control system.

Figure 4.8 shows the control performance without and with the low-pass filter and shows that the low-pass filter does not weaken the control performance. With the cavity control, the kinetic energy can be reduced not only at the structure resonance-dominated frequencies but also at the cavity resonance-dominated frequencies. The result shows that cavity control can provide significant transmitted noise. Therefore, cavity control strategies were further investigated, as discussed in Chapter 5.

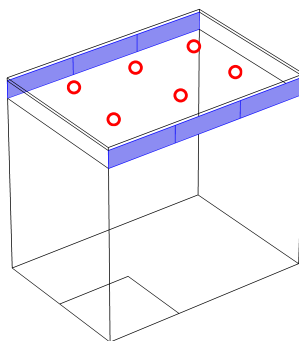


Figure 4.7: Distribution of control sets for cavity control.

Table 4.5: Numerical analysis of panel control positions, locus of $\det[\mathbf{I} + \mathbf{G}(j\omega)\mathbf{H}(j\omega)]$ from 10 Hz to 20 kHz: from 10 Hz to 1 kHz (blue solid lines) and from 1 kHz to 20 kHz (green dotted lines).

Configuration	Locus of $\det[\mathbf{I} + \mathbf{G}(j\omega)\mathbf{H}(j\omega)]$	Zoomed around (0, 0)
Cavity controlled		
Cavity controlled with the low-pass filter		

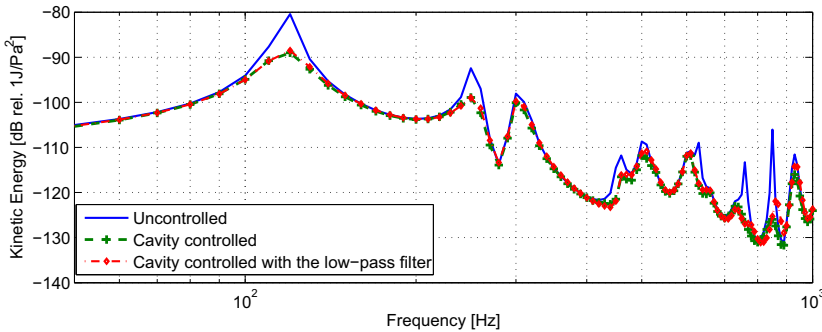


Figure 4.8: Simulated kinetic energy response of the radiating panel with cavity control.

4.4 Feedback combined control and comparisons

To improve the control performance, we applied structural control and cavity control to the system simultaneously, which is referred to as structural-cavity combination control. The stability was guaranteed with a fully coupled plant transfer matrix, in which 16 actuators and 16 sensors were simultaneously considered. All the open loop frequency response functions are computed above the crossover frequency, and every Nyquist plot does not cross or encircle the origin $(0, 0)$. In addition, we compared the control performance of the structural control, cavity control, and combination control based on identical stability indexes. The gain stability index, phase stability index, and modulus stability index in Table 4.6 are defined as the stability margins of the locus of $\det[\mathbf{I} + \mathbf{G}(j\omega)\mathbf{H}(j\omega)]$ from 10 Hz to 1 kHz. An infinity gain margin index means the smallest value at the x-axis of the locus of $\det[\mathbf{I} + \mathbf{G}(j\omega)\mathbf{H}(j\omega)]$ from 10 Hz to 1 kHz is larger than 1. Although the margin indexes from the full frequency spectrum should be considered, since the instability is caused at higher frequencies in practical applications, the stability at higher frequencies can be improved. For example, decreasing the distance between the loudspeaker and the microphone can improve the stability because the phase lag caused by the distance between the sensor and the actuator is decreased substantially, particularly at higher frequencies. Furthermore, the phase crossover frequency, which happens above 1 kHz, of the system is given to provide a complete view of the system.

Table 4.6: Numerical analysis of stabilities, kinetic energy reduction and radiated sound power reduction from 10 Hz to 1 KHz.

Combinations	6 loudspeakers (acc. source*)	10 pzt (inc. and rad. panel*)	6 loudspeakers (acc. source) and 10 pzt (inc. and rad. panel)
Control gain	0.00042	350(inc.);150(rad.)	0.00021(lsp.*);300(inc.);125(rad.)
Gain stability index	Inf.	Inf.	Inf.
Phase stability index	58.7	60.7	-61.0
Modulus stability index	0.87	0.98	0.96
Phase crossover frequency [10 Hz-20 KHz]	10 [KHz]	8841 [Hz]	7818 [Hz]
Total kinetic energy reduction($10 \log_{10}(\frac{\sum KE_{uncontrolled}}{\sum KE_{controlled}})$)[dB]			
	4.9	2.9	4.6
Total radiated sound power reduction($10 \log_{10}(\frac{\sum radiated\ power_{uncontrolled}}{\sum radiated\ power_{controlled}})$)[dB]			
	4.8	2.8	4.6

Abbreviations: acc., acceleration; inc., incident; rad., radiating; lsp, loudspeaker, and inf., infinity.

The controlled results are presented in three plots: the kinetic energy of the radiating panel, the sound pressure level (SPL) at 10 cm above the radiating panel and the radiated sound power level (SWL) of the radiating panel (Figs. 4.9 - 4.11). Moreover, we calculated the total kinetic energy reduction and the total radiated sound power reduction of each control method from 10 Hz to 1 kHz to provide a clearer index of the noise reduction (Table 4.6). The table shows that applying cavity control can reduce more of the radiating panel's kinetic energy and the total radiated sound power than the other two methods. Although the combination control method controls both the structure and cavity, the control gain is limited because of the stability constraint. Therefore, the combination control method cannot provide more noise reduction than the cavity control method.

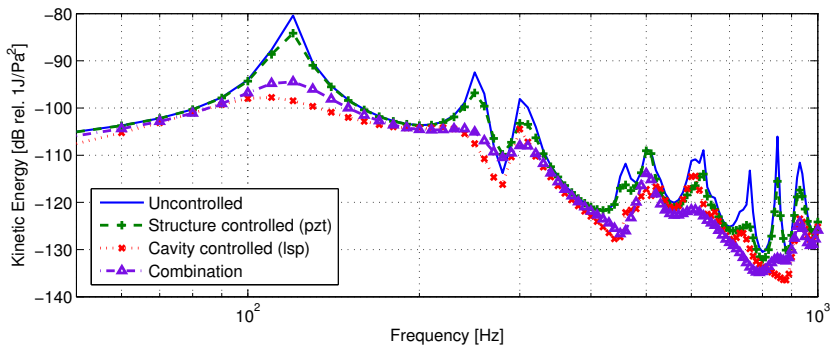


Figure 4.9: Simulated kinetic energy response of the radiating panel with various control methods.

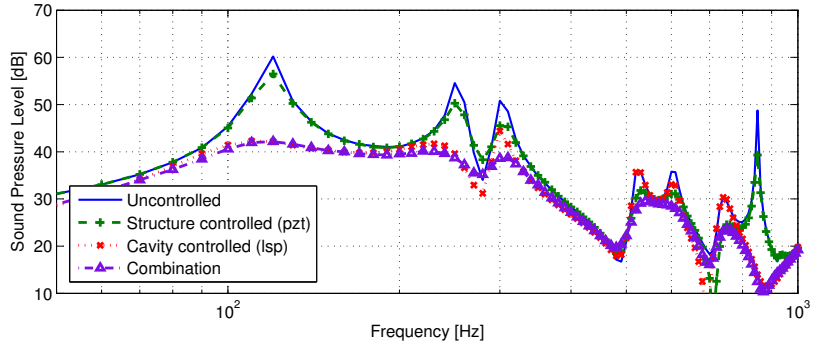


Figure 4.10: Simulated SPL response of the radiating panel with various control methods.

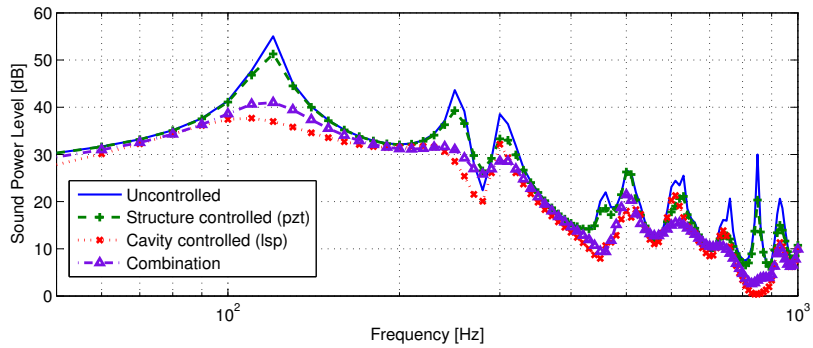


Figure 4.11: Simulated SWL response of the radiating panel with various control methods.

4.5 Conclusions

Various control configurations for reducing the transmitted sound through a double panel structure have been studied. The investigations explain the difficulty of reducing noise by only controlling the radiating panel in a double panel structure. Numerical analysis showed that with direct velocity feedback control, piezoelectric actuators should be simultaneously applied to the incident panel and radiating panel in a double panel structure. This strategy is required because the resonant energy in a double panel structure is not only determined by the radiating panel but also by the incident panel and cavity. Therefore, the structural control should be applied to both panels. However, the interaction between the two panels reduces the control stability and limits the control performance. Moreover, structural control can barely reduce the resonant energy, which is dominated by the cavity resonance. Similar conclusions have been obtained from experimental results.

To further improve the control performance, various combinations of structural control methods and cavity control methods have been numerically studied and compared. To maintain fairness, the comparison was based on identical control stability indexes. The analysis has shown that cavity control can provide more noise reduction than structural control. Therefore, further analysis of the cavity control is given in the following chapter.

Comparison of cavity control strategies

Part of this chapter is based on:

J. H. Ho and A. Berkhoff, "Comparison of various decentralised structural and cavity feedback control strategies for transmitted noise reduction through a double panel structure," Journal of Sound and Vibration, vol. 333, no. 7, pp. 1857–1873, 2014.

J. H. Ho and J. Kalverboer and A. Berkhoff, "Comparisons between various cavity and panel noise reduction control in double-panel structures," in THE ACOUSTICS 2012 HONG KONG (Invited), 13-18 May 2012, Hong Kong. pp. 1-6.

5.1 Introduction

From the previous comparison between various combinations of structural control methods and cavity control methods, we find that cavity control can provide significant noise reduction. Therefore, we present further investigations of various cavity sources in this chapter. Three types of cavity control sources are introduced, and the control performances are compared. The first type is a dynamic loudspeaker source, which operates as an acceleration source above the resonance frequency. The second type is an incident pressure source. The third type is controlling the pressure at the cavity boundaries. These three cavity control methods are applied at the boundaries of the cavity. The location of a cavity control source, which can be modeled as an acceleration source, incident pressure source, or pressure-controlled boundary, is marked in blue in Fig. 5.1. There are six cavity control sources along the cavity sides. To detect the error signal, there is one microphone in front of each control source.

In our model, sound wave radiation and propagation is governed in the frequency domain by

$$\nabla \hat{p} + j\omega \rho \hat{\mathbf{v}} = \mathbf{0}, \quad (5.1)$$

$$\nabla \cdot \hat{\mathbf{v}} + j\omega \kappa \hat{p} = 0, \quad (5.2)$$

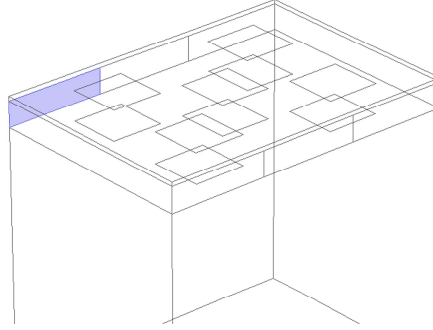


Figure 5.1: Cavity control source configuration.

where ∇ is the gradient in Eq. (5.1); $\nabla \cdot$ is the divergence in Eq. (5.2); \hat{p} [Pa] is the pressure; ρ [kg m^{-3}] is the density of air; $\hat{\mathbf{v}}$ [m s^{-1}] is the particle velocity and κ [Pa^{-1}] is the compressibility of air. Equation (5.1) is the equation of Newton's Law, and Eq. (5.2) is based on mass conservation.

The following sections provide the principles of the three cavity control sources: an acceleration source loudspeaker, an incident pressure source loudspeaker, and a pressure-controlled source loudspeaker.

5.1.1 Acceleration source loudspeaker

A dynamic loudspeaker is the most common type of loudspeaker. It can be assumed to operate as an acceleration source above the resonance frequency [126]. To model this type of loudspeaker, we control the acceleration of the loudspeaker surface. According to Eq. (5.1), the acceleration can produce an acoustic pressure \hat{p} to the system as follows,

$$-\mathbf{n} \cdot \nabla \hat{p} = \rho \mathbf{n} \cdot \hat{\mathbf{a}}, \quad (5.3)$$

in which \mathbf{n} is the normal vector to the loudspeaker surface and $\hat{\mathbf{a}} = j\omega \hat{\mathbf{v}}$ [m s^{-2}] is the acceleration of the loudspeaker surface. The acoustic source impedance of the loudspeaker is assumed to be infinite.

5.1.2 Incident pressure source loudspeaker

The incident pressure source loudspeaker is used to produce a pressure source with a non-reflecting source boundary. A non-reflecting boundary condition (NRBC) equation, derived by Givoli and Neta, is applied to the model to introduce an incident pressure source into the system without reflections at the system's boundary [127]. This equation is based on a reformulation of the Higdon Non-Reflecting Boundary Condition [128,129]. The Higdon NRBC relies on a series of linear partial differential equations. By adjusting the parameters of the boundary condition, the reflection coefficient can be reduced to zero for a certain incident angle. A higher order of the Higdon NRBC provides more incident angles that can be perfectly absorbed. Thus, less reflection is produced by the boundary. However, the order of the Higdon NRBC is limited in practical application because of computational difficulty. The Higdon NRBC orders and angles must be chosen based on experience to optimize the overall performance. The NRBC derived by Givoli and Neta uses additional auxiliary variables on the boundary to enable using the original Higdon NRBC up to any order. The second-order Givoli and Neta NRBC in the frequency domain is defined by

$$\mathbf{n} \cdot \nabla \hat{p} + jk\hat{p} + \frac{j\nabla^2 \hat{p}}{2k} = \mathbf{n} \cdot \nabla \hat{p}_i + jk\hat{p}_i + \frac{j\nabla^2 \hat{p}_i}{2k}, \quad (5.4)$$

where ∇^2 is the Laplacian, and k is the wave number. The pressure \hat{p} at the boundary can be derived if the incident pressure source \hat{p}_i [Pa] is known. Furthermore, this equation can present the interactions in near-real conditions without any derivatives beyond the second order.

An example of this incident pressure source is shown in Fig. 5.2. The right side of Fig. 5.2(a) acts as an incident pressure source loudspeaker with \hat{p}_i . In addition, a point source is present in the center. With these two sources, the pressure at the boundary (the right side of Fig. 5.2(a)) varies as the sum of these two pressure waves. Figure 5.2(b) is the pressure distribution along the right side of Fig. 5.2(a), where the x-axis is the pressure value and the y-axis is the position along this boundary. It can be observed that the pressure varies along the boundary.

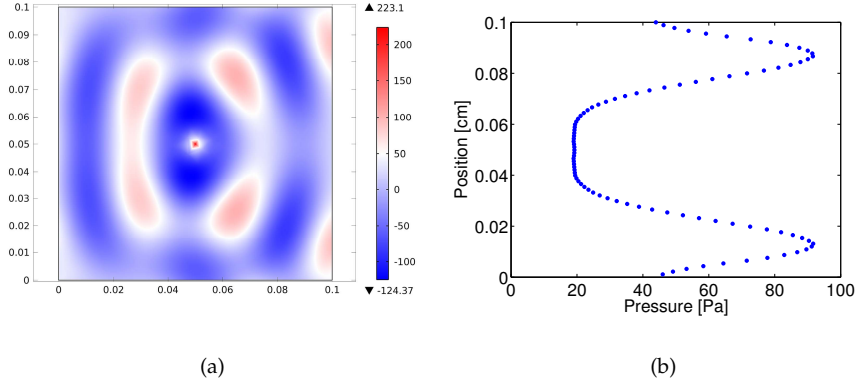


Figure 5.2: Incident pressure source illustration: (a) pressure distribution; (b) pressure along the boundary.

5.1.3 Pressure-controlled source loudspeaker

The third cavity control source is referred to as a pressure-controlled source loudspeaker. This cavity source controls the pressure at the boundary, which is the surface of the loudspeaker. The pressure \hat{p} at the boundary is controlled as our control pressure value \hat{p}_c [Pa]:

$$\hat{p} = \hat{p}_c. \quad (5.5)$$

An example of this pressure-controlled source loudspeaker is shown in Fig. 5.3. The right side of Fig. 5.3(a) acts as a pressure-controlled source loudspeaker with $\hat{p} = \hat{p}_0$. In addition, a point source is present in the centre. With the pressure-controlled source loudspeaker, the pressure at the controlled boundary (the right side of Fig. 5.3(a)) is maintained as the design value \hat{p}_0 , as shown in Fig. 5.3(b), where the x-axis is the pressure value and the y-axis is the position along this boundary.

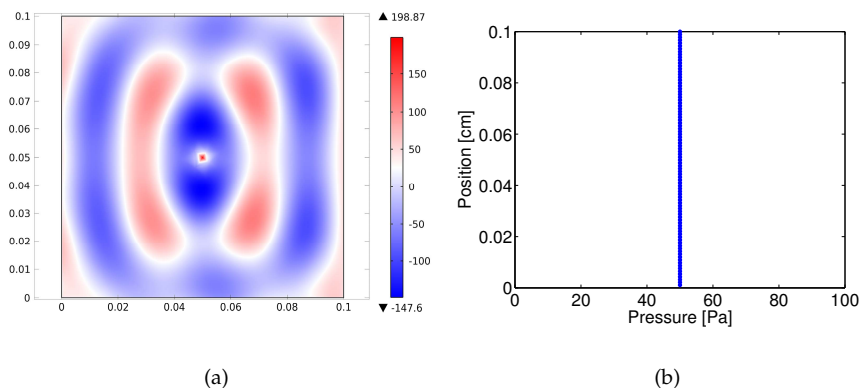


Figure 5.3: Pressure-controlled source illustration: (a) pressure distribution; (b) pressure along the boundary.

5.2 Cavity control performance comparisons

The noise reductions of these three cavity control sources are presented in three plots: the kinetic energy of the radiating panel, the sound pressure level at 10 cm above the radiating panel and the radiated sound power level of the structure (Figs. 5.4 - 5.6). The comparison is based on identical stability indexes (Table 5.1). The result shows that the pressure-controlled source loudspeaker can effectively reduce the broadband kinetic energy, but it increases the energy at certain frequencies, such as 600 Hz. In contrast, the incident pressure source loudspeaker does not increase the energy at any frequency below 1 kHz. Therefore, the broadband reduction of the kinetic energy is higher than it is for the other two source types, being 13.3 dB. This incident pressure source uses a non-reflecting boundary, which means that the energy can be propagated outside of the cavity. Although there are no practical loudspeakers that use this source, an incident pressure source loudspeaker can be created using a dynamic loudspeaker, a microphone, and a velocity sensor with a feedback control loop.

Table 5.1: Numerical analysis of stabilities, kinetic energy reduction and radiated sound power reduction from 10 Hz to 1 kHz.

Loudspeaker type	Acceleration source	Incident pressure source	Pressure-controlled source
Control gain	0.00042	0.2	0.029
Gain stability index	Inf.	34.6	Inf.
Phase stability index	58.7	59.8	59.8
Modulus stability index	0.87	0.62	0.75
Phase crossover frequency [10 Hz–20 kHz]	10 [kHz]	2187 [Hz]	6360 [Hz]
Total kinetic energy reduction($10 \log_{10}(\Sigma KE_{uncontrolled}/\Sigma KE_{controlled})$)[dB]			
	4.9	13.3	13.2
Total radiated sound power reduction($10 \log_{10}(\Sigma \text{radiated power}_{uncontrolled}/\Sigma \text{radiated power}_{controlled})$)[dB]			
	4.8	13.2	11.7

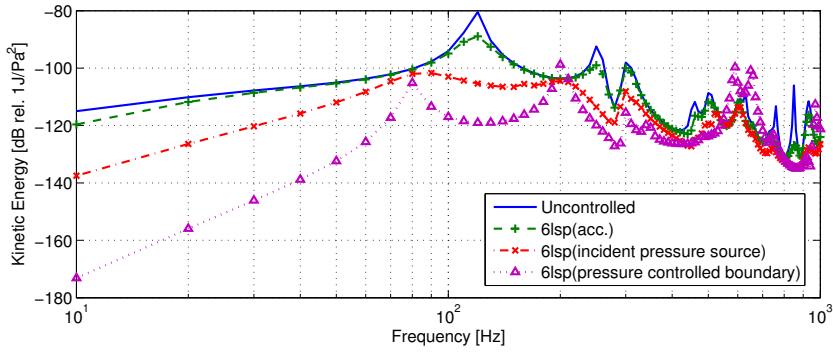


Figure 5.4: Simulated kinetic energy response of the radiating panel with various cavity control sources.

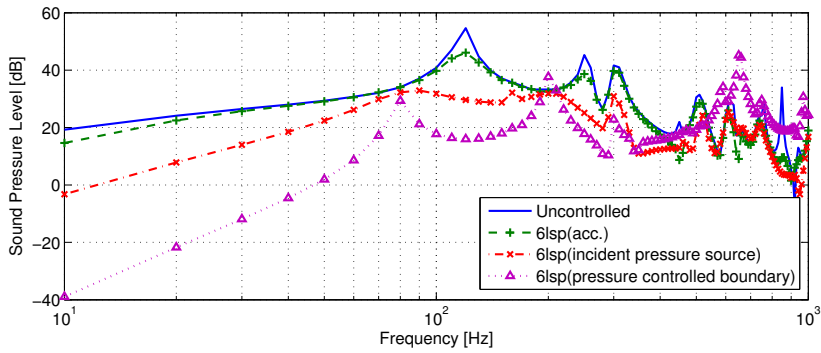


Figure 5.5: Simulated SPL response of the radiating panel with various cavity control sources.

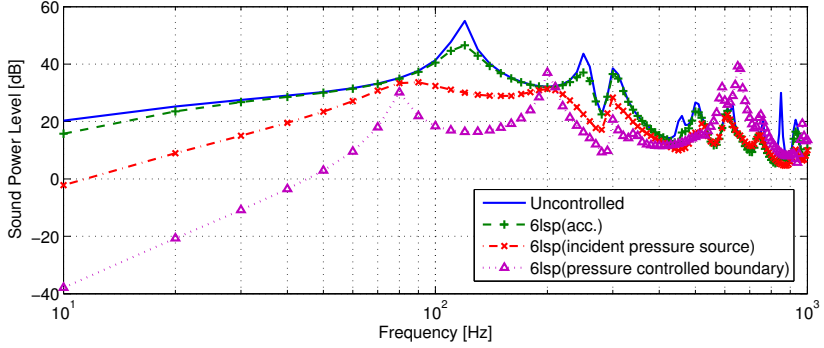


Figure 5.6: Simulated SWL response of the radiating panel with various cavity control sources.

5.3 Feed-forward control

In this section, decentralized feedback control is combined with decentralized harmonic feed-forward control to further reduce the transmitted noise through the double panel structure. We use the steepest-descent algorithm in the current work to have an adaptive feed-forward control system. The adaptation rule for the controller is given in Section 2.4.1. Furthermore, a control effort weight factor β is used to stabilize the feed-forward control system, details of which are described in Section 2.2.2. The control signals \mathbf{u} of the decentralized MIMO feed-forward control system are

$$\mathbf{u} = - \left[\hat{\mathbf{G}}^H \mathbf{G} + \beta \mathbf{I} \right]^{-1} \hat{\mathbf{G}}^H \mathbf{d}, \quad (5.6)$$

where \mathbf{G} is the plant transfer function of the control source, $\hat{\mathbf{G}}$ is the estimated plant transfer function, H denotes the Hermitian transpose, \mathbf{d} is the contribution of the primary source on the error sensor. The stability of the decentralized MIMO feed-forward control system is guaranteed if the real parts of the eigenvalues λ of the matrix $\hat{\mathbf{G}}\mathbf{G}^H + \beta\mathbf{I}$ are positive. If the system is unstable, β can be set to $-\min \text{Re}(\lambda)$ to make the system just stable [118].

First, various sensor-actuator combinations in feed-forward control are numerically analyzed. For the structural control method, accelerometers with piezoelectric patches on the incident panel, the radiating panel, and both panels are applied. For the cavity control method, microphones with incident

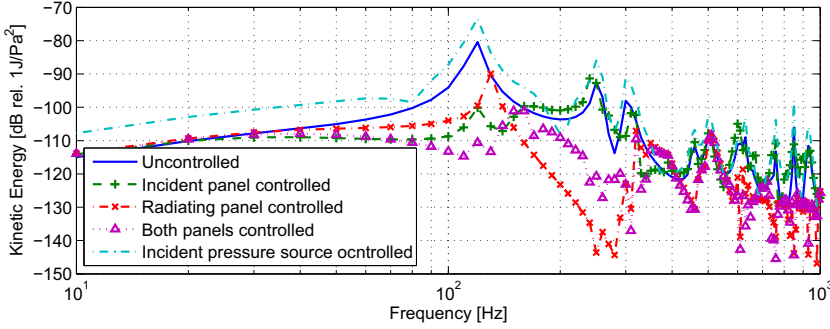


Figure 5.7: Simulated kinetic energy response of the radiating panel with various sensor-actuator configurations with decentralized harmonic feed-forward control.

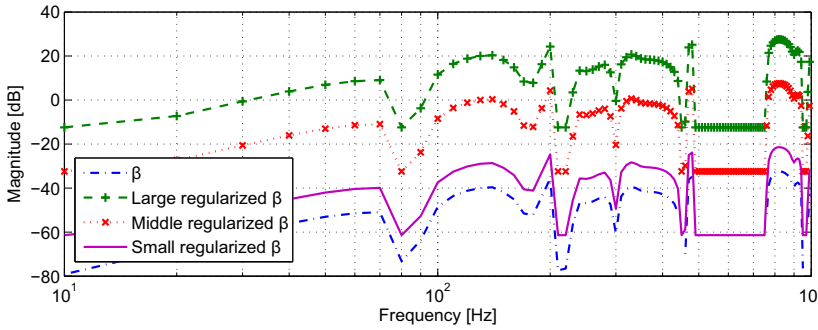


Figure 5.8: Values of β and regularized β .

pressure source loudspeakers are used. The results are shown in Fig. 5.7. The results indicate that piezoelectric patches on the radiating panel provide more transmitted noise reduction than the piezoelectric patches on the incident panel. Moreover, incident pressure source loudspeakers applied as the feed-forward cavity control sources even increase the transmitted noise. Since the error signals in the feed-forward cavity control method are the pressure inside the cavity, the cavity feed-forward control method does not guarantee the performance of the radiating panel. Nevertheless, the controller can be less aggressive if β in Eq. (5.6) is increased. We apply various β to the feed-forward cavity controller as shown in Fig. 5.8, where $\beta = -\min \text{Re}(\lambda)$. Regulariza-

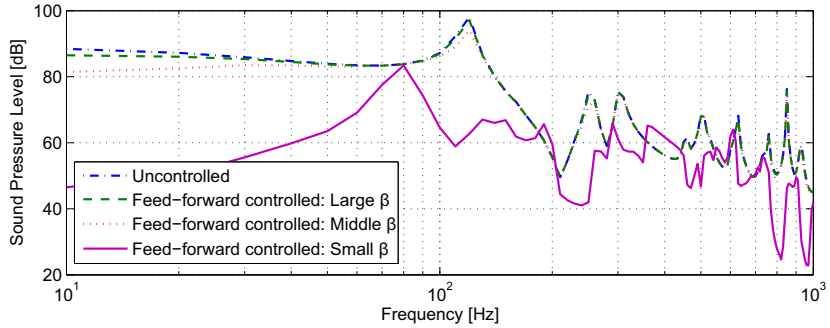


Figure 5.9: Incident pressure source feed-forward controlled with various β : simulated average sound pressure level inside the cavity.

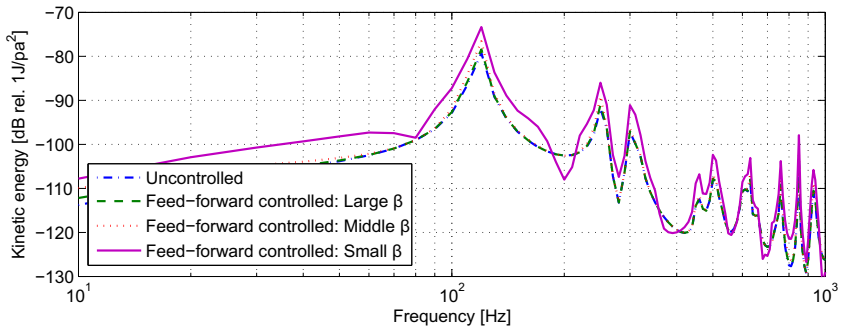


Figure 5.10: Incident pressure source feed-forward controlled with various β : simulated kinetic energy of the radiating panel.

tion is applied to large, middle, and small regularized β to limit the minimum β not being less than $1/1000$ of the maximum β . The average pressure inside the cavity and the kinetic energy of the radiating panel are presented in Figs. 5.9 and 5.10. As mentioned, small β leads to an aggressive controller and provides more pressure reduction. In contrast, large β gives small pressure reductions. On the other hand, small β leads to great increased kinetic energy of the radiating panel. Only a large β can avoid the increased kinetic energy of the radiating panel. Therefore, the incident pressure sources with pressure sensors inside the cavity for the feedback cavity control provide the largest trans-

mitted noise reduction among other sensor-actuator configurations. For the feed-forward cavity control method, this sensor-actuator configuration cannot reduce the transmitted noise through the double panel structure. The combination of decentralized feedback and feed-forward control is presented in Fig. 5.11. The incident pressure source, which can provide the largest reduction of transmitted noise in the previous section, is applied as the feedback cavity control source. This feedback control is combined with various feed-forward structural control configurations, which include piezoelectric patches on the incident panel, the radiating panel and both panels. The comparison indicates that piezoelectric patches on the radiating panel with feed-forward control combined with incident pressure source loudspeakers with feedback control can provide the largest transmitted noise reduction. The improvement of the control effect offered by the piezoelectric patches on the radiating panel with feed-forward control is presented in Fig. 5.12, where the green-dashed line presents the control effect of the decentralized feedback controller and the red-dotted line presents the control effect of the decentralized feedback and feed-forward combined controller. This combination provides the largest transmitted noise reduction through the double panel structure among all the other sensor-actuator configurations we introduced in Chapters 4 and 5.

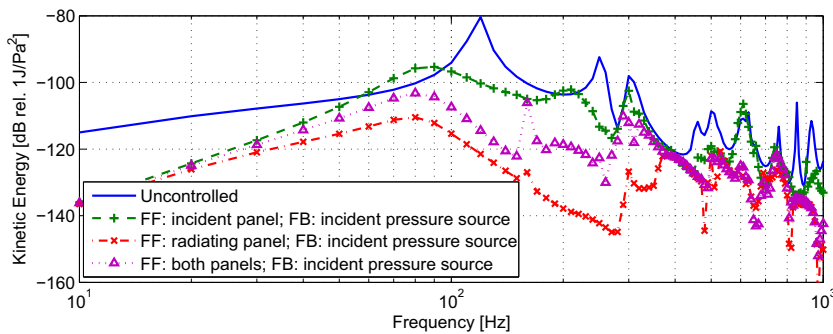


Figure 5.11: Simulated kinetic energy response of the radiating panel with feedback and feed-forward combined control, where incident pressure source loudspeakers are applied with feedback control and various sensor-actuator configurations are applied with feed-forward control.

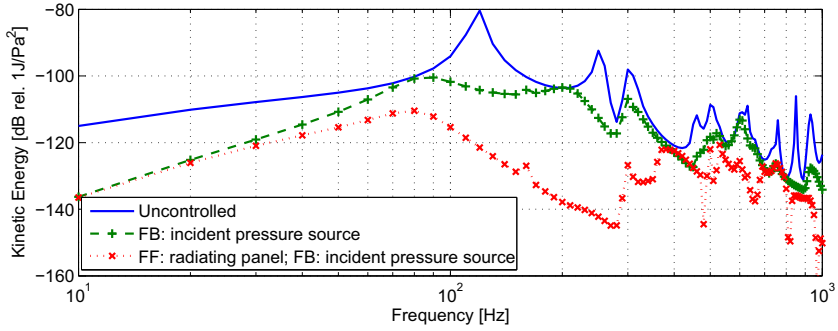


Figure 5.12: Simulated kinetic energy response of the radiating panel with feedback and feed-forward combined control providing the largest transmitted noise reduction, where incident pressure source loudspeakers are applied with feedback control and piezoelectric patches on the radiating panel with feed-forward control.

5.4 Conclusions

In this chapter, three types of cavity control sources for the feedback control were compared: an acceleration source loudspeaker, an incident pressure source loudspeaker, and a pressure-controlled source loudspeaker. The comparison has shown that the incident pressure source loudspeaker can achieve the largest total kinetic energy decrease of 13.3 dB and the largest total radiated sound power decrease of 13.2 dB within the frequency range from 10 Hz to 1 kHz.

To further improve the control effect, we combined decentralized direct feedback control with decentralized harmonic feed-forward control. From the noise reduction comparison between various sensor-actuator configurations, it was found that piezoelectric patches on the radiating panel with feed-forward control combined with incident pressure source loudspeakers with feedback control provided the largest transmitted noise reduction. This incident pressure source loudspeaker can be realized by using a dynamic loudspeaker, a microphone, and a velocity sensor with a feedback or feed-forward control loop. The development of incident pressure source loudspeakers is presented in the following chapter.

Development of incident pressure sources

Part of this chapter is based on:

J. H. Ho and A. Berkhoff, "Development of dynamic loudspeakers modified as incident pressure sources for noise reduction in a double panel structure," in 20th International Congress on Sound and Vibration (ICSV 20), 7-11 Jul. 2013, Bangkok, Thailand. pp. 1-7.

6.1 Introduction

This chapter presents the development of an incident pressure source, which was found to be an effective control source for reducing the transmitted noise through a double panel structure in Chapter 5. The double panel structure consists of two panels with air in between and offers the advantages of low weight, low sound transmission at high frequencies, and thermal insulation. Therefore, this structure is often applied in the aerospace and automotive industries. However, the main issues of the double panel structure are the resonance of the cavity and the high noise transmission at low frequencies. Both the two panels and the cavity cause the resonance, which limits the noise reduction performance. To improve the noise reduction of the double panel structure, many papers have discussed applying active structural acoustic control to the panels or active noise control to the cavity [1, 14, 16]. In Chapters 4 and 5, we considered the resonance of the panels and the cavity simultaneously and numerically compared various decentralized structural and cavity feedback control strategies based on identical control stability indexes, as described in Section 2.3.3. Cavity control by loudspeakers, which are modified to operate as incident pressure sources, was found to provide the largest noise reduction. As an extension of the previous chapters, this chapter presents the realization of this incident pressure source in one dimension by using a dynamic loudspeaker, a micro-

phone, and a particle velocity sensor with feed-forward control. The incident pressure source is defined as a pressure source for which there is no reflecting pressure from the incident boundary. In order to minimize the reflecting pressure from the boundaries, we apply a wave separation technique [130]. To improve the convergence rate and stability, the regularized modified filtered-error least mean square (RMFeLMS) algorithm described in Section 2.4.2 is applied to our real-time feed-forward control system [124, 125, 131]. Moreover, a numerical model shows that this incident pressure source can be obtained both in a one-dimensional duct and a three-dimensional cavity with feedback control.

This chapter has four main sections. Section 6.2 describes the incident pressure source development and the wave separation method. Section 6.3 shows the experimental setup and the real-time control result of the feed-forward control. Section 6.4 presents the numerical study of the incident pressure source development with feedback control. Finally, this dynamic loudspeaker modified control source is numerically applied to the double panel structure as the noise control source. Section 6.5 gives the conclusions.

6.2 Development of an incident pressure source

6.2.1 System configuration

The incident pressure source is defined as a pressure source for which there is no reflecting pressure from the incident boundary. In other words, the reflecting pressure from the solid surface vanishes. Therefore, we use the reflecting pressure instead of the total pressure as our error signal. The reflecting pressure can be derived by measuring the pressure and the velocity. Figure 6.1 shows our system configuration. A dynamic loudspeaker generates the primary source; another dynamic loudspeaker placed between the primary source and the solid surface gives the secondary source; one pressure sensor and one gradient pressure sensor, which functions as a particle velocity sensor, are placed at the same position in the duct to measure the error signal. The incident pressure source is realized by minimizing the reflecting pressure with a feed-forward controller or a feedback controller.

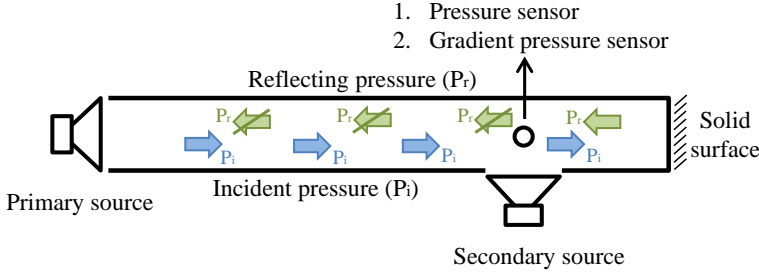


Figure 6.1: The configuration of the control system.

6.2.2 Wave separation technique

For plane wave propagation, the momentum equation in the time domain is written as

$$\rho \frac{\partial v}{\partial t} + \frac{\partial p}{\partial x} = 0, \quad (6.1)$$

where $\rho = \rho(x)$ [kg m^{-3}] is the density of the air; $p = p(x, t)$ [Pa] is the pressure; $v = v(x, t)$ [m s^{-1}] is the particle velocity; t [s] is the time and x indicates the wave propagate on x -axis. Assuming the incident pressure propagates in the positive x -direction, the incident pressure in the time domain can be expressed as $p_i(x, t) = \hat{p}_i \cos(kx - \omega t + \varphi)$, where \hat{p}_i is the amplitude of the incident pressure, which can be a function of frequency, k [m^{-1}] is the wave number, ω [rad s^{-1}] is the angular frequency, φ [rad] is the phase angle (an arbitrary value of the phase angle of the wave at the origin at $t = 0$). Using Eq. (6.1), the incident wave can be written as

$$\frac{\partial v_i}{\partial t} = \frac{1}{\rho} \hat{p}_i \sin(kx - \omega t + \varphi), \quad (6.2)$$

where $v_i = v_i(x, t)$ [m s^{-1}] is the particle velocity corresponding to the incident wave p_i [Pa]. v_i can be obtained as

$$v_i = \frac{\hat{p}_i}{\rho c} \cos(kx - \omega t + \varphi) = \frac{p_i}{\rho c}. \quad (6.3)$$

On the other hand, the reflecting pressure $p_r(x, t)$ propagates in the negative x -direction, and can be written as

$$p_r(x, t) = \hat{p}_r \cos(-kx - \omega t + \varphi), \quad (6.4)$$

where \hat{p}_r is the amplitude of the reflecting pressure, which can be a function of frequency. The particle velocity $v_r = v_r(x, t)$ [m s⁻¹] corresponding to the reflecting wave $p_r = p_r(x, t)$ [Pa] is

$$v_r = -\frac{\hat{p}_r}{\rho c} \cos(-kx - \omega t + \varphi) = -\frac{p_r}{\rho c}. \quad (6.5)$$

The total particle velocity and total pressure can be written as

$$v = v_i + v_r = \frac{p_i}{\rho c} - \frac{p_r}{\rho c}; \quad (6.6)$$

$$p = p_i + p_r. \quad (6.7)$$

Then the incident pressure and the reflecting pressure in the time domain can be expressed as

$$p_i = \frac{1}{2}(p + \rho cv); \quad (6.8)$$

$$p_r = \frac{1}{2}(p - \rho cv). \quad (6.9)$$

Equations (6.8) and (6.9) show that we can obtain the incident pressure and the reflecting pressure by measuring the pressure and the particle velocity.

6.3 One-dimensional realization with feed-forward control

6.3.1 Experimental setup

The regularized modified filtered-error adaptive least mean square (RM-FeLMS) algorithm is applied to the real-time feed-forward control implementation in this section. The details of RMFeLMS are described in Section 2.4.2. The experimental setup is shown in Fig. 6.2. A 250-cm-long duct is used; the radius of the duct cross section is 7.5 cm. The left end of the duct is the primary source generated by a dynamic loudspeaker, and the right end of the duct is a sealed solid surface. The primary noise is generated by filtering white noise with a simple low-pass filter. We use another dynamic loudspeaker as the secondary source, which is placed 206 cm away from the primary source. One pressure microphone and one gradient pressure microphone, which functions as the particle velocity sensor, are placed in the duct at the same position.

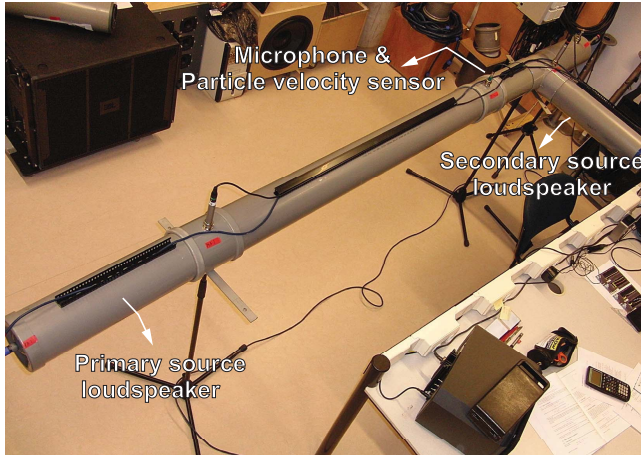


Figure 6.2: Experimental setup for real-time control.

6.3.2 Real-time control results

We evaluated two sensor-actuator configurations. Figure 6.3 shows these two sensor positions, sensor position 1 locates in front of the secondary source, sensor position 2 locates between the primary source and the secondary source. Configuration 1 uses the error sensors placed at sensor position 1, which is 206 cm away from the primary source. Configuration 2 uses the error sensors placed at sensor position 2, which is 155 cm away from the primary source.

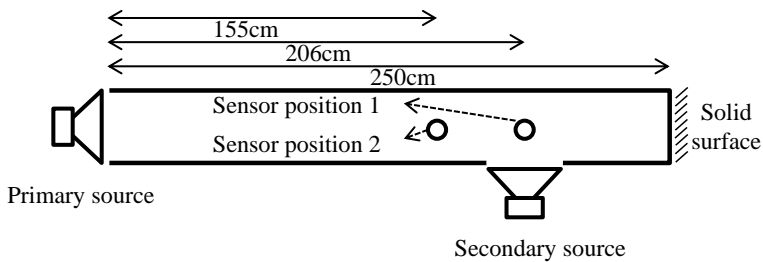


Figure 6.3: Sensor positions.

Figure 6.4 presents the reduction of the reflecting pressure, which is the error signal, with configuration 1 control. The results show that the RMFeLMS feed-forward control can effectively reduce the reflecting pressure with an average 26.2 dB reduction, assuming that the error sensor provides an exact measure of the reflected pressure. The total pressure measured at positions 1 and 2 is shown in Figs. 6.5 and 6.6. The resonance in the duct is removed by reducing the reflecting wave. Moreover, although the error sensor is placed at position 1, the improvement can also be seen at position 2. Figure 6.7 presents the reduction of the reflecting pressure with configuration 2 control. This configuration gives an average 25.4 dB reduction. The total pressure measured at position 1 and 2 is shown in Figs. 6.8 and 6.9. The duct resonance is effectively removed at position 2, as shown in Fig. 6.9. However, the control system cannot control the resonance behind the error sensor, for instance at position 1, as shown in Fig. 6.8. The result shows, with the RMFeLMS feed-forward control, that both configurations can effectively remove the resonance between the primary source and the error sensors and realize an incident pressure source.

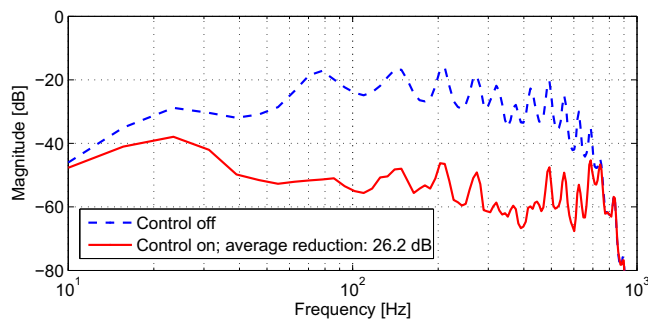


Figure 6.4: Reflecting pressure response: with real-time feed-forward configuration 1 control.

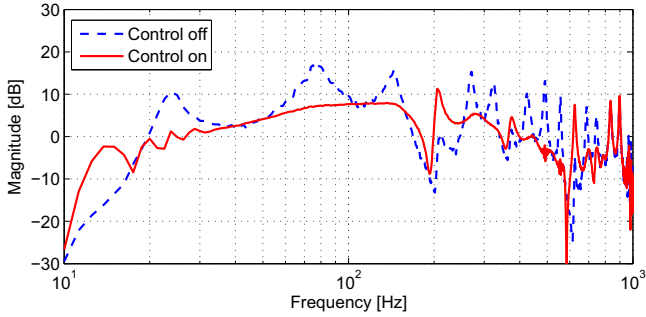


Figure 6.5: Total pressure response at sensor position 1: with real-time feed-forward configuration 1 control.

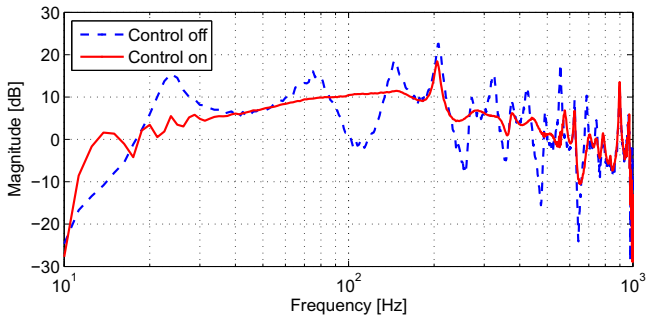


Figure 6.6: Total pressure response at sensor position 2: with real-time feed-forward configuration 1 control.

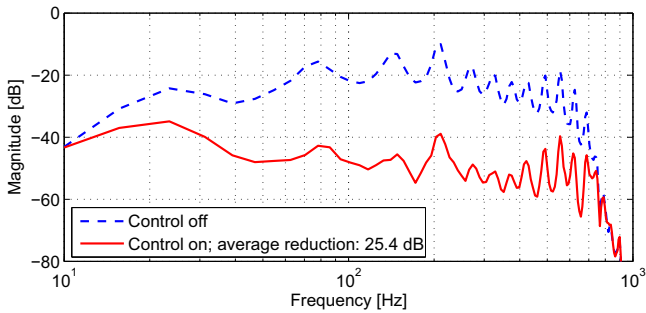


Figure 6.7: Reflecting pressure response: with real-time feed-forward configuration 2 control.

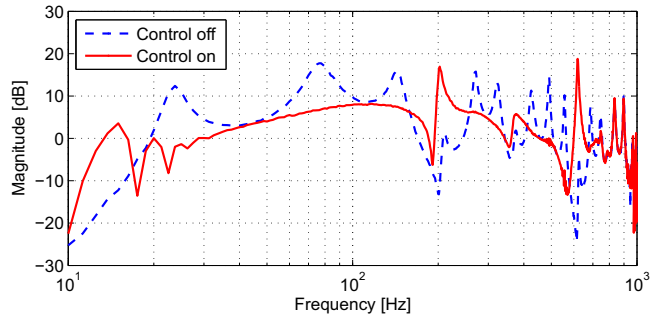


Figure 6.8: Total pressure response at sensor position 1: with real-time feed-forward configuration 2 control.

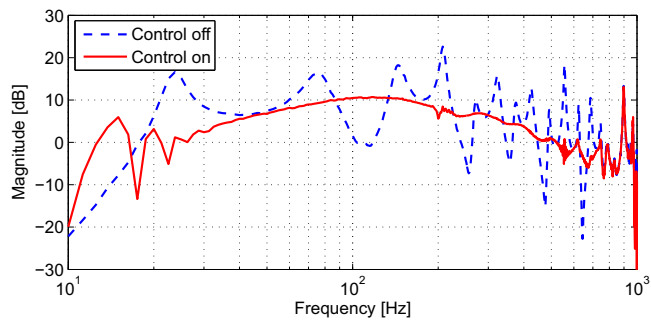


Figure 6.9: Total pressure response at sensor position 2: with real-time feed-forward configuration 2 control.

6.4 Numerical development with feedback control

6.4.1 Performance in a duct

In this section, we use the finite element method (FEM) with the COMSOL Multiphysics 4.3b (COMSOL, Inc., Burlington, MA 01803, USA) to model the duct, as described in Section 6.3. The walls of this 3D duct are rigid boundary surfaces and one of the duct-ends is the primary noise source as shown in Fig. 6.10. The model is meshed with tetrahedral elements. Two configurations are analyzed. In configuration 1, surface A is the control source and surface B is a rigid boundary surface. In configuration 2, surface A is a rigid boundary surface and surface B is the control source. With a feedback controller, the control source aims to minimize the pressure reflecting from the duct-end. The performance of modifying a dynamic loudspeaker operating as the incident pressure source is presented.

In theory, the stability of a feedback control system can be unconditionally guaranteed when the sensors and actuators are dual and collocated. Therefore, we use the average pressure and velocity over the surface of the control source as the error signals for the feedback controller. We have modeled the control configuration introduced in Section 6.3, where the control source locates 206 cm away from the primary noise source. This configuration is referred to as configuration 1, where surface A facing in the y -direction is the surface of

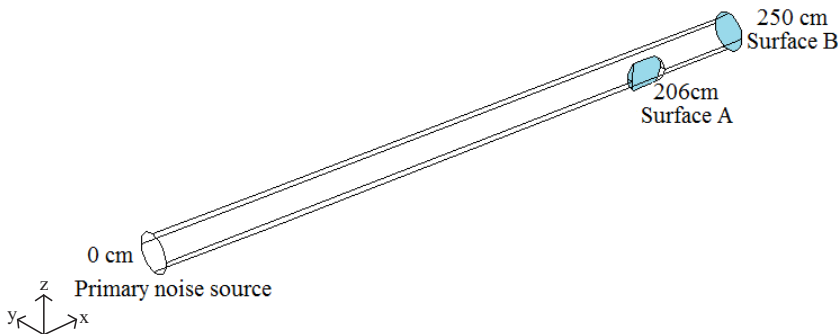


Figure 6.10: The configuration of the duct model:

Configuration 1: surface A is the control source and surface B is a rigid surface.

Configuration 2: surface A is a rigid surface and surface B is the control source.

the control source and surface B facing in the x-direction is the surface of the rigid duct-end, as shown in Fig. 6.10. However, the transfer function between the sensor and the actuator indicates that using pressure in the x-direction has a phase-lag problem as shown in Fig. 6.11. On the other hand, using pressure in the direction perpendicular to the surface of the control source as the error signal can provide a stable system.

In order to control the pressure in the x-direction with a stable feedback controller, we place the control source at the end of the duct facing in the x-direction. This configuration is referred to as configuration 2, where surface B facing in the x-direction is the surface of the control source and surface A facing in the x-direction is a rigid surface as shown in Fig. 6.10. The total pressure response along the duct with and without control is shown in Fig. 6.12. The x-axis is the distance to the primary source, the y-axis is the frequency, and the z-axis is the normalized SPL. To provide two distinguishable plots in the same figure, the controlled response is offset by -150 dB. The result presents that control configuration 2 greatly removes the resonance inside the duct. This in-

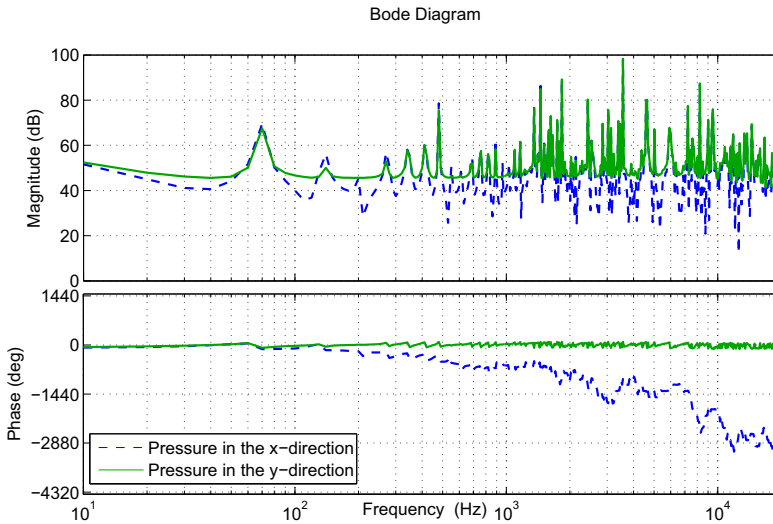


Figure 6.11: Transfer functions between the sensor and the actuator of control configuration 2. Blue-dash line: pressure in the x-direction as the error signal; green-solid line: pressure in the y-direction as the error signal.

icates that the reflecting pressure from the duct-end is effectively minimized. The detailed SPL response along the duct is shown in Fig. 6.13.

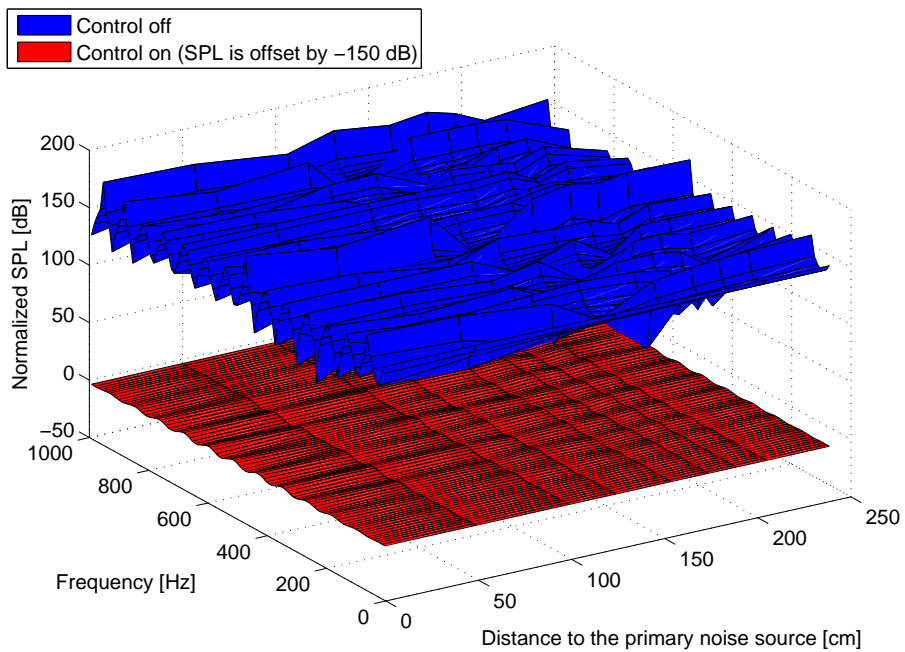


Figure 6.12: Normalized total pressure response along the duct: Blue-plot: uncontrolled; red-plot: controlled with configuration 2.

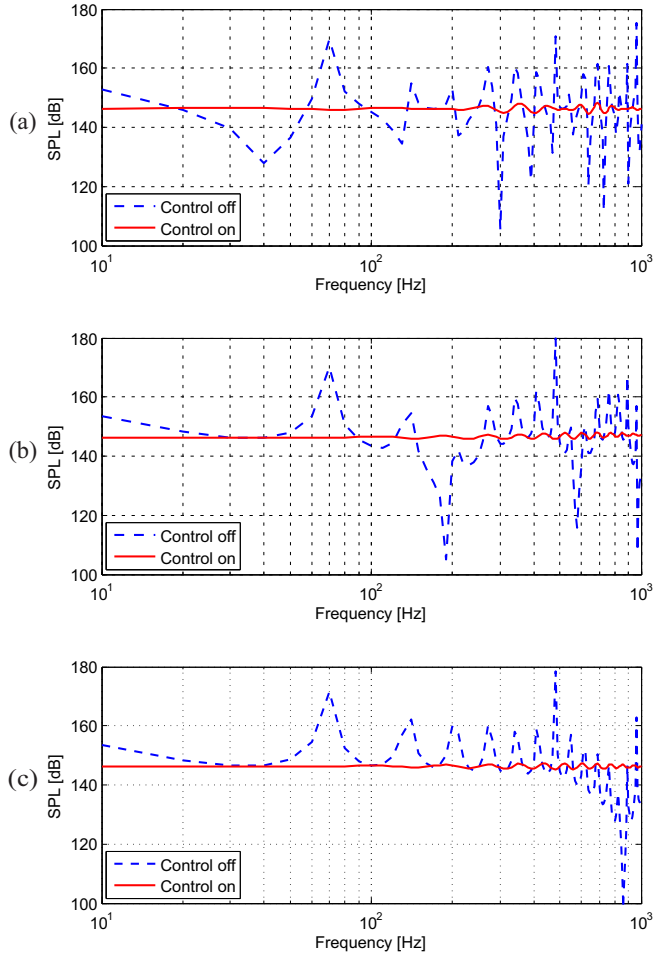


Figure 6.13: Simulated total pressure response: with feedback control configuration 1.
(a) SPL at 50 cm; (b) SPL at 206 cm; (c) SPL at 240 cm

6.4.2 Performance in a double panel structure

In Chapter 5, the results show that the incident pressure control source provides the largest noise reduction in a double panel structure. Although the incident pressure source has been experimentally and numerically obtained in the previous sections, the wave inside the duct is close to a one-dimensional wave propagation. Applying this modified loudspeaker source to the cavity control in a double panel structure requires further analysis, since the wave propagation in the double panel structure is a three-dimensional problem. This section presents the investigation and development of this incident pressure source applied to a three-dimensional cavity. To continue the results obtained in Sections 6.3 and 6.4, where the minimized reflecting pressure is used as an example of the incident pressure source, the minimized reflecting pressure is applied to the double panel structure control in this section. The minimized reflecting pressure can be implemented in COMSOL by using a non-reflecting boundary condition (NRBC) model [127]. A slight difference exists between applying the NRBC and applying the incident pressure source as the feedback control source to the system, as shown in Fig. 6.14. However, as both are regarded as the incident pressure source, they can both provide effective noise reduction. A detailed description and definition of the incident pressure control source is given in Section 5.1. Therefore, the following development aims to minimize the reflecting pressure in the cavity and to provide NRBC cavity sidewalls in order to reduce the transmitted noise through the double panel

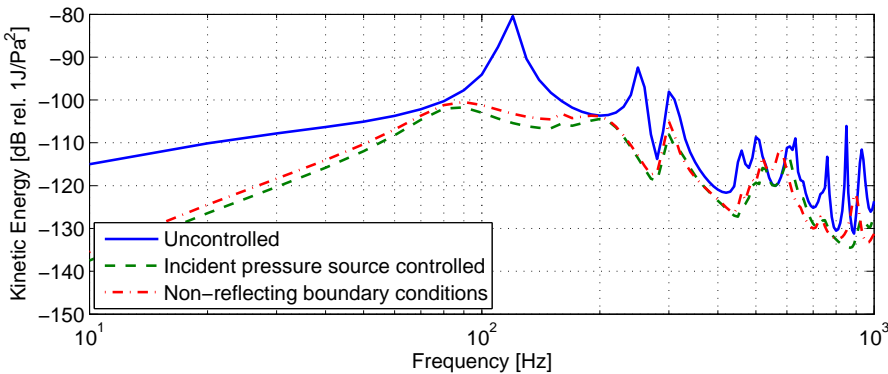


Figure 6.14: Simulated kinetic energy of the radiating panel of the double panel structure with various control strategies.

structure. Furthermore, as shown in Fig. 6.15, more NRBC sidewalls provide more transmitted noise reduction, since less resonance exists.

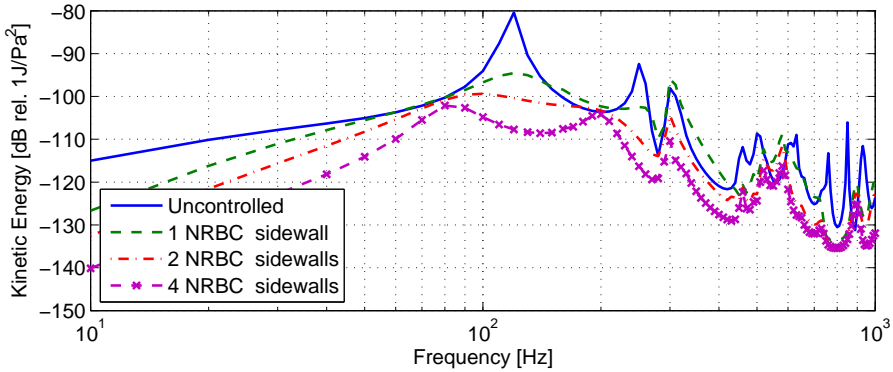


Figure 6.15: Simulated kinetic energy of the radiating panel of the double panel structure with various amount of non-reflecting cavity sidewalls

Reflecting pressure direction selection

The NRBC cavity sidewalls can be obtained by minimizing the reflecting pressure from the solid surface of the cavity sidewalls. However, unlike the duct control system, controlling the reflecting pressure inside the cavity is a three-dimensional issue. Further analysis of applying control sources facing in different directions is studied. Two loudspeakers facing in two different directions are analyzed, as shown in Fig. 6.16. Loudspeaker-X has the sound radiating surface perpendicular to the x-axis and loudspeaker-Y has the sound radiating surface perpendicular to the y-axis. As mentioned in the previous section, the error signals are obtained by the average total pressure and velocity over the loudspeaker surface. The transfer functions between the loudspeaker-X and the average pressure, pressure in the x-, y- and z-directions over the surface of the control source are shown in Fig. 6.17. The results indicate that using pressure in the x-direction as the error signal for loudspeaker-X provides better control stability than using pressure in the y- and z-directions. Similar results have been found in loudspeaker-Y as shown in Fig. 6.18. Using pressure in the y-direction as the error signal provides better control stability than using pressure in the x- and z-directions. This means using pressure in the direction perpendicular to the loudspeaker surface as the error signal provides a

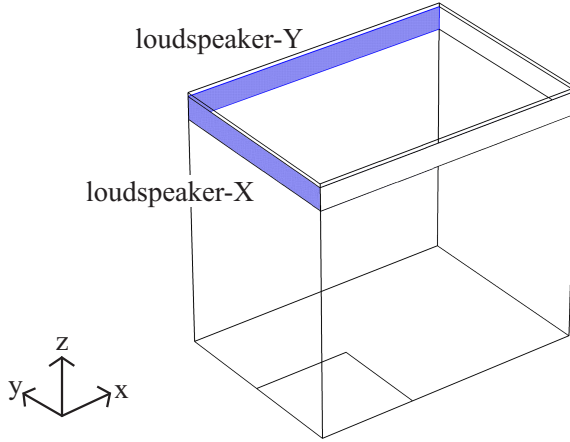


Figure 6.16: Configuration of control loudspeakers.

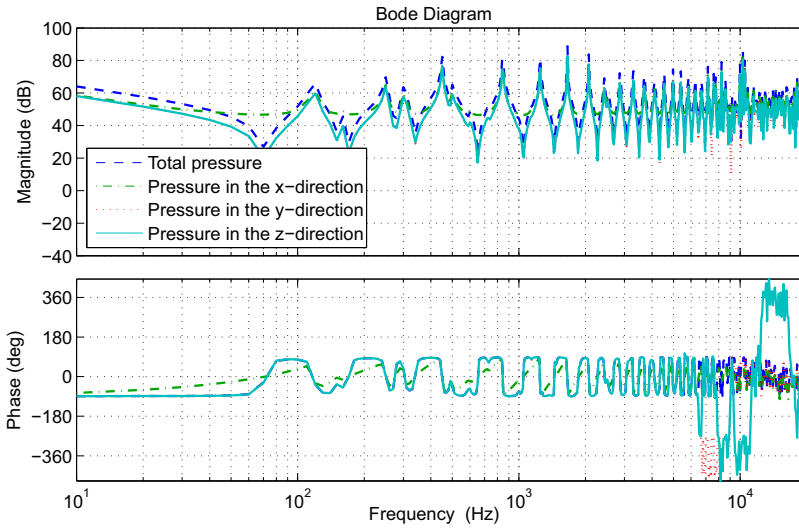


Figure 6.17: Transfer functions between the sensor and the actuator of loudspeaker-X.

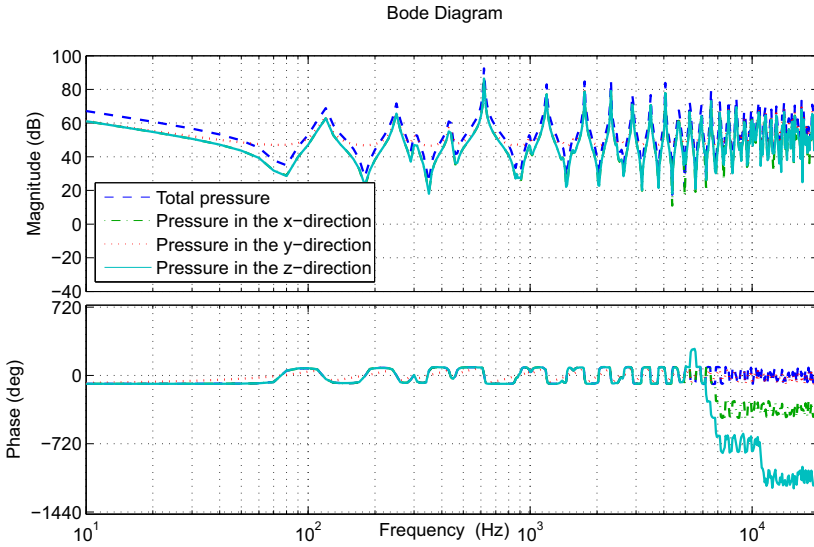


Figure 6.18: Transfer functions between the sensor and the actuator of loudspeaker-Y.

stable feedback control system. Therefore, we use pressure in the x-direction as the error signal for loudspeaker-X and use pressure in the y-direction as the error signal for loudspeaker-Y. Figure 6.19 presents the control performance of applying loudspeaker-X to minimize the total pressure or the pressure in the x-direction. The results show that a non-reflecting sidewall facing in the x-direction, which is labeled as NRBC-X, can be obtained by using loudspeaker-X to minimize the pressure in the x-direction. Moreover, instead of minimizing the total pressure, minimizing the pressure in the x-direction can effectively reduce the transmitted noise through the double panel structure. The same results are found in using loudspeaker-Y as shown in Fig. 6.20. A non-reflecting sidewall facing in the y-direction, which is labeled as NRBC-Y, can be obtained by using loudspeaker-Y to minimize the pressure in the y-direction. The transmitted noise can be effectively reduced by applying loudspeaker-Y to minimize the pressure in the y-direction. In conclusion, the incident pressure source can be obtained by applying a dynamic loudspeaker to minimize the pressure in the direction perpendicular to the loudspeaker surface with feedback control. And the transmitted noise can be effectively reduced by applying this modified dynamic loudspeaker.

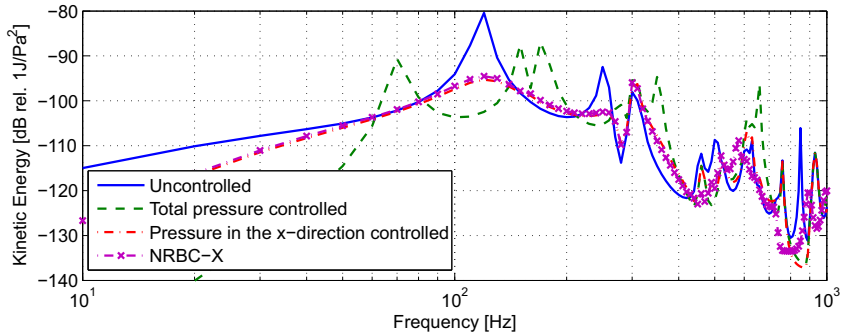


Figure 6.19: Simulated kinetic energy of the radiating panel of the double panel structure in three conditions: using loudspeaker-X to minimize total pressure or pressure in the x-direction; and applying a non-reflecting sidewall facing in the x-direction.

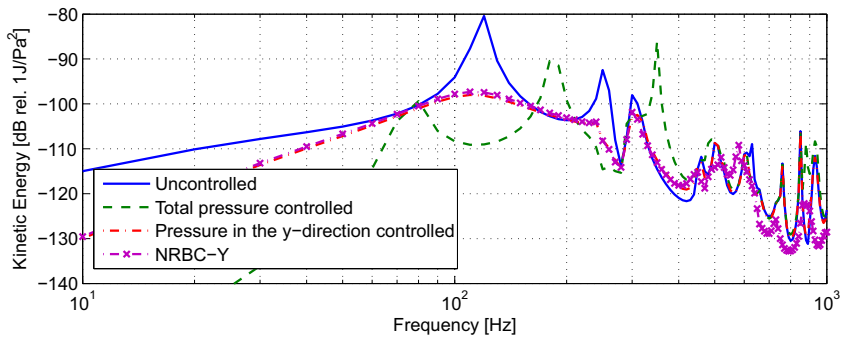


Figure 6.20: Simulated kinetic energy of the radiating panel of the double panel structure in three conditions: using loudspeaker-Y to minimize total pressure or pressure in the y-direction; and applying a non-reflecting sidewall facing in the y-direction.

MIMO control results

To increase the transmitted noise reduction, multiple controllers are applied to the system. The control results for a 2-channel MIMO control are presented in Fig. 6.21. The 2-channel MIMO control has two loudspeaker-Xs at the opposite side of the cavity. The results show that two non-reflecting sidewalls facing in the x-direction at the opposite side of the cavity, which is labeled as 2 NRBC-Xs, can be obtained by using two loudspeaker-Xs at the opposite side of the cavity for minimizing the pressure in the x-direction. Moreover, the 2-channel MIMO control provides more noise reduction than the SISO control. This agrees with Fig. 6.15, where more NRBC cavity sidewalls provide more transmitted noise reduction. The same results are found in applying two loudspeaker-Ys as shown in Fig. 6.22. More combinations of multiple controllers, which include another 2-channel MIMO control and a 4-channel MIMO control, are presented in Fig. 6.23. This 2-channel MIMO control has one loudspeaker-X and one loudspeaker-Y and the 4-channel MIMO control has two loudspeaker-Xs and two loudspeaker-Ys. However, the control gain of these two combinations is limited to the control stability and less noise reduction is provided than applying 2-loudspeaker-Xs or 2-loudspeaker-Ys control.

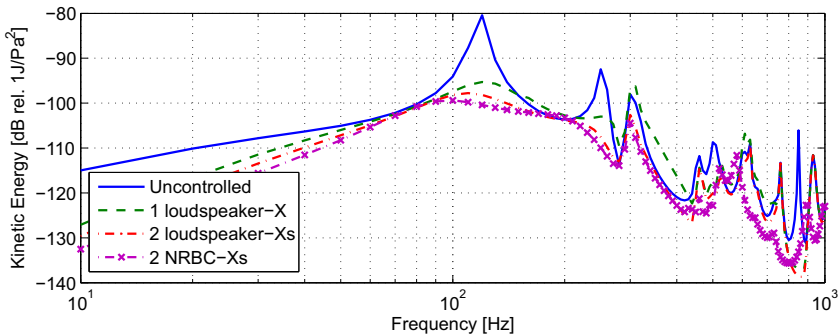


Figure 6.21: Simulated kinetic energy of the radiating panel of the double panel structure with NRBC and modified loudspeaker-X control.

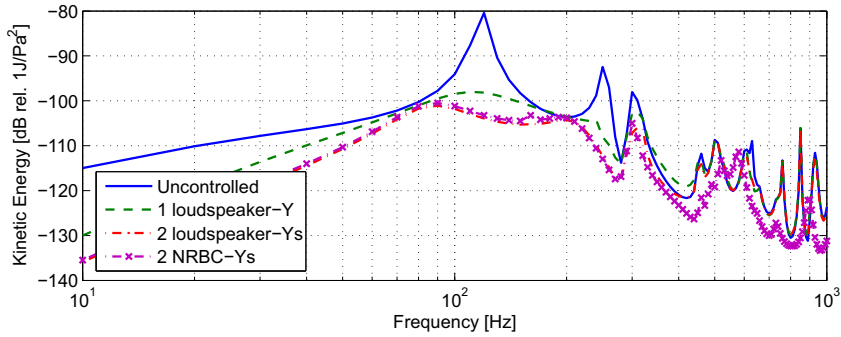


Figure 6.22: Simulated kinetic energy of the radiating panel of the double panel structure with NRBC and modified loudspeaker-Y control.

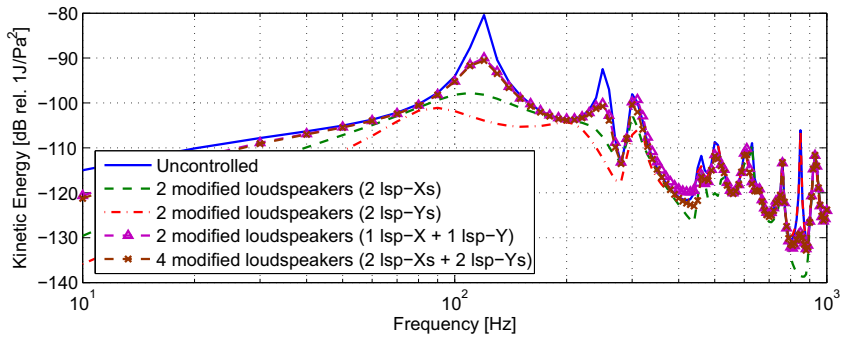


Figure 6.23: Simulated kinetic energy of the radiating panel of the double panel structure with multiple modified loudspeakers control.

A comparison was made between the control performance of the dynamic loudspeakers modified as the incident pressure sources and the other two cavity control sources introduced in Chapter 5, as shown in Fig. 6.24. This incident pressure source provides the largest transmitted noise reduction and is numerically obtained by modifying a dynamic loudspeaker.

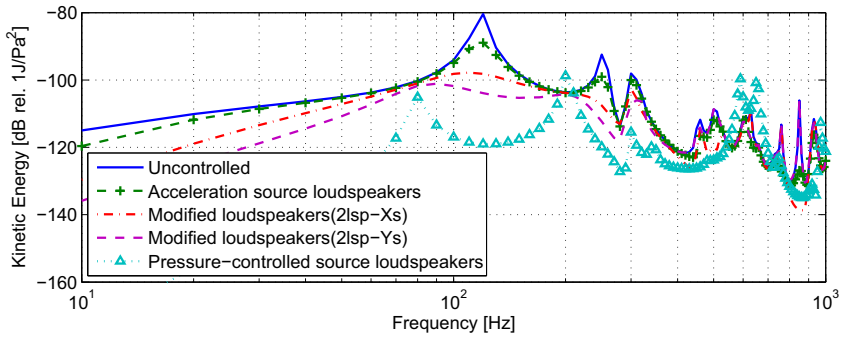


Figure 6.24: Simulated kinetic energy of the radiating panel of the double panel structure with various cavity control sources.

6.5 Conclusions

The one-dimensional real-time realization of the incident pressure source loudspeaker with feed-forward control is presented in this chapter. Our studies show that the reflecting pressure was reduced by 26.2 dB on average and that the pressure resonance in the duct can be effectively removed. Therefore, our work shows the incident pressure source loudspeaker can be realized by using a dynamic loudspeaker, a microphone, and a particle velocity sensor with a feed-forward controller. And a non-reflecting boundary condition can be realized by minimizing the reflecting pressure from the solid surface. Furthermore, this pressure source loudspeaker has been numerically developed both in a one-dimensional duct and in a three-dimensional cavity by using a dynamic loudspeaker, a distributed microphone and a distributed velocity sensor with a feedback controller. This dynamic loudspeaker modified as an incident pressure source loudspeaker, which is found to be the most effective noise control source for a double panel structure in Chapters 4 and 5, has been applied to the double panel structure and effectively reduces the transmitted noise.

Flat acoustic sources

This chapter is based on:

J. H. Ho and A. Berkhoff, "Flat acoustic sources with frequency response correction based on feedback and feed-forward distributed control," submitted to The Journal of the Acoustical Society of America.

7.1 Introduction

As we introduced in Chapter 1, a flat acoustic source is an alternative control source to reduce the transmitted noise through the double panel structure. The double panel structure provides noise insulation by the air gap between the two panels. A larger air gap offers less acoustic coupling because it has larger acoustic compliance. Consequently, compact partitions with narrow air gaps result in less acoustic insulation, especially at low frequencies. The insufficient acoustic insulation at low frequencies can be improved by applying the flat acoustic sources for active noise control, while sufficient insulation at high frequencies is provided by a narrow air gap.

In this chapter, a honeycomb sandwich structure is used as the sound radiation panel because this structure has a low density and high bending stiffness. These properties lead to low modal density and high electroacoustic conversion efficiency. Low modal density reduces the complexity of the panel vibration, which provides a more stable control condition. Furthermore, the honeycomb sandwich structure is combined with a thin cavity, and the face of the sandwich structure internal to the source is perforated to increase acoustic compliance and electroacoustic conversion efficiency [132]. The perforated honeycomb panel structure, which is the moving part of the acoustic source, is driven by multiple actuators. To obtain an even frequency response, distributed direct velocity feedback control is applied to control the acoustic and

structural resonances. However, the collocated decentralized feedback control can destabilize asymmetric modes caused by the coupling of the internal acoustic cavity and rigid body vibration of the moving panel, but a designed sensor-actuator configuration can effectively control these resonances. Moreover, response of the acoustic source can be improved, potentially by equalizing both the magnitude and phase response with digital filters [133–135]. For instance, an inner-outer factorization provides a technique to determine a minimum-phase transfer function with a stable inverse, which can be used to equalize the frequency response [136]. Based on the inner-outer factorization, a minimum-phase regularized inverse (MPRI) method is used to obtain the optimum frequency response equalization with limited inverse gain [124, 125]. An approximate method is the Linkwitz filter, which provides a simple method to compensate the response at low frequencies [137]. A comparison between the MPRI method and the Linkwitz filter is given. The principal contributions of the present work are (1) the use of a perforated honeycomb panel as the radiating panel in a thin acoustic source; (2) the distributed feedback control combined with feed-forward control applied to this panel; and (3) the detailed control stability analysis and the given sensor-actuator configuration design principles.

This chapter has four main sections. Section 7.2 describes a multichannel decentralized feedback control system for a fully coupled plant matrix and a method for control stability analysis, a perforated honeycomb panel structure combined with a cavity, and methods for compensating insufficient response at low frequencies. Section 7.3 describes the implementation, the experimental setup, and the numerical model. Section 7.4 presents the stability analysis of the system, where the excitation positions and Nyquist analysis are studied. Various control configurations are discussed in Section 7.5. The control performance, in terms of the measured sound pressure level (SPL) response above the flat panel loudspeaker, is presented and the control principles are given.

7.2 Method

7.2.1 Perforated honeycomb panel

The modal complexity of a panel should be as low as possible to allow the panel to be controlled with a relatively simple control system. Therefore, a honeycomb sandwich structure, which provides high stiffness and low density, is used as the sound-radiating panel. Moreover, the honeycomb sandwich struc-

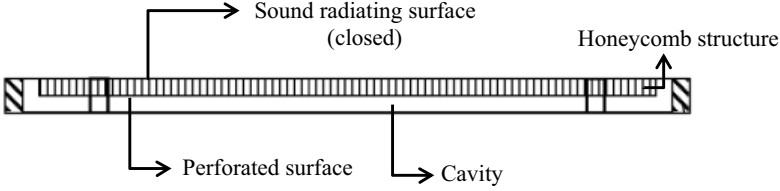


Figure 7.1: Side view of the flat panel loudspeaker configuration.

ture includes one perforated panel, which is connected to a cavity. Thus, the air inside the honeycomb structure can flow in and out to the cavity through the holes in the perforated panel. In other words, the total effective air volume is both the air inside the cavity and the air inside the honeycomb structure. Therefore, the effective air layer thickness is increased, and the dimensions of the cavity can be reduced. Figure 7.1 presents the configuration of the flat panel loudspeaker.

Moreover, the radius of the holes, the distance between the holes, and the area ratio of the holes to the perforated panel are considered to guarantee that the air can flow in and out through the perforated panel with a negligible viscous effect. Based on Beranek's model [138], the acoustic impedance Z_{perf} [N s m^{-3}] of the perforated plate is modeled by

$$Z_{perf} = \frac{\rho}{S_p \sigma} \left\{ \sqrt{2\eta\omega} \left[\frac{t_p}{r} + 2 \left(1 - \frac{\pi r^2}{d_h^2} \right) \right] + j\omega \left[t_p + 1.7r \left(1 - \frac{r}{d_h} \right) \right] \right\}, \quad (7.1)$$

where ρ [kg m^{-3}] is the density of air, S_p [m^2] is the area of the perforated plate, σ is the dimensionless area porosity, η is the dynamic viscosity, ω [rad s^{-1}] is the angular frequency, t_p [m] is the plate thickness, r [m] is the hole radius, d_h [m] is the distance between the holes and j is the unit imaginary number. This model is valid within the frequency range where the frequency f [Hz] satisfies

$$\frac{0.01}{\sqrt{f}} \leq r \leq \frac{10}{f}, \quad (7.2)$$

which indicates that the hole size is much smaller than the acoustic wavelength. For the perforated panel in this study, the model is valid between 15 Hz and 4 kHz. Neglecting the radiation impedance including mass effects, the acoustic impedance of the cavity and the honeycomb plate corresponds

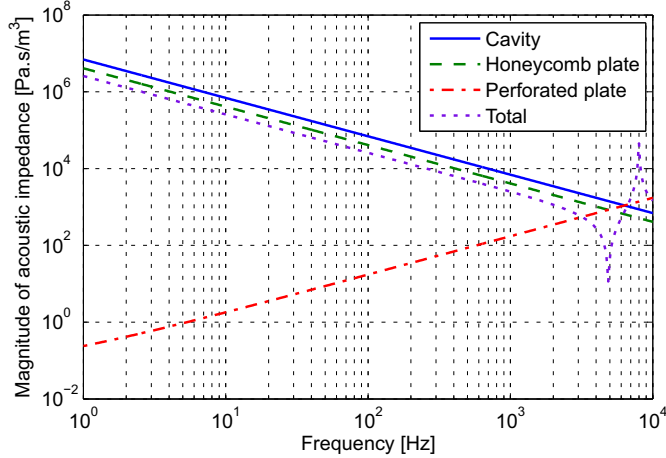


Figure 7.2: Lumped acoustic impedance load as seen by the back of the radiating structure.

to the air volume of the cavity and the hollow space of the honeycomb structure respectively. A lumped-element acoustic model of the perforated panel coupled with the cavity and actuators is constructed. The acoustic impedance frequency response of the perforated panel, honeycomb panel, and cavity is shown in Fig. 7.2. The acoustic impedance of the perforated panel is negligible compared to the cavity and honeycomb panel below 1 kHz.

7.2.2 Multiple decentralized feedback control

To improve the uneven sound frequency response of the panel, we apply a direct velocity feedback control on the panel. This direct velocity feedback control functions as active damping on the panel to flatten the peaks and dips of the response. Then, the feedback control signal is added to the driving signal of the loudspeaker to compensate the colored response. Figure 7.3 illustrates the signal block diagram of a feedback control system. $\mathbf{e}(j\omega)$ is the error signal matrix, where ω is the angular frequency [rad s^{-1}] and $j = \sqrt{-1}$. $\mathbf{G}(j\omega)$ is the plant transfer matrix; $\mathbf{u}(j\omega)$ is the feedback control signal matrix; $\mathbf{d}_d(j\omega)$ is the original driving source matrix, which is the error signal without the input feedback control signal; and $\mathbf{H}(j\omega)$ is the control matrix, which is a constant in

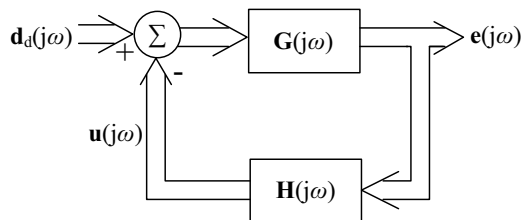


Figure 7.3: Feedback control systems.

the current work. The time-dependent signals are the real part of the complex vectors (i.e., the time-dependent error signal $e(t) = \text{Re}\{e(j\omega)e^{j\omega t}\}$).

From the block diagram in Figure 7.3, $e(j\omega)$ can be derived as

$$\mathbf{e}(j\omega) = [\mathbf{I} + \mathbf{G}(j\omega)\mathbf{H}(j\omega)]^{-1}\mathbf{d}_d(j\omega)\mathbf{G}(j\omega), \quad (7.3)$$

where \mathbf{I} is an identity matrix. To present the physical interactions between each control unit in a multiple-input and multiple-output (MIMO) control system, a fully coupled multiple channel plant transfer matrix $\mathbf{G}(j\omega)$ is applied:

$$\mathbf{G}(j\omega) = \begin{bmatrix} \mathbf{G}_{11}(j\omega) & \cdots & \mathbf{G}_{1m}(j\omega) \\ \vdots & \ddots & \vdots \\ \mathbf{G}_{l1}(j\omega) & \cdots & \mathbf{G}_{lm}(j\omega) \end{bmatrix}, \quad (7.4)$$

where $\mathbf{G}_{lm}(j\omega)$ is the transfer matrix from the m -th actuator to the l -th sensor.

In theory, the stability of a feedback control system can be unconditionally guaranteed when the sensors and actuators are dual and collocated [68]. However, non-ideal conditions exist in practical applications. For a single-input, single-output (SISO) control system, the Nyquist stability criterion is used to determine the stability of the system. The system is stable if and only if the Nyquist plot of $\mathbf{G}(j\omega)\mathbf{H}(j\omega)$ does not cross or encircle $(-1, 0)$. On the other hand, for a MIMO control system, the generalized Nyquist stability criterion is applied. The system is stable if and only if the locus of $\det[\mathbf{I} + \mathbf{G}(j\omega)\mathbf{H}(j\omega)]$ does not cross or encircle the origin $(0, 0)$ [13].

7.2.3 Feed-forward response correction filter

To equalize the response of the loudspeaker at low frequencies, the minimum-phase regularized inverse method (MPRI) method is used [124, 125, 136]. The inverse is based on an $L \times M$ -dimensional transfer function $\mathbf{G}(q)$ obtained from system identification [139], in which q is the unit delay operator. An identified state-space model is augmented with a regularizing function $\mathbf{G}_{reg}(q)$ which limits the gain of the inverse at frequencies for which the magnitude of $\mathbf{G}(q)$ is small. The augmented state-space model is defined by

$$\bar{\mathbf{G}}(q) = \begin{bmatrix} \mathbf{G}(q) \\ \mathbf{G}_{reg}(q) \end{bmatrix}. \quad (7.5)$$

An inner-outer factorization of the augmented state-space model

$$\bar{\mathbf{G}}(q) = \bar{\mathbf{G}}_i(q)\bar{\mathbf{G}}_o(q), \quad (7.6)$$

is used to determine an $M \times M$ -dimensional minimum-phase transfer function having a stable inverse, for which $\bar{\mathbf{G}}_o^{-1}(q)\bar{\mathbf{G}}_o(q) = \mathbf{I}_L$, in which \mathbf{I}_L is the identity matrix of dimensions L . The $L \times M$ -dimensional transfer function $\bar{\mathbf{G}}_i(q)$ is all-pass, i.e., $\bar{\mathbf{G}}_i^*(q)\bar{\mathbf{G}}_i(q) = \mathbf{I}_M$, in which the asterisk denotes the adjoint operator $\bar{\mathbf{G}}_i^*(q) = \bar{\mathbf{G}}_i^T(q^{-1})$, in which T denotes transpose and \mathbf{I}_M is the identity matrix of dimensions M . The all-pass property can be used to show that $\bar{\mathbf{G}}_o^*(q)\bar{\mathbf{G}}_o(q) = \bar{\mathbf{G}}^*(q)\bar{\mathbf{G}}(q) = \mathbf{G}^*(q)\mathbf{G}(q) + \mathbf{G}_{reg}^*(q)\mathbf{G}_{reg}(q)$. The inverse is used as the minimum-phase feed-forward response correction filter.

An approximate method to increase the insufficient response of the loudspeaker at low frequencies is to apply a Linkwitz filter as the feed-forward response correction filter. Figure 7.4 presents the frequency response of an uncompensated loudspeaker, a second-order Linkwitz filter, and a desired loudspeaker. The transfer function of the Linkwitz filter is obtained by dividing the transfer function of the desired loudspeaker with that of the uncompensated loudspeaker.

$$\mathbf{G}_u(s) = \frac{s^2 T_u^2}{s^2 T_u^2 + \frac{s T_u}{Q_u} + 1}, \quad (7.7)$$

$$\mathbf{G}_d(s) = \frac{s^2 T_d^2}{s^2 T_d^2 + \frac{s T_d}{Q_d} + 1}, \quad (7.8)$$

$$\mathbf{L}(s) = \frac{\mathbf{G}_d}{\mathbf{G}_u} = \frac{s^2 T_u^2 T_d^2 + \frac{s T_u T_d^2}{Q_u} + T_d^2}{s^2 T_u^2 T_d^2 + \frac{s T_u^2 T_d}{Q_d} + T_u^2}, \quad (7.9)$$

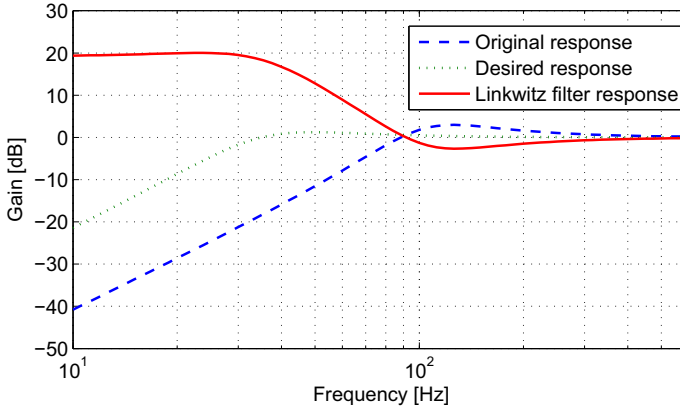


Figure 7.4: Frequency response: an uncompensated loudspeaker, a second-order Linkwitz filter, and a desired response.

where s is the Laplace transform parameter. Equation (7.7) presents the original Laplace-domain transfer function of the uncompensated loudspeaker $G_u(s)$. Equation (7.8) is the desired Laplace-domain transfer function of the loudspeaker $G_d(s)$. The Laplace-domain transfer function of the Linkwitz filter $L(s)$ is expressed as Eq. (7.9). T_u, Q_u, T_d , and Q_d are the coefficients related to the properties of the loudspeaker.

7.3 Implementation and numerical model

This section describes our implementation, experimental setup, and numerical model. First, the panel structure, driving force, control sensors, and measurement setup are described. Then, the acoustic-structural coupled numerical model is introduced. The model validation is presented in the final section.

7.3.1 Implementation

We used a 0.5-mm-thick aluminum panel as the closed upper layer of the honeycomb sandwich structure. The perforated lower layer was a 0.3-mm-thick perforated steel panel with holes 5 mm in diameter. These two panels were connected by an aluminum honeycomb structure, as shown in Fig. 7.5. The honeycomb sandwich panel had a volume of $605 \times 415 \times 22 \text{ mm}^3$ and a weight of 1.112 kg. The lower perforated panel was attached to a cavity with a depth of 13 mm. The perforated honeycomb panel was suspended by ethylene propylene diene monomer (EPDM) rubber with a thickness of 1 mm and a width of 15 mm. Five voice coil actuators (BEI Kimco Magnetics, type: LA18-12-000A, linear voice coil actuator) were mounted on the lower layer of the perforated honeycomb panel, as shown in Fig. 7.6. Each actuator provides a peak force of 44.5 N and a maximum stroke of 3 mm in both sides. The DC resistance and the force sensitivity of the actuator are 2.6Ω and 7.78 N/Ampere. Five accelerometers (B&K, type:4517-002, piezoelectric shear accelerometer), which functioned as the error sensor for the direct velocity feedback control, were mounted to the upper layer and collocated with the voice coil actuators. The real-time control platform was realized on a field-programmable gate array (FPGA) with a sam-

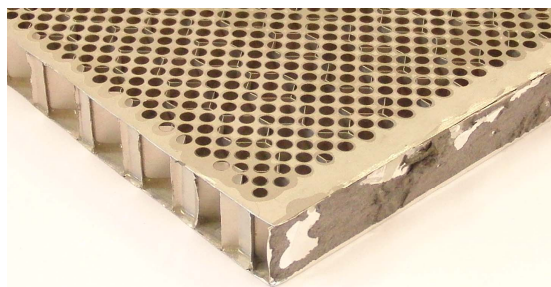


Figure 7.5: The perforated honeycomb panel.

pling frequency of 100 kHz. Furthermore, an amplifier designed by H. Kuipers, University of Twente, was applied to provide the driving current for the voice coil actuators. This amplifier delivered a proportional output current to an input voltage with a constant ratio of 2 Ampere/Volt. Detailed data of the voice coil actuator, the accelerometer and the amplifier can be found in Appendices A, B and C. The back view of the flat panel loudspeaker is shown in Fig. 7.7. The near field sound pressure was measured 5 cm above the panel, as shown in Fig. 7.8.

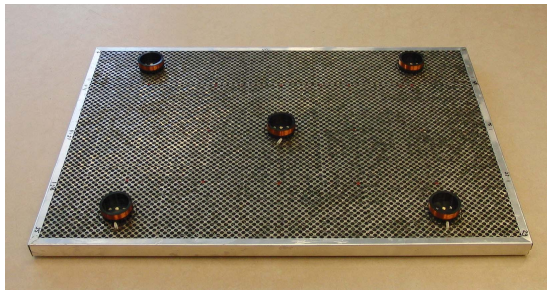


Figure 7.6: Five voice coil actuators were mounted on the perforated honeycomb panel as the driving actuators.

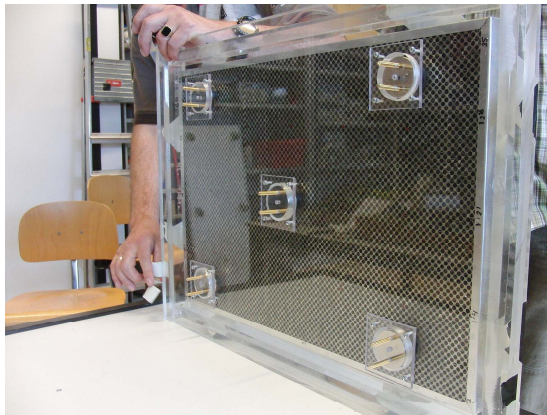


Figure 7.7: Back view of the flat panel loudspeaker.

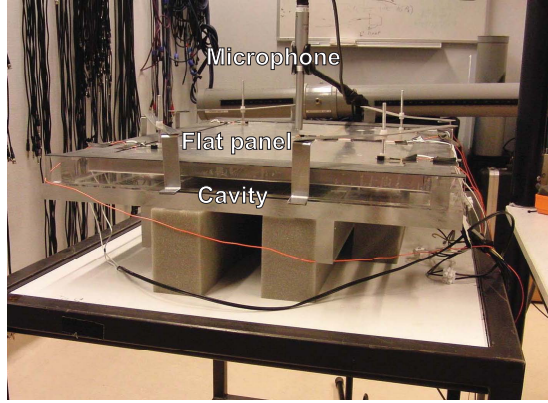


Figure 7.8: The radiated sound pressure level was measured 5 cm above the flat panel loudspeaker.

7.3.2 Numerical model

FEM model

We used the finite element method (FEM) with COMSOL Multiphysics 4.3b (COMSOL, Inc., Burlington, MA 01803, USA) to model our system. The acoustic and structural properties were considered simultaneously to more accurately model the system. Two domains, a fluid domain and a solid domain, were used to model the acoustic and structural properties. The interactions between these two domains were applied to both sides to provide a more accurate model. These two domains are linked as described below. In the solid domain, the pressure load (normal force per unit area) on the structure \mathbf{F}_p [N m^{-2}] produced by the fluid pressure p_a [Pa] on the fluid-solid interacting boundaries is given by

$$\mathbf{F}_p = -\mathbf{n} \cdot p_a, \quad (7.10)$$

where \mathbf{n} is the normal vector of the solid boundaries. In the acoustic fluid domain, the normal acceleration to the acoustic pressure a_n [m s^{-2}] on the fluid-solid interacting boundaries can be derived from the second derivatives of the structural displacements with respect to time \mathbf{u}_{tt} [m s^{-2}]:

$$a_n = \mathbf{n} \cdot \mathbf{u}_{tt}. \quad (7.11)$$

The interaction between the acoustic field and solid structure can be stud-

ied by applying Eqs. (7.10) and (7.11). The following simplifications have been made. First, a homogeneous solid panel was used to model the perforated honeycomb panel. Second, instead of modeling the air volume inside the honeycomb structure, the total effective air volume was modeled by increasing the air volume inside the cavity. Third, the force of the voice coil actuator was modeled as a point force. The weight of the voice coil actuators and accelerometers were modeled as additional masses on the panel according to their positions. Finally, the suspension was modeled as springs among the edges of the panel. The detailed model parameters are provided in Table 7.1.

Table 7.1: Model parameters.

	Parameters	Values	Unit
Flat panel	Dimensions	$605 * 415 * 22$	$[\text{mm}^3]$
	Density	201	$[\text{kg m}^{-3}]$
	Young's modulus	3.1	$[\text{GPa}]$
	Poisson's ratio	0.33	
	Loss factor	0.06	
Cavity	Inner dimensions	$605 * 415 * 28$	$[\text{mm}^3]$
	Rigid boundary		
Additional mass	Weight	0.4	$[\text{kg}]$
Suspensions	Spring constant per unit length (parallel to the panel surface)	666	$[\text{kN m}^{-2}]$
	Spring constant per unit length (normal to the panel surface)	66.6	$[\text{kN m}^{-2}]$
	Loss factor	0.4	

Model validation

Here, the resonance frequencies and kinetic energy responses obtained in the simulations and experiments are compared to validate our numerical model. First, an impact hammer modal test was conducted to measure the resonance frequencies of the honeycomb perforated panel, which was not attached to the cavity as shown in Fig. 7.9 [140]. Table 7.2 presents the measured and simulated resonance frequencies of the perforated honeycomb panel.



Figure 7.9: Setup of the impact hammer modal test.

Table 7.2: Resonance frequencies of the perforated honeycomb panel.

Resonant Mode	Experiment [Hz]	Simulation [Hz]	Error [%]
1	221	218	-1.4
2	256	243	-5.1
3	506	510	0.8
4	571	541	-5.3
5	611	643	5.2
6	775	752	-3.0

Then, the perforated honeycomb panel was attached to the cavity. The response of the panel was measured while the panel was excited by a shaker. The panel response was measured twice with two different excitation points to avoid measurement errors as shown in Fig. 7.10 [140]. The measured and simulated resonance frequencies of the panel-cavity coupled system are provided in Table 7.3.



Figure 7.10: Setup of the shaker test.

Table 7.3: Resonance frequencies of the panel-cavity coupled system.

Resonant Mode	Experiment [Hz]	Simulation [Hz]	Error [%]
1	42	40	-4.8
2	152	140	-7.9
3	195	170	-12.8
4	200	230	15.0
5	286	290	1.4
6	354	390	10.2
7	443	460	3.8
8	510	550	7.8

To further validate the model, the measured and simulated kinetic energy response of the panel, which was excited by five voice coil actuators, was compared, as shown in Fig. 7.11. The data obtained from the simulations and experiments differ because we used a homogeneous solid panel to model the honeycomb perforated panel. The results demonstrate that our numerical model can estimate our system with reasonable error.

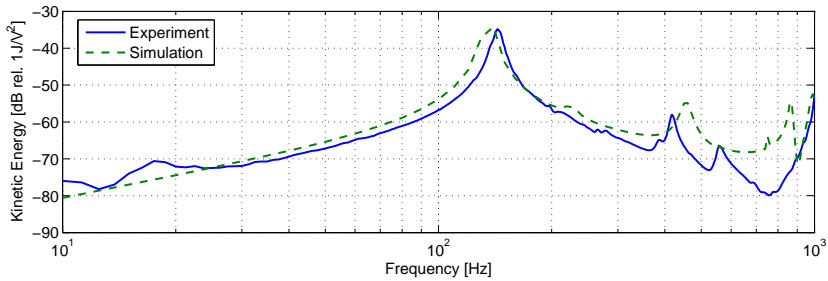


Figure 7.11: Kinetic energy response of the panel excited by five voice coil actuators in parallel connection.

7.4 Control stability

The vibration and sound radiation response of the flat panel greatly depends on the excitation positions. A designed excitation position can reduce the complexity of the response. A less complex control system can provide a more stable and easier feedback control condition. Therefore, we compared the panel response of various excitation positions to determine the excitation configuration. Moreover, a well-designed sensor-actuator configuration can increase the control stability in the feedback control system. Next, another stability analysis is presented. We used the Nyquist criterion and generalized Nyquist criterion to determine and present the control stability of our system. Three sensor-actuator configurations, which are two SISO control systems and one distributed MIMO control system, are presented. The frequency range of the analysis is 10 Hz to 1 kHz, where the benefit of this flat panel loudspeaker is expected.

7.4.1 Excitation positions

We applied voice coil actuators on the panel to excite the panel. However, the positions of the actuators affect the vibration response of the flat loudspeaker system. The energy of the near field sound pressure wave is related to the kinetic energy of the radiating panel at lower modes [122]. Therefore, the kinetic energy of the radiating panel can represent the near field sound. In this section, we used the kinetic energy response of the panel to analyze the effect of the excitation positions. The measured radiated sound pressure response of the panel is presented in the next section. Figure 7.12 presents three exci-

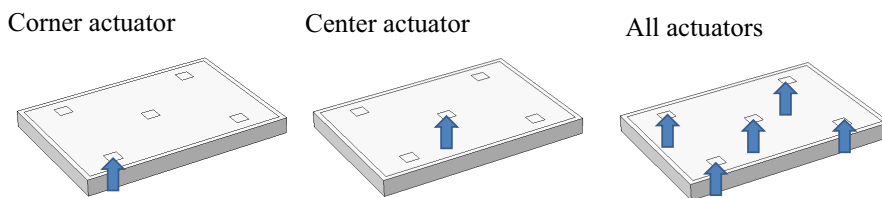


Figure 7.12: Excitation positions.

tation position configurations. The first configuration, where we applied one actuator located in the corner of the panel, provided an asymmetric excitation force. The second configuration, where we applied one actuator located in the center of the panel, provided a symmetric excitation force. The third configuration, where we applied five equally distributed actuators on the panel in parallel connection, provided a symmetric and equally distributed excitation force. Figure 7.13 presents the variations in the simulated kinetic energy response of the panel for varying excitation positions. The corner actuator, which located asymmetrically to the panel, excited numerous resonant modes of the system and caused high modal density. However, a symmetrically located actuator, for example the center actuator, excited fewer resonant modes than an asymmetrically located actuator. Moreover, applying an equally distributed excitation force, as in the all-actuator configuration, can further reduce the modal density. A less complex panel vibration can provide a more stable and easier feedback control condition. Therefore, the system design should avoid asymmetric excitation positions. Similar results were found in the measured data as shown in Figure 7.14. Furthermore, both the simulated and measured results indicated that there was a major resonance peak at very low frequencies when

the corner actuator was applied. The resonance frequency of this peak was mainly affected by the suspension properties. The approximate estimation of the suspension properties in our numerical model caused the difference in the resonance frequency of this peak. The mode shape is shown in Fig. 7.15. The excitation force should avoid amplifying this resonant mode, for instance, by applying the same excitation force to the upper-right and lower-left corners.

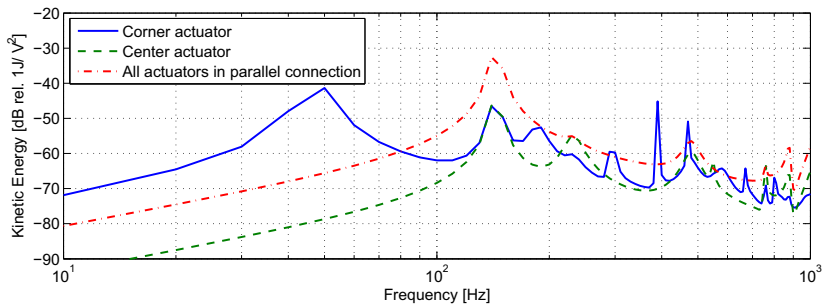


Figure 7.13: Simulated kinetic energy response of the panel with various excitation positions.

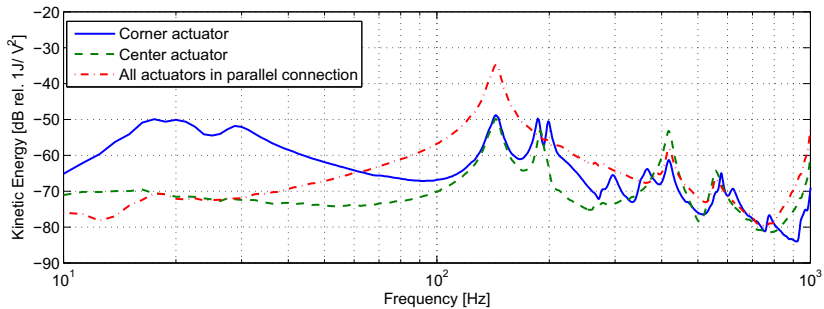


Figure 7.14: Measured kinetic energy response of the panel with various excitation positions.

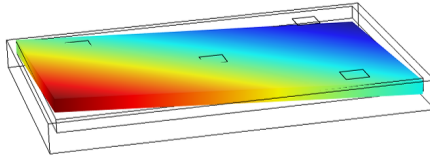
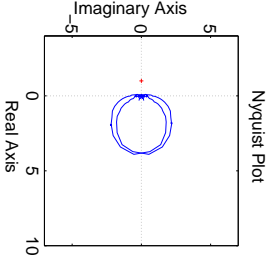
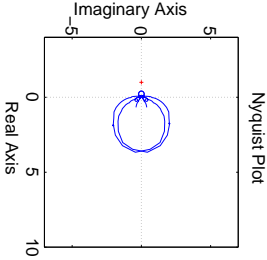
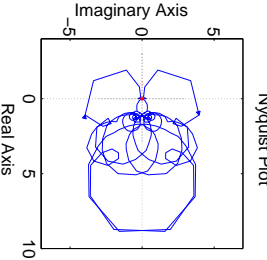


Figure 7.15: Illustration of the mode shape.

7.4.2 Nyquist stability analysis

The results from the previous section illustrate that driving all actuators with the same signal excites fewer resonant modes; in other words, a single-output control system with an equally distributed force provides a less complex system. However, a distributed control system with multiple controllers provides better controllability and can be applied to a large-scale system without a complicated control loop. Moreover, distributed multiple controllers have better failure tolerance in the sense that the failure of one controller does not directly affect other controllers. Therefore, in this section, we used the Nyquist criterion and generalized Nyquist criterion to determine the stabilities of the SISO and MIMO control systems. Two cases of the SISO feedback control system were analyzed. In the first case, the error signal was measured by the center sensor, and the same control signal was sent to all five actuators. In the second case, one of the corner sensors was used as the error sensor, and the five actuators were driven by the same control signal. The distributed MIMO control system discussed in this section used five sensors, and the control signal was fed back individually to the collocated actuators. The Nyquist plots and stability of these three cases with a same control gain are shown in Table 7.4. As introduced in Section 2.3.3, the gain stability index and phase stability index were used in the MIMO control system. From the analysis, both of the SISO control systems provide better stabilities than the MIMO control system. Furthermore, the crossover frequency of the MIMO control system occurs at a very low frequency with a small control gain. However, the response is more stable, except for the first resonant mode. This result agrees with the previous section. The system resonance at 15 Hz is effectively excited when driving on the corner actuator. The distributed MIMO control system drives these five actuators independently. Using non-identical driving forces yields the same effect as driving on the corner position only. Therefore, this type of excitation force should be avoided.

Table 7.4: Nyquist stability analysis.

	SISO with corner sensor	SISO with center sensor	MIMO 5 channels
Nyquist plot			
Gain margin \ stability index	17	2.4	0.98
Phase margin \ stability index	92	94	1.9
Gain crossover frequency [Hz]	28	417	15
Phase crossover frequency [Hz]	129	129	15

7.5 Control results

In this section, the SPLs measured above the flat panel loudspeaker resulting from various control configurations are presented. First, two configurations of the SISO feedback control system are presented. Then, a sensor-actuator configuration designed MIMO control system to further improve the performance is presented. Furthermore, the principles of sensor-actuator configuration design are provided. Another MIMO control configuration is presented as an example to demonstrate the principles. Finally, the feedback control is combined with a feed-forward control to improve the insufficient response of the flat loudspeaker at low frequencies.

7.5.1 Feedback control configurations

SISO control system

Section 7.4 illustrates that a SISO control provides more stability than a MIMO control in our system. Therefore, we began with the SISO control. We used only one sensor to obtain the error signal and then applied the identical control signal to all five voice coil actuators. Two sensor positions were analyzed in this study; the configurations are shown as Fig. 7.16. Because the accelerometer and voice coil actuator were neither dual nor collocated, the feedback control loop was only conditionally stable. The stability can be guaranteed when the Nyquist plot of $G(j\omega)H(j\omega)$ does not cross or encircle $(-1, 0)$. The Nyquist plots of the system are shown in Table 7.5. Figures zoomed in near $(-1, 0)$ are listed in Table 7.5 and confirm the stability.

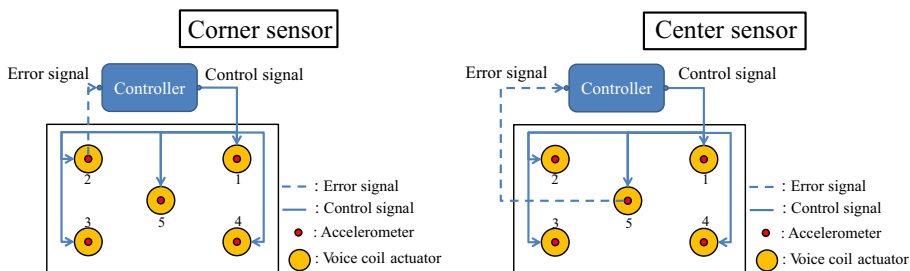


Figure 7.16: Two configurations of SISO control.

The near field SPL response of the control results is shown in Fig. 7.17. The first resonance peak was greatly reduced by both of the control configurations. However, the resonance peak at 420 Hz was only slightly reduced when using the corner sensor and was actually increased when using the center sensor. This resonance at 420 Hz causes control system instability, as shown in Table 7.5. Further sensor-actuator configuration design is necessary to further improve the SPL response.

Table 7.5: Two configurations of a SISO control, the Nyquist plot of $\mathbf{G}(j\omega)\mathbf{H}(j\omega)$ from 10 Hz to 1 kHz.

Configuration	the Nyquist plot of $\mathbf{G}(j\omega)\mathbf{H}(j\omega)$	Zoomed around (-1, 0)
Corner sensor		
Center sensor		

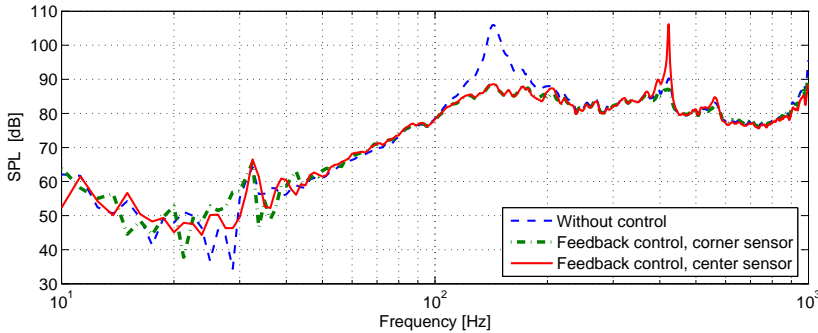


Figure 7.17: Measured SPL response of the flat loudspeaker with a SISO feedback control.

MIMO control system

To improve the control performance at 420 Hz, we further investigated the resonant mode shape at this frequency. Figure 7.18 presents the mode shape at 420 Hz for both the measured and simulated results. The mode shape illustrates that the center point moves opposite to the corner points at this frequency. Therefore, use of either the center sensor or corner sensor cannot fully present the vibration of the panel. Additional sensors are necessary to accurately detect the vibration of the panel. Nevertheless, the figure illustrates that these four corner points move together at this resonance frequency. Therefore, two sensors are sufficient to further improve the control performance at 420 Hz. We applied two sensors, with one center sensor as the error sensor to the center actuator and one corner sensor as the error sensor to the four corner actuators. Figure 7.19 shows the sensor-actuator configuration. The Nyquist plots of the system are shown in Table 7.6. The figures zoomed in around the

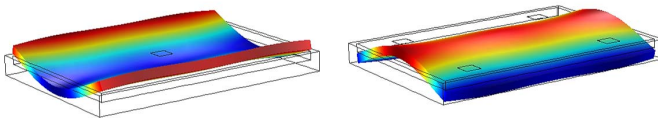


Figure 7.18: Mode shape at 420Hz.

origin are listed in the table to confirm the stability of the system. The near field SPL response of the control results is shown in Fig. 7.20. With this 2-channel control, both the first resonance peak and the resonance peak at 420 Hz can be effectively reduced. The result illustrates that all of the resonance peaks below 1 kHz can be effectively reduced by this control configuration.

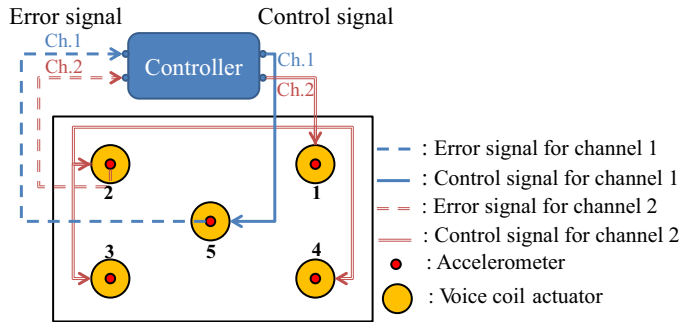
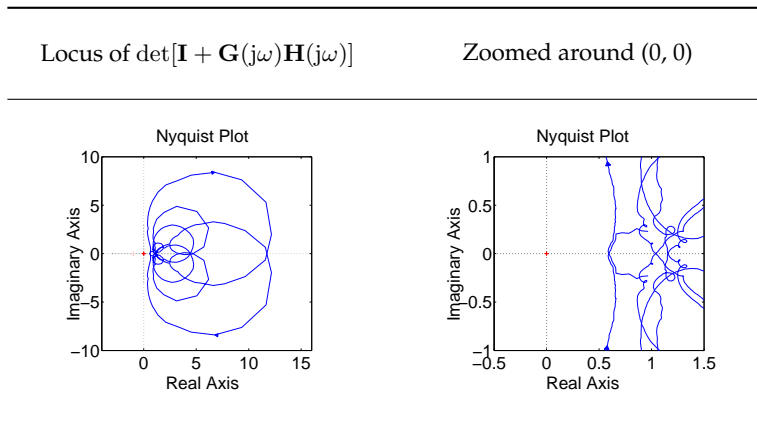


Figure 7.19: Configuration of the 2-channel MIMO control.

Table 7.6: 2-channel MIMO control, locus of $\det[\mathbf{I} + \mathbf{G}(j\omega)\mathbf{H}(j\omega)]$ from 10 Hz to 1 kHz.



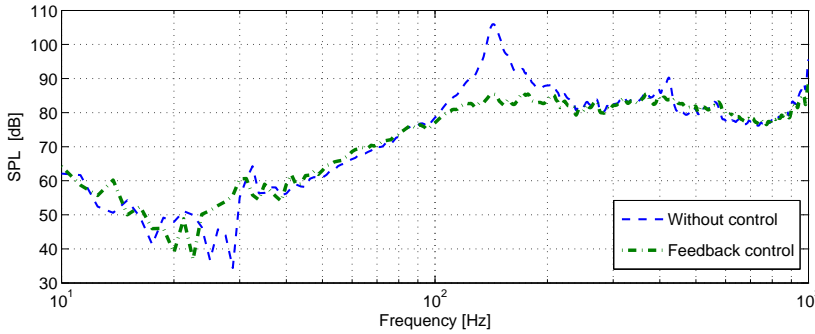


Figure 7.20: Measured SPL response of the flat loudspeaker with a 2-channel MIMO feedback control.

Example

A further sensor-actuator analysis based on the previous results is presented in this section. The design follows two principles. First, the excitation positions should be symmetric, and second, the sensor-actuator configuration should consider the fact that the center point moves in the opposite direction to the corner points at the resonance frequency 420 Hz. As an example, a 3-channel MIMO control system was measured in this study. Three sensors were applied: the center sensor as the error sensor to the center actuator and two corner sensors as the error sensors to two pairs of the corner actuators, as shown in Fig. 7.21.

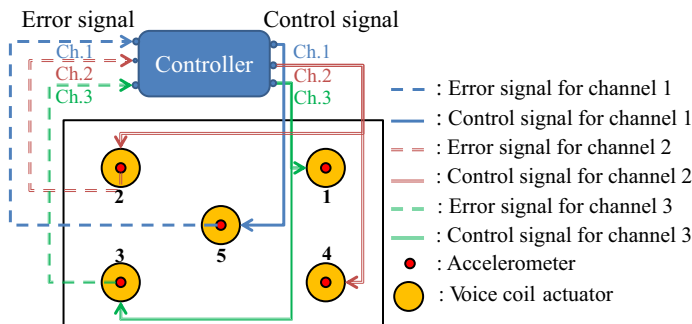


Figure 7.21: Configuration of the 3-channel MIMO control.

The Nyquist plots of the system are shown in Table 7.7. The figure zoomed in near the origin is shown in the table to confirm the stability of the system. The near field SPL response of the 3- and 2-channel control configurations is shown in Fig. 7.22. The figure illustrates that the 3- and 2-channel MIMO control systems performed similarly.

Table 7.7: 3-channel MIMO control, locus of $\det[\mathbf{I} + \mathbf{G}(j\omega)\mathbf{H}(j\omega)]$ from 10 Hz to 1 kHz.

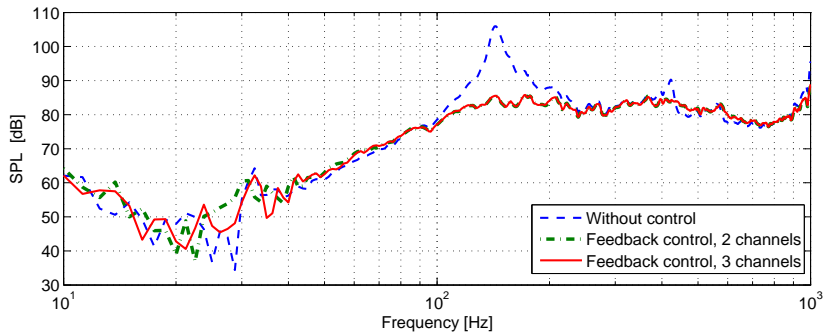
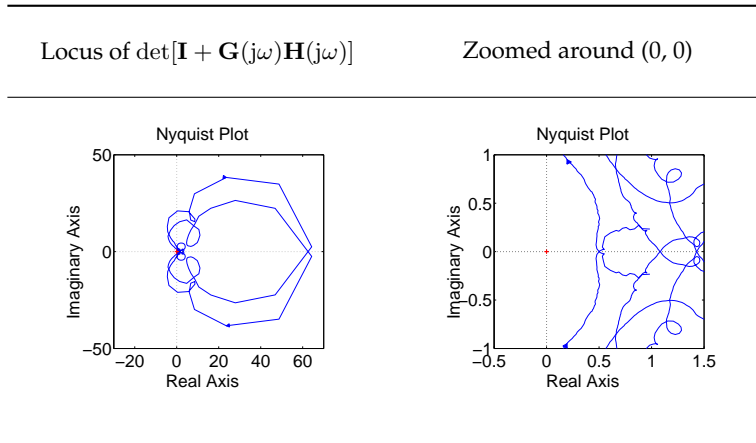


Figure 7.22: Measured SPL response of the flat loudspeaker with a MIMO feedback control: 2-channel configuration and 3-channel configuration.

7.5.2 Response equalization at low frequencies

In this section, we applied a feed-forward response correction filter to further improve the insufficient response of the loudspeaker at low frequencies. Three filters, which includes two MPRI filters and one Linkwitz filter, to compensate the measured feedback controlled response are presented in Fig. 7.23. The first MPRI filter equalized a single pressure response and the second MPRI filter was obtained by five accelerometers. The result indicates there is good potential for the MPRI filter applied in a MIMO control system. Furthermore, the second-order Linkwitz filter gives similar compensation to the MPRI filter, which offers the optimum response equalization as shown in Fig. 7.24. Therefore, we implemented the second-order Linkwitz filter with 35 and 105 Hz cut-off frequencies to the real-time control system. The measured near field SPL response above the loudspeaker resulting from 2- and 3-channel dis-

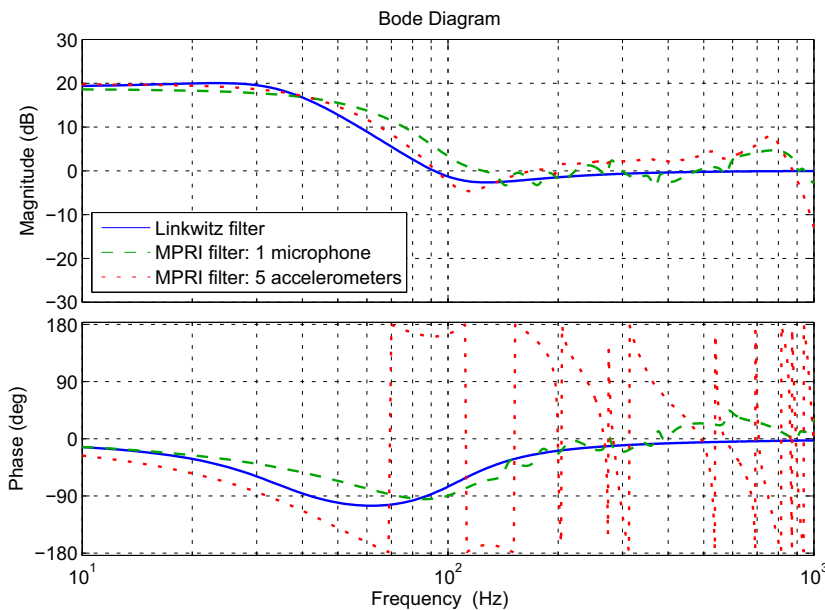


Figure 7.23: Bode plot of three filters based on measured feedback controlled response: the Linkwitz filter, the MPRI filter with one microphone, and the MPRI filter with five accelerometers.

tributed feedback and feed-forward combined MIMO control systems is shown in Fig. 7.25. The response illustrates that with the feed-forward control, the attenuated response of the loudspeaker at low frequencies can be compensated without affecting the feedback control performance.

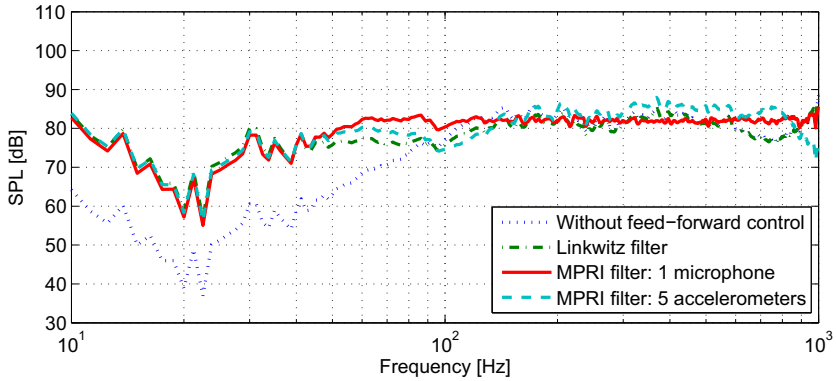


Figure 7.24: Simulated SPL response equalization based on measured feedback controlled response: without equalization, with the Linkwitz filter, the MPRI filter with one microphone, and the MPRI filter with five accelerometers.

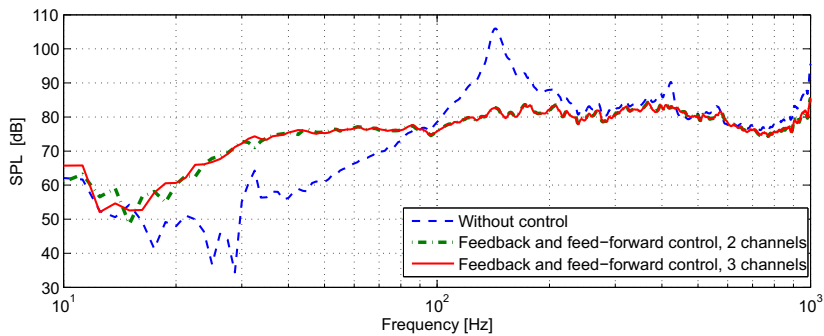


Figure 7.25: Measured SPL response of the flat loudspeaker with a feedback and feed-forward combined MIMO control: 2-channel configuration and 3-channel configuration.

7.6 Conclusions

This chapter presents an acoustic source with a small thickness that provides an even sound frequency response. The real-time control results indicate that the frequency response of the radiated sound from a perforated honeycomb panel combined with a thin cavity can be greatly improved by applying a simple and stable distributed feedback and feed-forward combined control to the panel. However, an inappropriate sensor-actuator configuration could easily destabilize the asymmetric resonant modes caused by the coupling of the internal acoustic cavity and the rigid body vibration of the panel. In particular, it was shown that a straightforward decentralized controller based on collocated force actuators and velocity sensors fails to meet the performance requirement because of a destabilizing mode at 15 Hz. The detailed stability analysis in this chapter illustrates that more sensor-actuator control channels cannot guarantee the control stability. In contrast, fewer channels can provide a stable control system if the sensor-actuator configuration follows the design principle that the excitation force should be symmetrically applied on the panel. A designed set of independent combinations of symmetric driving patterns with corresponding velocity feedback controllers can effectively control both the fundamental mass-air resonance and lower bending modes of the panel. However, the minimum number of sensors depends on the mode shapes within the working bandwidth. The perforated honeycomb panel presented in this work provides efficient space utilization and a lower modal density. Therefore, the distributed feedback control system can effectively flatten the sound frequency response of the perforated honeycomb panel below 1 kHz with only two accelerometer sensors. Finally, as an example of the compensation scheme for the response at low frequencies, the Linkwitz filter, which provides a similar result to the optimum equalization offering by the MPRI filter in this study, was applied as the feed-forward control. A flat frequency response in the range of 30 Hz to 1 kHz with deviations smaller than 3 dB was obtained.

Conclusions

8.1 Conclusions

In this thesis, we have presented methods to reduce transmitted noise through a double panel structure and have developed control sources to improve the performance. In this final chapter, we summarize our research results, answer the research questions and suggest potential directions for future work.

- **Decentralized structural feedback control**

Both numerical analysis and experimental results showed that with direct velocity feedback control, piezoelectric actuators should be simultaneously applied to the incident panel and radiating panel in a double panel structure. This strategy is required because the resonant energy in a double panel structure is not only determined by the radiating panel but also by the incident panel and cavity. Therefore, structural control should be applied to both panels. However, the interaction between the two panels reduces the control stability and limits the control performance. Moreover, structural control can barely reduce the resonant energy, which is dominated by the cavity resonance.

- **Decentralized cavity feedback control**

A comparison has shown that for the configuration presented in the current work, cavity control can provide more noise reduction than structural control and structural-cavity combined control. Therefore, three types of cavity control sources were compared: an acceleration source loudspeaker, an incident pressure source loudspeaker, and a pressure-controlled source loudspeaker. The results have shown that the incident pressure source loudspeaker can achieve the largest total kinetic energy

decrease of 13.3 dB and the largest total radiated sound power decrease of 13.2 dB within the frequency range from 10 Hz to 1 kHz.

- **Decentralized feed-forward and feedback combined control**

To further improve the transmitted noise reduction, we combined the decentralized direct feedback control with the decentralized harmonic feed-forward control. Comparison between various sensor-actuator configurations indicates that using piezoelectric patches on the radiating panel with feed-forward control combined with incident pressure source loudspeakers with feedback control can provide the largest transmitted noise reduction for the double panel structure presented in the current work within the frequency range from 10 Hz to 1 kHz.

- **One-dimensional realization of the incident pressure source loudspeaker**

The incident pressure source is a pressure source for which there is no reflecting pressure from the boundary. This source can be realized by minimizing the reflecting pressure from the solid surface. A one-dimensional incident pressure source loudspeaker has been realized by using a dynamic loudspeaker, a microphone, a particle velocity sensor and a feed-forward controller. The real-time measurement showed that the reflecting pressure was reduced by 26.2 dB on average and that the pressure resonance in the duct can be effectively removed.

- **Three-dimensional model of the incident pressure source loudspeaker**

The three-dimensional incident pressure source has been numerically modeled by using a dynamic loudspeaker, a distributed microphone and a distributed velocity sensor with feedback control. Similar to the one-dimensional case, the incident pressure source is obtained by minimizing the reflecting pressure. Minimizing the reflecting pressure in the direction perpendicular to the loudspeaker surface can provide better control performance than minimizing the total pressure or the reflecting pressure in other directions. This dynamic loudspeaker modified as the incident pressure source loudspeaker has been numerically applied to the double panel structure and the transmitted noise was effectively reduced.

- **Frequency response improvement of a flat panel loudspeaker**

To improve the frequency response of the flat panel loudspeaker, two methods were applied. The frequency response of a flat panel loudspeaker can be flattened by applying direct velocity feedback control on

the panel, and the insufficient acoustic response of the loudspeaker at low frequencies can be compensated by applying frequency equalization based feed-forward control. Real-time control results indicate that the frequency response of the radiated sound from a perforated honeycomb panel combined with a thin cavity can be greatly improved by applying a simple and stable distributed feedback and feed-forward combined control to the panel.

- **Stability of driving the flat panel loudspeaker**

An inappropriate sensor-actuator configuration could easily destabilize the asymmetric resonant modes caused by the coupling of the internal acoustic cavity and the rigid body vibration of the panel. The detailed stability analysis in Chapter 7 illustrates that more sensor-actuator control channels cannot guarantee the control stability. In contrast, fewer channels can provide a stable control system if the sensor-actuator configuration follows the design principle that the excitation force should be symmetrically applied on the panel.

- **Performance of the perforated honeycomb panel loudspeaker**

The principles of driving the flat panel loudspeaker with stable direct feedback control have been presented. Moreover, the perforated honeycomb panel presented in this work provides efficient space utilization and low modal density. Therefore, the distributed feedback control system can effectively flatten the sound frequency response of the perforated honeycomb panel below 1 kHz with only two accelerometer sensors. Finally, a second-order Linkwitz filter, which was found to provide similar performance to the optimum frequency equalization offered by the MPRI filter in this study, was applied to compensate the insufficient response at low frequencies. A flat frequency response in the range of 30 Hz to 1 kHz with deviations smaller than 3 dB was obtained.

The main contributions of the current work are:

- Various decentralized feedback control strategies, including structural and acoustic sensor-actuator configuration designs, to reduce noise transmission through the double panel structure have been numerically compared, all of which are based on identical control stability indexes.
- Effective decentralized feed-forward and feedback combined control strategies for the transmitted noise reduction through the double panel structure are presented.

- A one-dimensional incident pressure source has been realized by using a dynamic loudspeaker, a microphone and a particle velocity sensor with feed-forward control. A three-dimensional incident pressure source has been numerically modeled by using a dynamic loudspeaker, a distributed microphone and a distributed velocity sensor with feedback control.
- A flat panel loudspeaker with small thickness, which can offer a flat frequency response in the range of 30 Hz to 1 kHz with deviations smaller than 3 dB, is realized.

8.2 Answers to the research questions

We shall now answer the research questions posed in Chapter 1.

- **What kind of resonance dominates transmitted noise through a double panel structure?**

The results show that in the range of 10 Hz to 1 kHz, every resonance peak of the transmitted noise response of the double panel structure presented in the current work is dominated by one of the following: the incident panel resonance, the radiating panel resonance, or the cavity resonance. However, there is no single structural/cavity resonance that dominates the transmitted noise resonance in the whole frequency range.

- **With decentralized feedback control, controlling which part of the double panel structure offers more transmitted noise reduction: the cavity, the incident panel, or the radiating panel?**

Both numerical analysis and experimental results showed that with direct velocity feedback control, piezoelectric actuators should be simultaneously applied to the incident panel and radiating panel in a double panel structure. However, because of the interference between these two panels, the control gain of both panels was limited. Moreover, direct velocity feedback control can barely reduce the resonant energy, which is dominated by the cavity resonance. The comparison indicates that decentralized feedback cavity control can provide more noise reduction than decentralized feedback structural control for the configuration presented in the current work within the frequency range from 10 Hz to 1 kHz.

- **Can the decentralized feedback control performance be further improved by combining other control strategies?**

We have combined decentralized direct feedback control with decentralized harmonic feed-forward control. With the noise reduction comparison between various sensor-actuator configurations, piezoelectric patches on the radiating panel with feed-forward control combined with incident pressure source loudspeakers with feedback control was found to effectively provide further transmitted noise reduction.

- **Do we already have good control sources for the transmitted noise control? If not, what kind of control source is needed?**

Two effective control sources have been introduced and developed in our work:

1. Incident pressure source loudspeaker

A one-dimensional incident pressure source has been realized by using one dynamic loudspeaker, a microphone, a particle velocity sensor and a feed-forward controller. Furthermore, this modified loudspeaker has been numerically modeled in three dimensions by using a dynamic loudspeaker, a distributed microphone, a distributed velocity sensor, and a feedback controller.

2. Flat panel loudspeaker

A flat panel loudspeaker with a small thickness that provides a smooth sound frequency response in the range of 30 Hz to 1 kHz with deviations smaller than 3 dB has been developed by using a perforated honeycomb panel and a designed set of independent combinations of symmetric driving patterns with corresponding velocity feedback controllers.

8.3 Potential directions for future work

- **Use other error signals for the incident pressure control sources in the feed-forward part.**

In Chapter 5, we found that the incident pressure sources provide the largest transmitted noise reduction for the configuration presented in the current work within the frequency range from 10 Hz to 1 kHz when used as the feedback control sources. However, the incident pressure sources hardly provide any noise reduction in the feed-forward part. An interesting direction for future analysis is to use other error signals for the

incident pressure source control in feed-forward control. For instance, the error sensors on the radiating panel.

- **Realize the incident pressure source with feedback control.**

A three-dimensional model has shown that this incident pressure source can be obtained by using a dynamic loudspeaker, a distributed microphone and a distributed velocity sensor with feedback control. And this incident pressure source applied as the feedback control source provides the largest transmitted noise reduction among other control sources presented in the current work. Therefore, a three-dimensional realization of this incident pressure source with feedback control is an interesting topic for further exploration.

- **Use piezoelectric patches as the actuators of the flat panel loudspeaker.**

Energy consumption is an issue for loudspeakers at low frequencies. Compared to moving-coil actuators, piezoelectric actuators as the loudspeaker driving actuators provide several advantages: (1) theoretically, piezoelectric actuators can keep large strain/displacement without power consumption; (2) the energy has the potential to be continuously transferred between the piezoelectric materials and the compressed air in the cavity; and (3) piezoelectric actuators have compact dimensions. Therefore, using piezoelectric patches as the actuators is a potentially interesting research direction.

- **Use carbon fiber reinforced plastic for the sound radiation panel of the flat panel loudspeaker.**

The sound radiation panel of the flat panel loudspeaker with a low density and high bending stiffness offers low modal density and high electroacoustic conversion efficiency. Low modal density reduces the complexity of the panel vibration, which provides a more stable control condition. Therefore, we use a honeycomb sandwich structure as the sound radiation panel. In the current work, the honeycomb sandwich panel is made of metal materials. The performance of the flat panel loudspeaker can be improved by replacing the metal part with a material which has low density and high stiffness, such as carbon fiber reinforced plastic (CFRP).

Bibliography

- [1] Q. Mao and S. Pietrzko, "Experimental study for control of sound transmission through double glazed window using optimally tuned Helmholtz resonators," *Applied Acoustics*, vol. 71, no. 1, pp. 32–38, 2010.
- [2] F. Fahy and J. Walker, *Fundamentals of Noise and Vibration*. London: E. & F.N. Spon, 1998.
- [3] F. Fahy and P. Gardonio, *Sound and structural vibration: radiation, transmission and response*, 2nd ed. London: Academic Press, 2007.
- [4] J. Pan and C. Bao, "Analytical study of different approaches for active control of sound transmission through double walls," *The Journal of the Acoustical Society of America*, vol. 103, no. 4, pp. 1916–1922, 1998.
- [5] O. E. Kaiser, S. J. Pietrzko, and M. Morari, "Feedback control of sound transmission through a double glazed window," *Journal of Sound and Vibration*, vol. 263, no. 4, pp. 775–795, 2003.
- [6] J. P. Carneal and C. R. Fuller, "An analytical and experimental investigation of active structural acoustic control of noise transmission through double panel systems," *Journal of Sound and Vibration*, vol. 272, no. 3–5, pp. 749–771, 2004.
- [7] P. A. Nelson and S. J. Elliott, *Active Control of Sound*, 1st ed. London: Academic Press, 1992.
- [8] A. P. Berkhoff, "Piezoelectric sensor configuration for active structural acoustic control," *Journal of Sound and Vibration*, vol. 246, no. 1, pp. 175–183, 2001.
- [9] P. Gardonio, E. Bianchi, and S. J. Elliott, "Smart panel with multiple decentralized units for the control of sound transmission. Part I: theoretical predictions," *Journal of Sound and Vibration*, vol. 274, no. 1–2, pp. 163–192, 2004.
- [10] P. Gardonio, E. Bianchi, and S. J. Elliott, "Smart panel with multiple decentralized units for the control of sound transmission. Part II: design of the decentralized control units," *Journal of Sound and Vibration*, vol. 274, no. 1–2, pp. 193–213, 2004.
- [11] E. Bianchi, P. Gardonio, and S. J. Elliott, "Smart panel with multiple decentralized units for the control of sound transmission. Part III: control system implementation," *Journal of Sound and Vibration*, vol. 274, no. 1–2, pp. 215–232, 2004.

- [12] B. Petitjean and I. Legrain, "Feedback controllers for active vibration suppression," *Journal of Structural Control*, vol. 3, no. 1-2, pp. 111–127, 1996.
- [13] S. J. Elliott, P. Gardonio, T. C. Sors, and M. J. Brennan, "Active vibroacoustic control with multiple local feedback loops," *The Journal of the Acoustical Society of America*, vol. 111, no. 2, pp. 908–915, 2002.
- [14] S. J. Pietrzko and Q. Mao, "New results in active and passive control of sound transmission through double wall structures," *Aerospace Science and Technology*, vol. 12, pp. 42–53, 2008.
- [15] N. Alujević, P. Gardonio, and K. D. Frampton, "Smart double panel with decentralized active dampers for sound transmission control," *American Institute of Aeronautics and Astronautics Journal*, vol. 46, no. 6, pp. 1463–1475, 2008.
- [16] N. Alujević, P. Gardonio, and K. D. Frampton, "Smart double panel for the sound radiation control: Blended velocity feedback," *American Institute of Aeronautics and Astronautics Journal*, vol. 49, no. 6, pp. 1123–1134, 2011.
- [17] F. Fahy and J. Walker, *Advanced Applications in Acoustics, Noise and Vibration*. London: Spon Press, 2004.
- [18] L. Maestrello, "Measurement of noise radiated by boundary layer excited panels," *Journal of Sound and Vibration*, vol. 2, no. 2, pp. 100–115, 1965.
- [19] L. Maestrello, "Design criterion of panel structure excited by turbulent boundary layers," *Journal of Aircraft*, vol. 5, no. 4, p. 321–328, 1968.
- [20] W. R. Graham, "Boundary layer induced noise in aircraft, part I: The flat plate model," *Journal of Sound and Vibration*, vol. 192, no. 1, pp. 101–120, 1996.
- [21] W. R. Graham, "Boundary layer induced noise in aircraft, part II: The trimmed flat plate model," *Journal of Sound and Vibration*, vol. 192, no. 1, pp. 121–138, 1996.
- [22] M. H. C. Hannink, "Acoustic resonators for the reduction of sound radiation and transmission," Ph.D. thesis, University of Twente, Enschede, The Netherlands, 2007.
- [23] F. J. Fahy and C. Schofield, "A note on the interaction between a Helmholtz resonator and an acoustic mode of an enclosure," *Journal of Sound and Vibration*, vol. 72, no. 3, pp. 365–378, 1980.
- [24] J. M. Mason and F. J. Fahy, "The use of acoustically tuned resonators to improve the sound transmission loss of double-panel partitions," *Journal of Sound and Vibration*, vol. 124, no. 2, pp. 367–379, 1988.
- [25] M. Qibo and S. Pietrzko, "Control of sound transmission through double wall partitions using optimally tuned Helmholtz resonators," *Acta Acustica United With Acustica*, vol. 91, pp. 723–31, 2005.
- [26] M. Qibo and S. Pietrzko, "Experimental study for control of sound transmission through double glazed window using optimally tuned Helmholtz resonators," *Applied Acoustics*, vol. 71, pp. 32–8, 2010.

- [27] N. W. Hagood and A. von Flotow, "Damping of structural vibrations with piezoelectric materials and passive electrical networks," *Journal of Sound and Vibration*, vol. 146, no. 2, pp. 243–268, 1991.
- [28] W. W. Clark, "Vibration control with state-switched piezoelectric materials," *Journal of Intelligent Material Systems and Structures*, vol. 11, no. 4, pp. 263–271, 2000.
- [29] L. R. Corr and W. W. Clark, "Comparison of low-frequency piezoelectric switching shunt techniques for structural damping," *Smart Materials and Structures*, vol. 11, no. 3, p. 370, 2002.
- [30] C. Richard, D. Guyomar, D. Audigier, and G. Ching, "Semi-passive damping using continuous switching of a piezoelectric device," in *Proceedings of SPIE International Symposium on Smart Structures and Materials: Damping and Isolation*, vol. 3672, 1999, pp. 104–111.
- [31] C. Richard, D. Guyomar, D. Audigier, and H. Bassaler, "Enhanced semi-passive damping using continuous switching of a piezoelectric device on an inductor," in *Proceedings of SPIE International Symposium on Smart Structures and Materials: Damping and Isolation*, vol. 3989, 2000, pp. 288–299.
- [32] J. P. Den Hartog, *Mechanical vibrations*, 4th ed. New York: McGraw-Hill, 1956.
- [33] J. Q. Sun, M. R. Jolly, and M. A. Norris, "Passive, adaptive and active tuned vibration absorbers—a survey," *Journal of Mechanical Design*, vol. 117, pp. 234–242, 1995.
- [34] C. R. Fuller, J. P. Maillard, M. Mercadal, and A. H. von Flotow, "Control of aircraft interior noise using globally detuned vibration absorbers," *Journal of Sound and Vibration*, vol. 203, no. 5, pp. 745–761, 1997.
- [35] S. Keye, R. Keimer, and S. Homann, "A vibration absorber with variable eigenfrequency for turboprop aircraft," *Aerospace Science and Technology*, vol. 13, no. 4–5, pp. 165–171, 2009.
- [36] L. Kela and P. Vähöja, "Recent studies of adaptive tuned vibration absorbers/neutralizers," *Applied Mechanics Reviews*, vol. 62, no. 6, p. 060801, 2009.
- [37] C. Hirunyapruk, M. J. Brennan, B. R. Mace, and W. H. Li, "A tunable magneto-rheological fluid-filled beam-like vibration absorber," *Smart Materials and Structures*, vol. 19, no. 5, p. 055020, 2010.
- [38] S. J. Elliott, P. A. Nelson, I. M. Stothers, and C. C. Boucher, "Preliminary results of in-flight experiments on the active control of propeller-induced cabin noise," *Journal of Sound and Vibration*, vol. 128, no. 2, pp. 355–357, 1989.
- [39] J. P. Carneal, M. Giovanardi, C. R. Fuller, and D. Palumbo, "Re-active passive devices for control of noise transmission through a panel," *Journal of Sound and Vibration*, vol. 309, no. 3–5, pp. 495–506, 2008.

- [40] R. L. Clark and C. R. Fuller, "A model reference approach for implementing active structural acoustic control," *The Journal of the Acoustical Society of America*, vol. 92, no. 3, pp. 1534–1544, 1992.
- [41] C. R. Fuller, C. A. Rogers, and H. H. Robertshaw, "Control of sound radiation with active/adaptive structures," *Journal of Sound and Vibration*, vol. 157, no. 1, pp. 19–39, 1992.
- [42] S. J. Elliott and M. E. Johnson, "Radiation modes and the active control of sound power," *The Journal of the Acoustical Society of America*, vol. 94, no. 4, pp. 2194–2204, 1993.
- [43] C. Guigou, Z. Li, and C. R. Fuller, "The relationship between volume velocity and far-field radiated pressure of a planar structure," *Journal of Sound and Vibration*, vol. 197, no. 2, pp. 252–254, 1996.
- [44] B. T. Wang and C. R. Fuller, "Near-field pressure, intensity, and wave-number distributions for active structural acoustic control of plate radiation: theoretical analysis," *The Journal of the Acoustical Society of America*, vol. 92, no. 3, pp. 1489–1498, 1992.
- [45] A. P. Berkhoff, "Broadband radiation modes: estimation and active control," *The Journal of the Acoustical Society of America*, vol. 111, no. 3, pp. 1295–305, 2002.
- [46] T. C. Sors and S. J. Elliott, "Modelling and feedback control of sound radiation from a vibrating panel," *Smart Materials and Structures*, vol. 8, no. 3, p. 301, 1999.
- [47] P. Gardonio and S. J. Elliott, "Smart panels for active structural acoustic control," *Smart Materials and Structures*, vol. 13, no. 6, p. 1314, 2004.
- [48] P. D. Fonseca, P. Sas, and H. V. Brussel, "A comparative study of methods for optimising sensor and actuator locations in active control applications," *Journal of Sound and Vibration*, vol. 221, no. 4, pp. 651–679, 1999.
- [49] M. H. H. Oude Nijhuis, "Analysis tools for the design of active structural acoustic control systems," Ph.D. thesis, University of Twente, Enschede, The Netherlands, 2003.
- [50] Y. Aoki, P. Gardonio, and S. J. Elliott, "Rectangular plate with velocity feedback loops using triangularly shaped piezoceramic actuators: Experimental control performance," *The Journal of the Acoustical Society of America*, vol. 123, no. 3, pp. 1421–1426, 2008.
- [51] J. Rohlfing, P. Gardonio, and D. J. Thompson, "Comparison of decentralized velocity feedback control for thin homogeneous and stiff sandwich panels using electrodynamic proof-mass actuators," *Journal of Sound and Vibration*, vol. 330, no. 5, pp. 843–867, 2011.
- [52] N. Alujević, K. D. Frampton, and P. Gardonio, "Stability and performance of a smart double panel with decentralized active dampers," *American Institute of Aeronautics and Astronautics Journal*, vol. 46, no. 7, pp. 1747–1756, 2008.

- [53] P. D. Man, A. Francois, and A. Preumont, "Active control of noise transmission through double wall structures. An overview of possible approaches," in *the 6th National Congress on Theoretical and Applied Mechanics*, May 2003.
- [54] S. J. Elliott, *Signal Processing for Active Control*. London: Academic Press, 2001.
- [55] P. Gardonio, Y. S. Lee, S. J. Elliott, and S. Debost, "Analysis and measurement of a matched volume velocity sensor and uniform force actuator for active structural acoustic control," *The Journal of the Acoustical Society of America*, vol. 110, no. 6, pp. 3025–3031, 2001.
- [56] C. Hong and S. J. Elliott, "Local feedback control of light honeycomb panels," *The Journal of the Acoustical Society of America*, vol. 121, no. 1, pp. 222–233, 2007.
- [57] M. Morari, *Robust process control*. London: Prentice-Hall, 1989.
- [58] A. Jakob and M. Möser, "Active control of double-glazed windows. Part II: Feedback control," *Applied Acoustics*, vol. 64, no. 2, pp. 183–196, 2003.
- [59] K. J. Åström, U. Borisson, L. Ljung, and B. Wittenmark, "Theory and applications of self-tuning regulators," *Automatica*, vol. 13, no. 5, pp. 457–476, 1977.
- [60] L. J. Eriksson and M. C. Allie, "Use of random noise for on-line transducer modeling in an adaptive active attenuation system," *The Journal of the Acoustical Society of America*, vol. 85, no. 2, pp. 797–802, 1989.
- [61] K. J. Åström and B. Wittenmark, *Adaptive Control*, 2nd ed. New York: Addison-Wesley, 1995.
- [62] G. C. Goodwin and K. S. Sin, *Adaptive Filtering Prediction and Control (Information and Systems Science Series)*. London: Prentice-Hall, 1984.
- [63] K. J. Åström, "Adaptive feedback control," *Proceedings of the IEEE*, vol. 75, no. 2, pp. 185–217, 1987.
- [64] K. J. Åström, "Adaptive control around 1960," *Control Systems, IEEE*, vol. 16, no. 3, pp. 44–49, 1996.
- [65] C. R. Fuller, S. J. Elliott, and P. A. Nelson, *Active Control of Vibration*. London: Academic Press, 1996.
- [66] R. L. Clark, W. R. Saunders, and G. P. Gibbs, *Adaptive Structures*. New York: John Wiley & Sons, 1998.
- [67] J. Q. Sun, "Some observations on physical duality and colocation of structural control sensors and actuators," *Journal of Sound and Vibration*, vol. 194, no. 5, pp. 765–770, 1996.
- [68] M. J. Balas, "Direct velocity feedback control of large space structures," *Journal of Guidance, Control, and Dynamics*, vol. 2, no. 3, pp. 252–253, 1979.
- [69] V. Jayachandran and J. Q. Sun, "Unconditional stability domains of structural control systems using dual actuator–sensor pairs," *Journal of Sound and Vibration*, vol. 208, no. 1, pp. 159–166, 1997.

- [70] D. Wagg, I. Bond, and P. Weaver, *Adaptive structures: engineering applications*. New York: John Wiley & Sons, 2007.
- [71] A. Preumont, *Vibration Control of Active Structure*, 3rd ed. London: Springer, 2012.
- [72] M. Zilletti, S. J. Elliott, and P. Gardonio, "Self-tuning control systems of decentralised velocity feedback," *Journal of Sound and Vibration*, vol. 329, no. 14, pp. 2738–2750, 2010.
- [73] N. A. Lynch, *Distributed Algorithms*. San Francisco: Morgan Kaufmann, 1996.
- [74] R. D'Andrea and G. E. Dullerud, "Distributed control design for spatially interconnected systems," *Automatic Control, IEEE Transactions on*, vol. 48, no. 9, pp. 1478–1495, 2003.
- [75] E. Scholte and R. D'Andrea, "Active vibro-acoustic control of a flexible beam using distributed control," in *American Control Conference*, vol. 3, June 2003, pp. 2640–2645.
- [76] K. D. Frampton, "Vibro-acoustic control with a distributed sensor network," *The Journal of the Acoustical Society of America*, vol. 119, no. 4, pp. 2170–2177, 2006.
- [77] T. Tao and K. D. Frampton, "Experiments on distributed active vibration control of a simply supported beam," *Smart Materials and Structures*, vol. 15, no. 6, p. 1858, 2006.
- [78] P. Cobo and M. Cuesta, "Hybrid passive-active absorption of a microperforated panel in free field conditions," *The Journal of the Acoustical Society of America*, vol. 121, no. 6, pp. EL251–EL255, 2007.
- [79] P. Sas, C. Bao, F. Augusztinovicz, and W. Desmet, "Active control of sound transmission through a double panel partition," *Journal of Sound and Vibration*, vol. 180, no. 4, pp. 609–625, 1995.
- [80] C. Bao and J. Pan, "Experimental study of different approaches for active control of sound transmission through double walls," *The Journal of the Acoustical Society of America*, vol. 102, no. 3, pp. 1664–1670, 1997.
- [81] X. Pan, T. J. Sutton, and S. J. Elliott, "Active control of sound transmission through a double-leaf partition by volume velocity cancellation," *Journal of the Acoustical Society of America*, vol. 104, no. 5, pp. 2828–2835, 1998.
- [82] J. H. Ho and A. Berkhoff, "Comparison of various decentralised structural and cavity feedback control strategies for transmitted noise reduction through a double panel structure," *Journal of Sound and Vibration*, vol. 333, no. 7, pp. 1857–1873, 2014.
- [83] F. Fahy, *Sound and Structural Vibration*. London: Academic Press, 1985.
- [84] J. P. Carneal and C. R. Fuller, "Active structural acoustic control of noise transmission through double panel systems," *American Institute of Aeronautics and Astronautics Journal*, vol. 33, no. 4, pp. 618–623, 1995.

- [85] O. Kaiser, A. Julius, S. Pietrzko, and M. Morari, "Uncontrollable modes in double wall panels," in *the 17th International Congress on Acoustics*, 2001, pp. 7–9.
- [86] K. Idrisi, M. E. Johnson, A. Toso, and J. P. Carneal, "Increase in transmission loss of a double panel system by addition of mass inclusions to a poro-elastic layer: A comparison between theory and experiment," *Journal of Sound and Vibration*, vol. 323, no. 1–2, pp. 51–66, 2009.
- [87] C. J. Naify, C. M. Chang, G. McKnight, and S. R. Nutt, "Scaling of membrane-type locally resonant acoustic metamaterial arrays," *The Journal of the Acoustical Society of America*, vol. 132, no. 4, pp. 2784–2792, 2012.
- [88] J. Zhou, A. Bhaskar, and X. Zhang, "Sound transmission through a double-panel construction lined with poroelastic material in the presence of mean flow," *Journal of Sound and Vibration*, vol. 332, no. 16, pp. 3724 – 3734, 2013.
- [89] J. Zhou, A. Bhaskar, and X. Zhang, "The effect of external mean flow on sound transmission through double-walled cylindrical shells lined with poroelastic material," *Journal of Sound and Vibration*, vol. 333, no. 7, pp. 1972 – 1990, 2014.
- [90] T. G. H. Basten, "Noise reduction by viscothermal acousto-elastic interaction in double wall panels," Ph.D. thesis, University of Twente, Enschede, The Netherlands, 2001.
- [91] S. J. Elliott and P. A. Nelson, "Active noise control," *Signal Processing Magazine, IEEE*, vol. 10, no. 4, pp. 12–35, 1993.
- [92] B. K. Henderson, S. A. Lane, J. Gussy, S. Griffin, and K. M. Farinholt, "Development of an acoustic actuator for launch vehicle noise reduction," *The Journal of the Acoustical Society of America*, vol. 111, no. 1, pp. 174–179, 2002.
- [93] W. P. J. de Bruijn and M. M. Boone, "Application of wave field synthesis in life-size videoconferencing," in *Audio Engineering Society Convention 114*, March 2003.
- [94] R. Small, "Direct-radiator loudspeaker system analysis," *Audio and Electroacoustics, IEEE Transactions on*, vol. 19, no. 4, pp. 269–281, 1971.
- [95] D. Beer, M. Jahr, A. Reich, and M. Schuster, "The air spring effect of flat panel speakers," in *Audio Engineering Society Convention 124*, May 2008.
- [96] N. Harris and M. J. Hawksford, "The distributed-mode loudspeaker (DML) as a broad-band acoustic radiator," in *Audio Engineering Society Convention 103*, September 1997.
- [97] J. Panzer and N. Harris, "Distributed-mode loudspeaker radiation simulation," in *Audio Engineering Society Convention 105*, September 1998.
- [98] N. J. Harris and M. O. J. Hawksford, "Introduction to distributed mode loudspeakers (DML) with first-order behavioural modelling," *Circuits, Devices and Systems, IEE Proceedings*, vol. 147, no. 3, pp. 153–157, 2000.

- [99] M. M. Boone, "Multi-actuator panels (MAPs) as loudspeaker arrays for wave field synthesis," *Journal of Audio Engineering Society*, vol. 52, no. 7/8, pp. 712–723, 2004.
- [100] M. Kuster, D. De Vries, D. Beer, and S. Brix, "Structural and acoustic analysis of multiactuator panels," *Journal of Audio Engineering Society*, vol. 54, no. 11, pp. 1065–1076, 2006.
- [101] B. Pueo, J. J. López, G. Ramos, and J. Escolano, "Efficient equalization of multi-exciter distributed mode loudspeakers," *Applied Acoustics*, vol. 70, no. 5, pp. 737–746, 2009.
- [102] B. Pueo, G. Ramos, and J. J. Lopez, "Strategies for bass enhancement in multiactuator panels for wave field synthesis," *Applied Acoustics*, vol. 71, no. 8, pp. 722–730, 2010.
- [103] J. H. Ho and A. Berkhoff, "Comparisons between various cavity and panel noise reduction control methods in double-panel structures," *The Journal of the Acoustical Society of America*, vol. 131, no. 4, p. 3501, 2012.
- [104] M. Salikuddin and H. K. Tanna, "Active noise control system," US Patent US4 689 821 A, 1987.
- [105] D. E. Ivers, M. R. Jolly, M. A. Norris, and W. E. Schmidt, "Active systems and devices including active vibration absorbers," WO Patent WO9 612 121, 1996.
- [106] M. C. Heath, D. E. Ivers, M. A. Norris, D. J. Rossetti, and S. C. Southward, "Active structural control system and method including active vibration absorbers (AVAs)," WO Patent WO1 998 006 089 A1, 1998.
- [107] V. Shridhar and D. Wertz, "System for active noise control based on audio system output," US Patent US8 189 799 B2, 2012.
- [108] G. D. Billoud, "Active noise control system for closed space such as aircraft cabins," WO Patent WO1 997 012 360 A1, 1997.
- [109] K. Sakamoto, T. Inoue, A. Takahashi, and Y. Kobayashi, "Vehicular active noise/vibration/sound control system, and vehicle incorporating such system," US Patent US7 876 910 B2, 2011.
- [110] S. J. Elliott, P. A. Nelson, and I. M. Stothers, "Active vibration control," European Patent EP0 285 632 B1, 1993.
- [111] S. J. Elliott and I. M. Stothers, "Time domain adaptive control system," WO Patent WO1 995 026 521 A1, 1995.
- [112] M. Mercadal, P. M. Tappert, and A. H. von Flotow, "Apparatus and method for active control of sound transmission through aircraft fuselage walls," US Patent US6 078 673 A, 2000.
- [113] I. M. Stothers, I. A. Scott, and S. J. Elliott, "Noise attenuation system for vehicles," US Patent US20 050 232 435 A1, 2005.

- [114] M. Wurm, "Adaptive noise control system," US Patent US8 565 443 B2, 2013.
- [115] F. G. Pla and H. Rajiyah, "Active noise control using a tunable plate radiator," US Patent US5 618 010 A, 1997.
- [116] A. O. Andersson, "Active control system and method for reducing engine noise and vibration," European Patent EP0 372 590 B1, 1993.
- [117] A. P. Berkhoff and J. M. Wesselink, "Combined MIMO adaptive and decentralized controllers for broadband active noise and vibration control," *Mechanical Systems and Signal Processing*, vol. 25, no. 5, pp. 1702–1714, 2011.
- [118] S. J. Elliott and C. C. Boucher, "Interaction between multiple feedforward active control systems," *Speech and Audio Processing, IEEE Transactions on*, vol. 2, no. 4, pp. 521–530, 1994.
- [119] S. Skogestad and I. Postlethwaite, *Multivariable Feedback Control: Analysis and Design*. New York: John Wiley & Sons, 2005.
- [120] P. Gardonio and N. Alujević, "Double panel with skyhook active damping control units for control of sound radiation," *The Journal of the Acoustical Society of America*, vol. 128, no. 3, pp. 1108–1117, 2010.
- [121] G. D. Martin, "On the Control of Flexible Mechanical Systems," Ph.D. thesis, Stanford University, Stanford, CA, 1978.
- [122] M. E. Johnson and S. J. Elliott, "Active control of sound radiation using volume velocity cancellation," *The Journal of the Acoustical Society of America*, vol. 98, no. 4, pp. 2174–2186, 1995.
- [123] R. H. Cannon and D. E. Rosenthal, "Experiments in control of flexible structures with noncolocated sensors and actuators," *Journal of Guidance, Control, and Dynamics*, vol. 7, no. 5, pp. 546–553, 1984.
- [124] A. P. Berkhoff and G. Nijse, "A rapidly converging filtered-error algorithm for multichannel active noise control," *International Journal of Adaptive Control and Signal Processing*, vol. 21, no. 7, pp. 556–569, 2007.
- [125] A. P. Berkhoff, "A technique for improved stability of adaptive feedforward controllers without detailed uncertainty measurements," *Smart Materials and Structures*, vol. 21, no. 6, p. 064003, 2012.
- [126] M. Rossi, *Acoustics and electroacoustics*. Norwood: Artech House, 1988.
- [127] D. Givoli and B. Neta, "High-order non-reflecting boundary scheme for time-dependent waves," *Journal of Computational Physics*, vol. 186, no. 1, pp. 24–46, 2003.
- [128] R. L. Higdon, "Absorbing boundary conditions for difference approximations to the multi-dimensional wave equation," *Mathematics of Computation*, vol. 47, no. 176, pp. 437–459, 1986.

- [129] R. L. Higdon, "Numerical absorbing boundary conditions for the wave equation," *Mathematics of Computation*, vol. 49, no. 179, pp. 65–90, 1987.
- [130] H. Zhu, R. Rajamani, and K. A. Stelson, "Active control of acoustic reflection, absorption, and transmission using thin panel speakers," *The Journal of the Acoustical Society of America*, vol. 113, no. 2, pp. 852–870, 2003.
- [131] J. M. Wesselink and A. P. Berkhoff, "Fast affine projections and the regularized modified filtered-error algorithm in multichannel active noise control," *The Journal of the Acoustical Society of America*, vol. 124, no. 2, pp. 949–960, 2008.
- [132] A. P. Berkhoff, "Sound generator," US Patent US20 100 111 351 A1, 2010.
- [133] R. Greenfield and M. J. Hawksford, "Efficient filter design for loudspeaker equalization," *Journal of Audio Engineering Society*, vol. 39, no. 10, pp. 739–751, 1991.
- [134] M. Karjalainen, E. Piirilä, A. Järvinen, and J. Huopaniemi, "Comparison of loudspeaker equalization methods based on DSP techniques," *Journal of Audio Engineering Society*, vol. 47, no. 1/2, pp. 14–31, 1999.
- [135] G. Ramos and J. J. López, "Filter design method for loudspeaker equalization based on IIR parametric filters," *Journal of Audio Engineering Society*, vol. 54, no. 12, pp. 1162–1178, 2006.
- [136] V. Ionescu and C. Oara, "Spectral and inner-outer factorizations for discrete-time systems," *Automatic Control, IEEE Transactions on*, vol. 41, no. 12, pp. 1840–1845, 1996.
- [137] S. Linkwitz, "A three-enclosure loudspeaker system with active delay and crossover: Part 1, 2, 3," *Speaker Builder*, vol. 2-4/80, pp. 12–25, 1980.
- [138] L. L. Beranek, *Acoustics*. New York: McGraw-Hill, 1954.
- [139] L. Ljung, *System Identification Toolbox 7: User's Guide*. Natick: The MathWorks, Inc., 2007.
- [140] J. C. Villamil Oostra, "Design and analysis of a flat sound generator," Master thesis, University of Twente, Enschede, The Netherlands, 2012.

Nomenclature

Greek

α	Convergence coefficient
β	Control effort weighting factor
η	Dynamic viscosity
κ	Compressibility of air
λ	Eigenvalue
μ	Convergence factor
ρ	Density of air
ω	Angular frequency

Operators and functions

j	Imaginary unit ($j=\sqrt{-1}$)
$\text{Re}(\mathbf{A})$	Real part of \mathbf{A}
$\text{Im}(\mathbf{A})$	Imaginary part \mathbf{A}
\mathbf{A}^H	Hermitian transpose of \mathbf{A}
\mathbf{A}^T	Transpose of \mathbf{A}
\mathbf{A}^{-1}	Inverse of \mathbf{A}
$\text{trace}(\mathbf{A})$	Trace of \mathbf{A}
$\det(\mathbf{A})$	Determinant of \mathbf{A}
$\min(\mathbf{A})$	Minimum value of \mathbf{A}
$\frac{\partial \mathbf{A}}{\partial \mathbf{B}}$	Derivative of \mathbf{A} with respect to \mathbf{B}
$\nabla \mathbf{A}$	Gradient of \mathbf{A}
$\nabla \cdot \mathbf{A}$	Divergence of \mathbf{A}
$\nabla^2 \mathbf{A}$	Laplacian of \mathbf{A}
q	Unit delay operator

Scalars

a_n	Normal acceleration to the surface
c	Sound speed
C_a	Damping of vibration absorber
C_s	Damping of vibrating structure
d_{31}	Piezoelectric strain coefficient
d_h	Distance between the holes
E_p	Young's modulus of the piezoelectric patch
f	Frequency
g_m	Gain margin
h	Distance
J	Cost function
k	Wave number
K	Number of reference sensors
K_a	Spring stiffness of vibration absorber
K_s	Spring stiffness of vibrating structure
KE	Kinetic energy of the radiating panel
L	Number of error sensors
M	Number of actuators
M_a	Mass of vibration absorber
M_p	Moment per unit length
M_s	Mass of vibrating structure
n	The n -th iteration
p	Pressure (time domain)
\hat{p}	Pressure (frequency domain)
p_a	Pressure in the fluid domain
\hat{p}_c	Control pressure value
p_i	Incident pressure
\hat{p}_i	Amplitude of the incident pressure
p_m	Phase margin
\hat{p}_o	Specific control pressure value
p_r	Reflecting pressure
\hat{p}_r	Amplitude of the reflecting pressure
Q_u	Property coefficients of the uncompensated loudspeaker
Q_d	Property coefficients of the desired loudspeaker
r	Hole radius
s	Laplace domain parameter
s_m	Modulus margin
S_p	Area of the perforated plate
t	Time
t_p	Plate thickness
T_d	Property coefficients of the desired loudspeaker
T_u	Property coefficients of the uncompensated loudspeaker
v	Particle velocity
v_i	Particle velocity in the incident direction
v_r	Particle velocity in the reflecting direction
V	Voltage
Z_{perf}	Acoustic impedance of the perforated plate

Vectors and matrices

$\hat{\mathbf{a}}$	Acceleration
\mathbf{d}	Primary noise source signals
$\hat{\mathbf{d}}$	Estimated primary noise source signals
\mathbf{e}_a	Auxiliary error signals
\mathbf{F}_p	The pressure load (normal force per unit area) on the structure surface produced by the fluid pressure
\mathbf{G}	Plant transfer function
$\bar{\mathbf{G}}$	Augmented plant transfer function
$\hat{\mathbf{G}}$	Estimated plant transfer function
$\bar{\mathbf{G}}_i$	Minimum-phase plant transfer function
$\bar{\mathbf{G}}_o$	All-pass plant transfer function
\mathbf{G}_{rp}	Transfer function between the secondary sources and the reference sensors
\mathbf{G}_{reg}	Regularized function
\mathbf{G}_u	Transfer function of the uncompensated loudspeaker
\mathbf{G}_d	Transfer function of the desired loudspeaker
\mathbf{H}	Control matrix
\mathbf{I}	Identity matrix
\mathbf{I}_L	L-dimensional identity matrix
\mathbf{I}_M	M-dimensional identity matrix
\mathbf{L}	Transfer function of the Linkwitz filter
\mathbf{n}	Normal vector of the surface
\mathbf{P}	Primary transfer function
\mathbf{u}	Control signals
\mathbf{u}_I	Imaginary part of control signals
\mathbf{u}_R	Real part of control signals
\mathbf{u}_{opt}	Optimal control signals
\mathbf{u}_{tt}	Second derivatives of the structural displacements with respect to time
$\hat{\mathbf{v}}$	Particle velocity
\mathbf{W}	Control filter
\mathbf{W}_i	The i -th control filter
\mathbf{x}_{ref}	Reference signals
\mathbf{x}_d	Delayed reference signals
\mathbf{y}	Secondary signals

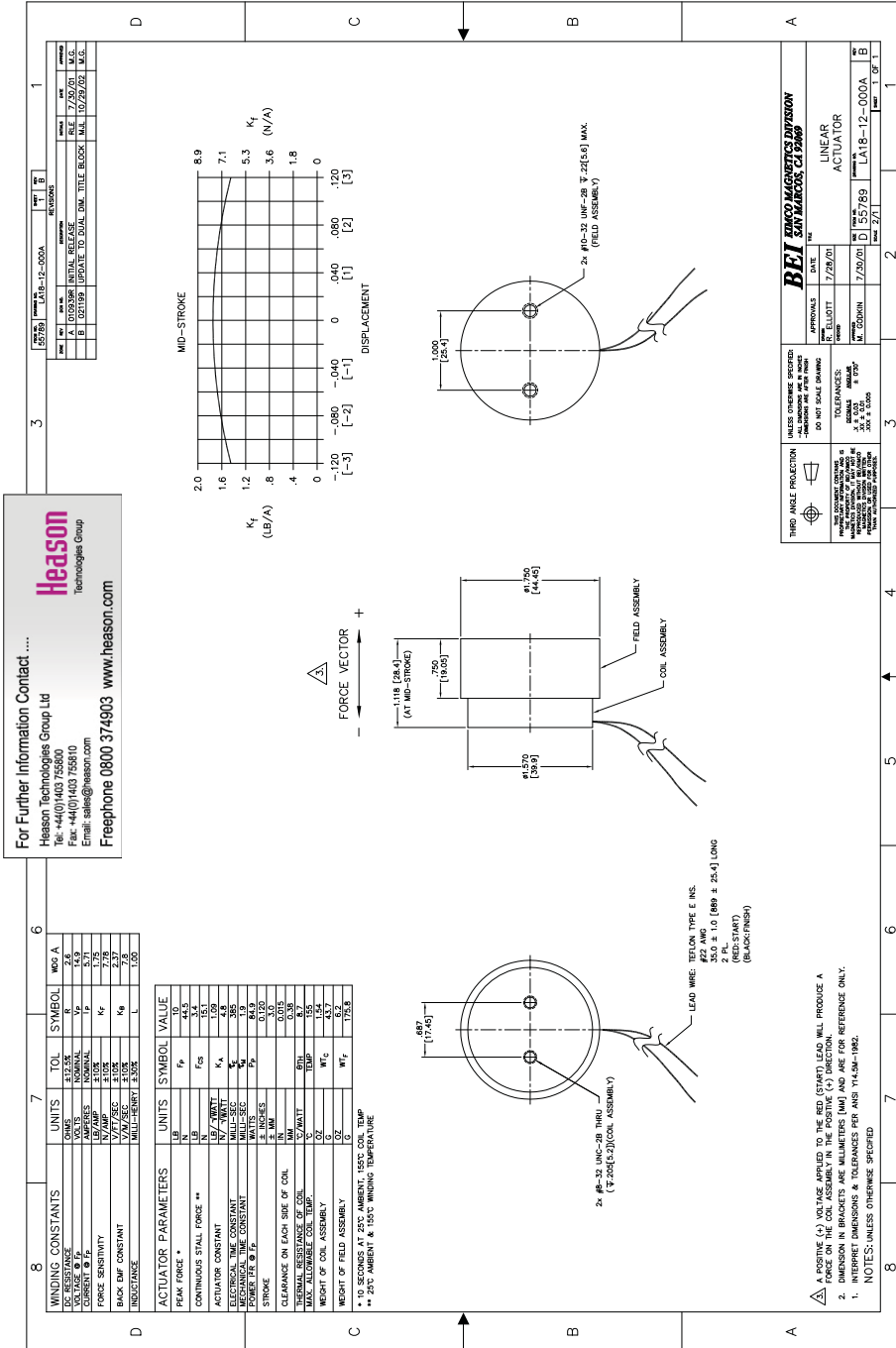
Abbreviations

acc.	Acceleration
ANC	Active noise control
ASAC	Active structural acoustic control
ASC	Active structural control
ATVA	Adaptive tuned vibration absorber
AVA	Active vibration absorber
AVC	Active vibration control
CFRP	Carbon fiber reinforced plastic
dB	Decibel
DML	Distributed mode loudspeaker
DVFB	Direct velocity feedback
EPDM	Ethylene propylene diene monomer
FEM	Finite element method
Filtered-x LMS	Filtered-reference least mean square
FPGA	Field-programmable gate array
FLXLMS	Filtered-reference least mean square
IMC	Internal model control
inc.	Incident
LMS	Least mean square
lsp	Loudspeaker
MAP	Multi-actuator panel
MIMO	Multiple-input and multiple-output
MPRI	Minimum-phase regularized inverse
MR	magneto-rheological
NRBC	Non-reflecting boundary condition
PZT	Piezoelectric
rad.	Radiation
RMFeLMS	Regularized modified filtered-error least mean square
SISO	Single-input and single-out
SPL	Sound pressure level
SWL	Sound power level
TVA	Tuned vibration absorber
WFS	Wave field synthesis

Appendices

APPENDIX A

Datasheet of the voice coil actuator



APPENDIX B

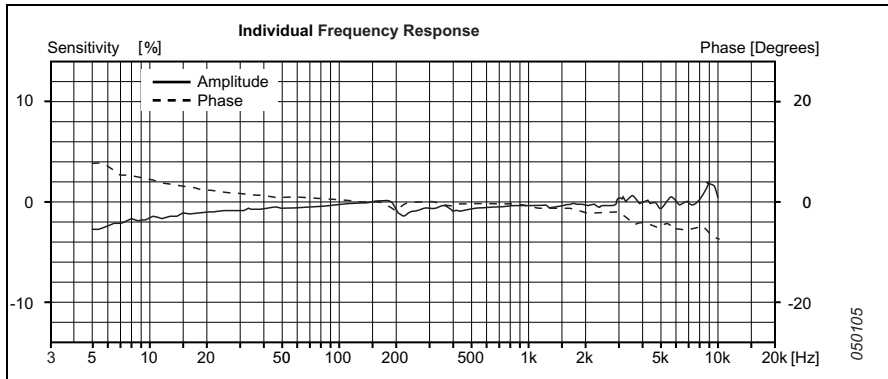
Datasheet of the accelerometer

**Specifications – Miniature DeltaTron Accelerometers
Types 4517 and 4517-002**

	Units	4517	4517-002
Dynamic Characteristics			
Voltage Sensitivity (@ 160Hz)	mV/g	10 ±10%	
Measuring Range	g	±500	
Frequency Response		See typical amplitude response	
Mounted Resonance Frequency	kHz	75	
Amplitude Response ±10% (typical) ^a	Hz	1 to 20000	
Residual Noise	mg	6	
Transverse Sensitivity	%	<5	
Electrical Characteristics			
Output Impedance	Ω	< 100	
DC Output	At room temperature	V	10 ±15%
Bias Voltage	In specified temp. range	V	8 to 16
Power Supply		mA	2 to 20
Start-up Time		s	<1
Grounding		Case grounded	Insulated
Environmental Characteristics			
Temperature Range	°C (°F)	-51 to +121 (-60 to +250)	
Humidity		Hermetically sealed	
Max. Operational Shock (peak)	g pk	5000	
Base Strain Sensitivity	Equiv. g/μ strain	0.08	0.05
Thermal Transient Sensitivity	Equiv. %/°C (%/°F)	0.05 (0.03)	
Thermal Shock Sensitivity	ms ² /°C (g/°F)	2.6 (0.15)	
Physical Characteristics			
Dimensions		See outline drawing	
Weight	gram (oz.)	0.6 (0.021)	1.0 (0.035)
Case Material		Titanium	
Connector		3-56 UNF thread	
Mounting		Adhesive	

a. Individual frequency response calibration up to 10 kHz

All values are typical at 25°C (77°F) unless measurement uncertainty is specified

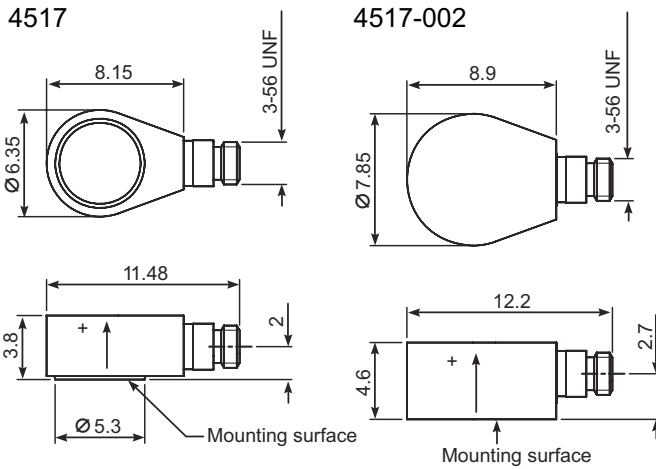




4517

4517-002

Figure B.1: Accelerometers: B&K 4517 and 4517-002.



All dimensions in mm

Figure B.2: Dimensions of the accelerometers.

APPENDIX C

Amplifier

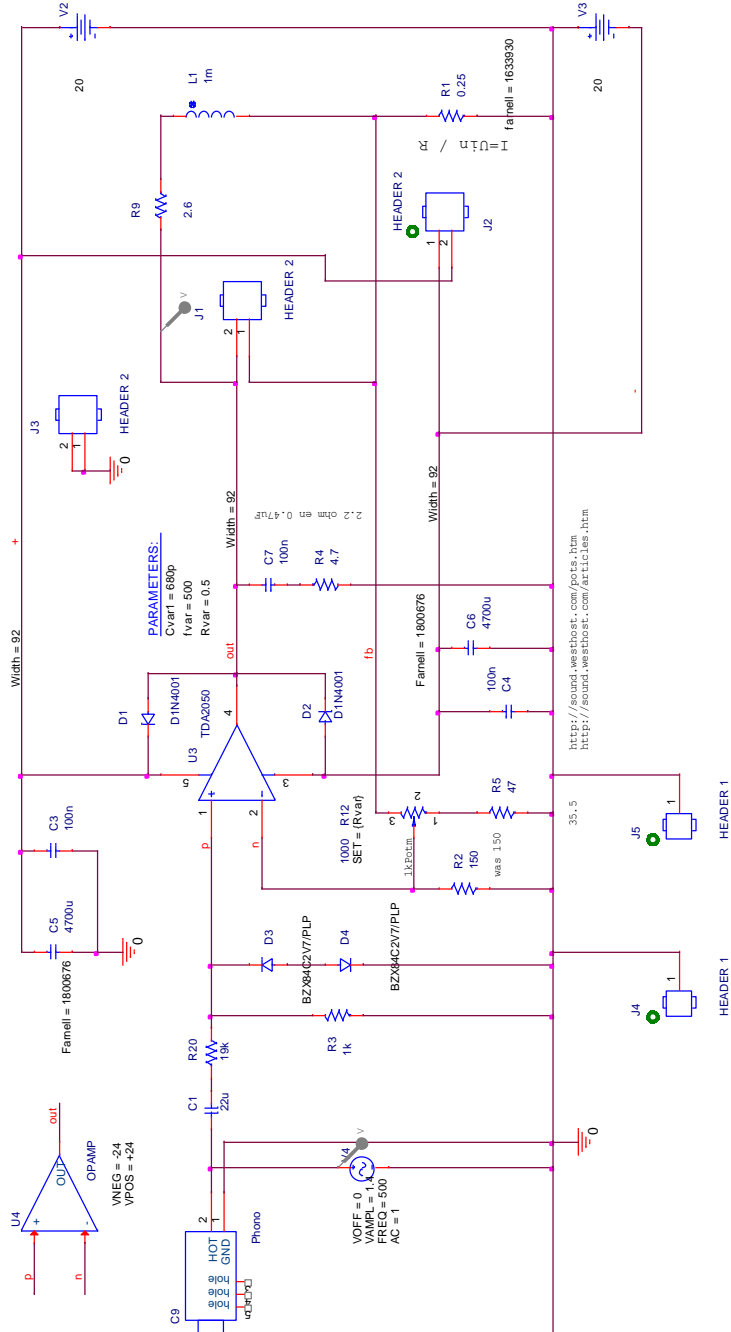


Figure C.1: Schematics of the amplifier for driving the voice coil actuators.

About the author

Jen-Hsuan was born in Taichung, Taiwan, in 1984. She received her BSc in Civil Engineering and MSc in Engineering Science and Ocean Engineering from National Taiwan University (Taipei, Taiwan) in 2006 and 2008, respectively. In April 2010 she started her PhD at the University of Twente (Enschede, the Netherlands), in the Signals and Systems group. In October 2013, she joined the Applied Mechanics group. Her PhD research focused on structural acoustics and active noise control.

List of Journal Papers

- J. H. Ho and A. Berkhoff, "Flat acoustic sources with frequency response correction based on feedback and feed-forward distributed control," submitted to *The Journal of the Acoustical Society of America*.
- J. H. Ho and A. Berkhoff, "Comparison of various decentralised structural and cavity feedback control strategies for transmitted noise reduction through a double panel structure," *Journal of Sound and Vibration*, vol. 333, no. 7, pp. 1857–1873, 2014.

List of Conference Papers

- A. Berkhoff, and J. H. Ho, "Flat sources for active acoustic shielding based on distributed control of a vibrating plate coupled with a thin cavity," in *42nd International Congress and Exposition on Noise Control Engineering (Inter-Noise 2013)*, 15-18 Sep. 2013, Innsbruck, Austria.
- J. H. Ho and A. Berkhoff, "A low density, high stiffness flat loudspeaker with improved sound frequency response," in *21st International Congress on Acoustics (ICA 2013)*, 2-7 Jun. 2013, Montreal, Canada. pp. 1-5.
- J. H. Ho and A. Berkhoff, "Development of dynamic loudspeakers modified as incident pressure sources for noise reduction in a double panel structure," in *20th International Congress on Sound and Vibration (ICSV 20)*, 7-11 Jul. 2013, Bangkok, Thailand. pp. 1-7.

- J. H. Ho and J. Kalverboer and A. Berkhoff, "Comparisons between various cavity and panel noise reduction control in double-panel structures," in *THE ACOUSTICS 2012 HONG KONG* (Invited), 13-18 May 2012, Hong Kong. pp. 1-6.
- J. H. Ho and A. Berkhoff, "Noise reduction in double panel structures by cavity and panel resonance control," in *18th International Congress on Sound and Vibration (ICSV 18)*, 10-14 Jul. 2011, Rio de Janeiro, Brazil. pp. 1-8.
- J. H. Ho and A. Berkhoff, "Panel resonance control and cavity control in double-panel structures for active noise reduction," in *22nd International Conference on Adaptive Structures and Technologies (ICAST 2011)*, 10-13 Oct. 2011, Corfu, Greece. pp. 1-10.

Presentation

- J. H. Ho and J. Kalverboer and A. Berkhoff, "Cavity control and panel control strategies in double-panel structures for transmitted noise reduction," in *NAG Symposium on Active Noise and Vibration Control 2012*, 6 Jun. 2012, Utrecht, The Netherlands.

Acknowledgments

Finally, I've come to this page! However, it isn't easy to write these acknowledgments since there are too many people whom I want to thank. If you are reading this, you are most certainly someone I am grateful to. Please do forgive me if I forget to mention your name here; after this whole thesis-writing thing, I find my brain is still rebooting.

First I would like to thank to my supervisor, Arthur Berkhoff. I still remember how cold it was when I came here for the interview in December four years ago. However, after I saw your enthusiasm for research and your friendly attitude towards people, I thought The Netherlands might not be that cold after all. Every time I felt frustrated in my results during my Ph.D. research, your enthusiasm simply encouraged me. Thank you for your support and patience while guiding me through this journey. I enjoyed working with you and I will miss hearing you say, "Excellent".

I would also like to thank my promotor, André de Boer, and Prof. Kees Slump. André, thank you for supporting me during the last year of my Ph.D. Your clear and energetic responses made everything simple and efficient. I really liked to work and discuss with you. Kees, thank you for providing us with a great working environment. I will miss your smile and the coffee you brew.

This work was supported by STW's (the Dutch foundation for technical sciences') project IMPEDANCE (Integrated Modules for Power Efficient Distributed Active Noise Cancelling Electronics). I would like to thank all the project partners for the useful discussions in our project meetings.

Many thanks go to the secretaries in SAS and TM. Thank you for not only the administrative work, but also for always helping when needed. Sandra, I will miss our chats about cooking, market shopping and travelling that we had in the coffee corner. Debbie, I will miss your cheerful and energetic laugh.

I would like to express my gratitude to Geert Jan, Henny, and Axel for all the support in the laboratory. Without your support, I would probably still be struggling to measure data instead of writing these acknowledgements. Also Geert Jan, thank you for always saving my computer, no matter what I did to it. I will always remember "Borrel" shouting from the coffee corner.

Thanks to all my officemates in SAS. To the people in CA3344, thank you for tolerating my noisy talk. Obviously, my study about noise control failed with respect to myself. Thanks to Pinar and Chris, for all the cheerful moments we shared; life in Enschede would not be so perfect without you. Chris, thank you for teaching me Dutch,

and most importantly, thank you for being my classic Dutch example. I will always remember to bring a “Hagelslag” with me for the perfect vacation outside The Netherlands. Pinar, thank you for your good sense of humor; I enjoyed all the funny stories and observations we shared. To Tauseef, thank you for preferring to work late in the office, so we could share an evening coffee in the office before my deadlines. To Chanjuan, thank you for teaching me a lot of CS knowledge and helping me to fit into CA3344. To Robin, thank you for being the less classic Dutch example in our office and helping me to calibrate my impression on Dutch culture. To Abhishek, thank you for your confidence that encouraged me while I felt frustrated. To Haiyun, thank you for always having interesting chatting topics. To Rita, as you said, I would also thank you for our political, historical, philosophical – and especially, gastronomical – discussions about random topics. To Xiaoying, thank you for inviting me for your Asian cooking, which I will miss a lot. To Sjoerd, thank you for discussing acoustic topics with me and being the other Ph.D. student who is also dealing with sound in SAS. To Meiru, thank you for all the incredible and puzzling stories you shared with us; you broadened my horizons. To Raymond, thank you for all the interesting chats on various topics. To Berk, Julia, Gert, Almar, Anne, Bas, Dirk Jan, Roel, Bianca, Gerbert, Sanja, Luuk, Ferdi, Olga, Jan, and Yuxi, thank you for all the nice chats at lunch and coffee time.

Thanks to all my officemates in TM. To Marieke, thank you for introducing me to the culture of TM and The Netherlands. To Dirk, thank you for all the interesting discussions about mixed-international culture and the purely local Twente culture. I now know the SOP of a Dutch dinner and party: I should always end the dinner with “koffie en/of ijs” and start the party with a cup coffee – but no more than two cups. To Jurnan, thank you for all the interesting performances you gave. Yes, seeing you talking is like seeing a talk show. To Derek, thank you for sharing your experiences in Taiwan; it’s always very interesting to know how foreign people think of our country. To Andrea, thank you for bringing the warmth of Latin America to our office. To Anne, thank you for showing me a different type of humor. To Bo, Semih, Jos, Shaojie, Chao, Martin, Ted, Marcel, Daan, Ysbrand, Ton, Tiedo, Bert, Richard, Timo, Nico, Emile, Johan, and Jason, thank you for the nice chats during our coffee breaks.

I would also like to thank all the members of Cabezota. Thank you for always enjoying our matches, whether we won or lost. The tournaments were great: sleeping in the handball field with hundreds of people and waking up early to rock music. The summer tournament that came with BBQ and beer was the best. Serving in the sports bar was also lots of fun. I really had a great time in Cabezota.

Thank you to my dear friends in Enschede and The Netherlands. To Ingeborg, thank you for all the nice game times and great food we had, and thanks to your cute girl, Noa, for playing with us. To Anneke and Gerrit, thank you for your warm greetings and for caring; your parties are very “gezelligheid”. To Shuo, Yiping, and Xueling, thanks for teaching me the local language and sharing your experiences. To Yung-Ching, Juo-Lan, Dong-Po, Yu-Chuan, Chien-Ching, Kai-Fan, Qiuju, Gil, Yunyun, Yuna, Haifeng, Yvonne, Allison, Songyue, and Derec, thank you for the cozy gatherings. To Astor and

Doreen, thank you for all the nights we spent chatting non-stop and being the greatest hosts in Amsterdam.

I would also like to thank Skype and Facebook. Thank you for helping me stay connected with Hsin-Chieh, Pei-You, Yu-Fang, Yi-Chieh, Dolores, Coco, Chiung-Wen, and all my friends, who now live in Taiwan, Europe and the USA. To all my friends, thank you for living all over the world, so I can always find one to talk to no matter what time it is. Without your company, I would not feel this happy every day.

I would also like to express my gratitude to Prof. Chih-Kung Lee, and Prof. Wen-Jong Wu, for your support while guiding me in NTU. Without your support, I would not come to this page.

Finally, I want to thank my family. To my mom, dad, aunts, and uncles, thank you for your unlimited support and caring. To my brother, even though we always make fun of each other, you mean a lot to me. I especially want to thank my grandparents for giving me a great childhood and values which I am still proud to believe in. And to Wei-Shu, thank you for sharing my happiness and sadness. With your patience, support, and encouragement, I was able to overcome every difficulty.

親愛的家人們: 謝謝你們一直以來不論距離遠近, 總是以各種方式支持著我, 願與你們一起分享我完成博士論文的喜悅。有你們真好!

親愛的爺爺奶奶: 謝謝你們給我的童年回憶, 希望我能令你們感到欣慰, 我永遠懷念著你們。

Jen-Hsuan Ho

賀仁萱

Enschede, June 2014